**Peer Review File**

**Manuscript Title:** Targeting Immune Fibroblast Cell Communication in Heart Failure

## Reviewer Comments & Author Rebuttals

### Reviewer Reports on the Initial Version:

Referees' comments:

Referee #1 (Remarks to the Author):

In this manuscript by Amrute J.M., Luo X., and colleagues, the authors used various multi-omic methods to dissect the fibroblast activation states that emerge following acutely infarcted and chronically failing human hearts. This well-written manuscript relies heavily on elegant computational investigation and inferences of complex biology in human cardiac tissues to make several novel claims. Cell interaction analyses and spatial transcriptomics were used to identify areas of fibrosis that were predicted to be driven by IL1b signaling from CCR2 macrophages to activate fibroblasts. Macrophage IL-1 signaling into fibroblasts in cardiac tissue is highly relevant however macrophage-specific deletion of IL1 would be necessary to validate this prediction. The authors also proposed that fibroblasts expressing FAP diverge into distinct myofibroblasts and pro-fibrotic fibroblast populations. While this idea is novel it requires proper in vivo lineage tracing studies to validate the in silico predictions. The authors further described that FAP+ fibroblasts treated with a neutralizing antibody against IL1b differentiated into a myofibroblast lineage that was not observed in isotype-treated control. However, this observation was not corroborated in their mouse model with fibroblast specific knockout of IL1R. While I appreciate that the authors attempted to use a fibroblast specific knockout of IL1R (Il1rfl/fl Dermo1-Cre) to demonstrate that IL1b signaling to fibroblast is necessary for cardiac fibrosis, the only readout was reduced trichrome staining. While I applaud the authors' computational efforts to characterize an interesting axis of myeloid-fibroblast cross talk in human cardiac disease, this manuscript lacks sufficient quantitative in vivo evidence to support their claims.

Referee #2 (Remarks to the Author):

Amrute et al. use multi-omics data and relevant mouse models to elucidate immune-fibroblast crosstalk in the context of heart failure. They find a subset of CCR2+ macrophages that signal to fibroblast via IL-1b and rewire their gene regulatory network and differentiation trajectory towards a pro-fibrotic fibroblast phenotype. Il1b deficient mice or treatment with anti-IL1b alleviates fibrosis and reprograms fibroblasts. The manuscript is well written and interesting, but is very abundant in computational predictions with only some validation.
Major critiques:
• The first part of the paper essentially reports fibroblasts clusters during cardiac inflammation/fibrosis with the value of presenting human data y comparison with mouse models, to show reasonable

alignment. The data at this point is purely in silico with poor validating value on what the different fibroblast clusters represent, beyond correlation with disease. Is there any other more rigorous metric to demonstrate this alignment?

• The role of RUNX1 in the regulation of FAP+ pro-fibrotic fibroblast is predicted, not tested by any experimental approach. Sometimes, this is not clearly stated in the document like in lines 573-575: “We identify a macrophage subset in humans which signals to fibroblasts via IL-1 β and modulates fibroblast activation, lineage specification via a RUNX1 orchestrated gene regulatory network”.

• About the expansion of myeloid cells and fibroblast mentioned in lanes 184-187, there is not reference to any figure supporting this statement.

• In the second section of the Results, relative to “Expansion of pathologic fibroblast subsets in acute MI and chronic heart failure”, the authors categorize fibroblasts as perivascular or interstitial to justify their focus on the F9 subset because “Given the fibrosis associated transcriptional signature of F9 fibroblasts and their localization within the infarct and fibrotic regions of the myocardium” (226-228). However, this categorization is just based in few images of spatial transcriptomics, with no distance quantification and without showing any data on vessels localization for comparison (lanes 208-210 and 222-225, Supplementary Figure 4D).

• In Figure 5, the effect of anti-IL1b treatment is moderate and substantial number of FAP+ fibroblasts still exist in AngII/PE group compared to Sham group. Are there other pathways that can activate fibroblasts? Or the effect of the antibody is not strong? Do Il1r f/f Dermo1-Cre mice show a strong reduction of FAP+ fibroblast population compared to the control mice group? Along this line, it´d be relevant to show whether treatment with anti-IL1b improves cardiac function, not only fibrosis as shown in Fig.4p.

• Fig4A: can the rationale and methodological approach behind the nichenet search explained better? which is the dataset used for this? which cell types are considered in this search? The call for TGFb and IL1b seem more of a biased call than an actual search.

• Related to the above, Fig4i: the correlation between POSTN/RUNX1 with NFKB is interesting but again no specific for IL1b, is the cytokine actually expressed at these sites enriched in F9 fibroblasts? beyond in silico predictions, the paper generally lacks from direct validation e.g. by immunofluroesence, genetic models (reporters, loss of function), etc. to confirm predictions. For example, can the authors show that Il1b+ macrophages associate physically with Meox+ or Postn+ or FAP+ fibroblasts? This point is particularly relevant since it is clear that F9 fibroblasts are predicted to be in large areas of the myocardium (Fig.S16), so it's unclear the specificity and resolution of the transcriptional profiling performed by spatial seq.

• The production of Il1b by macrophages as causal to fibroblast reprogramming and fibrosis is predicted, not demonstrated. It would be necessary to genetically disrupt Il1b expression specifically by macrophages.

• Fig4A: can the rationale and methodological approach behind the nichenet search explained better? which is the dataset used for this? which cell types are considered in this search? The call for TGFb and IL1b seem more of a biased call than an actual search.

• Fig.5B: the cytometry plots reveal a continuum of fibroblasts in FAP expression, unlike what one would expect, and the minor shifts are interpreted as IL1b regulating "fibroblast specification". This unclear separation was then used to sort FAPpos vs FAPneg cells for scRNAseq. It is unclear to me why this

approach was followed rather than direct sequencing of all fibroblasts in the anti-IL1b treated and untreated groups to build a fibroblast map with all states.

• Minor:
• The predictions shown in Fig.5k-l merging mouse and human data are shallow and only predictive and not quantified in any way. More conclusive experiments in the mouse during actual transcriptomics of the compared groups would be needed to make a relevant point.
• page 6: there is no defined perivascular or interstitial spatial niches that I can tell in FIg.S4. How are these discriminated or described?
• The Fig2N call in page 8 seems to be incorrect in the actual figure. Related to this, the choice of ENRA to examine openness of the locus and association with HF is a bit random, what about RUNX1 and MEOX1?
• The data regarding the immune-fibroblast niche and T-cell is rather descriptive and preliminary. How do you connect this data to your main story of macrophage–fibroblast crosstalk? How do T-cells affect the fibroblast phenotype if at all? I would suggest leaving these data out of the paper.
• Likewise, in Fig.5G the use of the new tool CellOracle to predict perturbations in Runx1KO fibroblasts is interesting but speculative and out of place in this paper. what is the intention of adding it and how does it link with anti-Il1b treatment?
• Misspelling: line 183: aobserved
• typo: line 442 should be Fig5C, not 5A, right?
• it´s impossible for me read the heading of some panels, eg. Fig.3C
• IL-1, IL-B and IL-1B are mixed throughout the document. Please choose one for consistency

Referee #3 (Remarks to the Author):

This interesting study examines populations of human and mouse cardiac cells, with an emphasis on subpopulations of fibroblasts, during the heart's response to injury. The findings are potentially very impactful and the datasets will be useful to the field. Inclusion of human data is a strength. An enormous amount of data is analyzed—a strength, because of the efforts to reconcile with previous research, and a weakness, because following what was done is extremely challenging. Parsing observation from interpretation is tough with the limited description of the different analyses performed. The authors should make a stronger effort to clearly describe what has been done in each of the comparative analyses in the main text, perhaps paring down some of the extensive analyses to explain in sufficient detail those that would need to be repeated by future investigators wishing to examine these subpopulations of cells. Additional characterization of the effect of Il1 beta on cardiac phenotypes would strengthen the paper. Other feedback:

The legend says that Figure 1D is "RNA and protein" data, whereas the results say the clusters were based on differential gene expression. Please clarify in main text how these clusters were defined.

What data are the basis for this claim: "Accumulation of fibroblasts was seen across pathological

conditions beginning 1 week after acute MI"? Is this a temporal analysis based on a subset of patients with different times out from MI? What markers were used for fibroblasts in this conclusion?

Please list in the figure which 'canonical markers' were used to determine cell populations in Figure 1I.

RNA and ATAC data should be split out and analyzed in parallel, in addition to the combined method in Figure 1. Are the accessibility changes around the same canonical genes sufficient to retrieve the same clusters using only the ATAC data? What differences in clustering exist when these datasets are not combined?

Expanding on the last point, a strength of snRNA and ATAC with Multiome is that, in principle, the experiment can reveal whether the accessibility changes and expression changes are happening in the same cell. What is the observation in the present study? Also, the investigators are missing a chance to dig deeper into how the accessibility and expression data identify the same or different features of these populations of cells. What subpopulations of cells are identified only with RNA or only with ATAC?

Regarding this sentence: "Using RNA derived annotations, we called peaks and found feature marker peaks for the major cell types (Fig. 1J)." What is a 'feature marker peak'? Unclear what is shown in this figure and how it was generated. Likewise Figure 1K needs a better description to understand what is going on.

Are the 'classical' fibroblast markers used for ground state clustering in Figure 2a the genes Pl16, CCDC80 and FBLN1 from Figure 2B? Please be explicit.

The description in the results and the figure legend are insufficient to understand what the authors observe in the figure and how they come to this conclusion: "Spatial transcriptomics data from human heart indicated that fibroblast populations were located within defined perivascular and interstitial spatial niches (Supplementary Fig. 4B – D)." On the basis of what observation was 'were located in defined…niches' determined? What would the alternative look like (i.e. what is a control showing the absence of defined localization)?

Please specify in each of the panels of Figure 2 whether RNA, ATAC or both are used for clustering and analyses. Legend says CITED, so this is protein information too? Please clarify in results and legend text.

Regarding this statement: "F2 and F9 fibroblasts resided within distinct regions of the myocardium (Supplementary Fig. 4D)"; what this figure appears to show is F2 expression in perivascular and F9 in interstitial sections, but not the opposite analysis, which would be required to make this conclusion. Please clarify. These data are intriguing and hint that the investigators may have uncovered different populations involved in perivascular vs interstitial fibrosis.

Related to the last point: many bulk RNA seq or PCR based measurements of gene activation in hearts and isolated fibroblasts show activation of acta2 and postn, whereas these authors demonstrate these

genes are not active in the same cells (Figure 2B), an important observation.

Regarding this statement: “Furthermore, RUNX1 and MEOX1 increased along the F9 lineage but not the other lineages (Fig. 2L)”, did the authors investigate the other fibroblast clusters or just F2 v F9 as shown in Fig 2L? All clusters should be analyzed.

Figure 2N is labeled as betweenness centrality in the legend and differential ATAC accessibility in the results. Both would be interesting to see.

For the differential ATAC accessibility, how many of the other marker genes in this cluster also have differential ATAC accessibility and in how many of the cases does it move in the predicted manner (e.g. more accessible, more transcribed)? Is accessibility of the gene body or a nearby regulatory element considered?

The comparison with previously published mouse scRNA-seq data is a strength of this work. Regarding these analyses: what is meant by ‘strong mapping across all populations’? I understand the coloring in SFigure 6B, but as a control, what comparison would produce weak mapping? What would this look like?

If you map previously published data onto your CITED-seq clusters, how do you avoid overfitting? This analysis gives the impression that one would generate the same clusters from these different datasets with the same data analysis methods, but without using the cell type assignments from one to label the other. But I do not think this is what has been done here. Do you regenerate the clusters in Figure 6A without reference to the CITED data in your study? It sounds like you are using the already generated clusters and mapping onto them the expression data from other mouse studies. If this is the case, how similar are the data if you just cluster them completely independently of each other (i.e. cluster the mouse data without reference to the human data)? Either way, please make this clearer in results and figures. These same questions apply to Figure 3.

Regarding this statement: “Multiple biological and technical replicates were included, individually hash tagged, and pooled to minimize any potential batch effects (Fig. 3F).” If the replicates were separately bar coded, the authors should be able to retrieve the individual sample information and analyze this variability. Such analyses would be very useful to the field towards the goal of understanding variability in single cell measurements.

How Figure 4J was generated and what it shows is unclear. Also for Figure 4M. The relationship between ‘spatial niches’ and ‘spatial clusters’ is unclear.

Please show level of Il1beta and Il1 receptor protein expression in control, Il1rflox/flox dermo1-cre, and both strains with AngII/PE in macrophages and cardiac fibroblasts. Also, the level of circulating Il1beta should be tested in all these conditions.

The ability of Il1beta to influence ventricular remodeling by inhibiting fibrosis has been known for some

time (PMID: 11691538). The experiments in Figure 5 add detail to the molecular features of the different cells contributing to this phenomenon. The investigators need to show whether Il1b mAb treatment influences fibrosis in this model and the effects on systolic and diastolic cardiac function.

Given the known role of Il1b in fibrosis, it is uncertain how the reader will use the information in this paper for future studies. Efforts by the authors to make clearer how to repeat identification and characterization of the fibroblast subpopulations described in this study, and whether these subpopulations are differentially involved in the effects of Il1b, would increase the impact of the study.

**Author Rebuttals to Initial Comments:**

Referee #1 (Remarks to the Author):

In this manuscript by Amrute J.M., Luo X., and colleagues, the authors used various multi-omic methods to dissect the fibroblast activation states that emerge following acutely infarcted and chronically failing human hearts. This well-written manuscript relies heavily on elegant computational investigation and inferences of complex biology in human cardiac tissues to make several novel claims. Cell interaction analyses and spatial transcriptomics were used to identify areas of fibrosis that were predicted to be driven by IL1b signaling from CCR2 macrophages to activate fibroblasts. Macrophage IL-1 signaling into fibroblasts in cardiac tissue is highly relevant however macrophage-specific deletion of IL1 would be necessary to validate this prediction. The authors also proposed that fibroblasts expressing FAP diverge into distinct myofibroblasts and pro-fibrotic fibroblast populations. While this idea is novel it requires proper in vivo lineage tracing studies to validate the in-silico predictions.

We thank the reviewer for the insightful comments and suggestions. To experimentally validate the computationally derived claims, we have added several new mouse models and performed in vivo cardiac injury experiments focused on the functional role of IL-1 signaling and fibroblast lineage tracing. We have also added new human data to further support our conclusions.

Point 1: "Macrophage IL-1 signaling into fibroblasts in cardiac tissue is highly relevant however macrophage-specific deletion of IL1 would be necessary to validate this prediction". To mechanistically investigate the impact of targeting IL-1β on cardiac function, we generated IL-1β$^{flox/flox}$ Ccr2$^{creERT2}$ mice to specifically knockout IL-1β in CCR2+ monocytes and monocyte-derived macrophages. We focused specifically on CCR2+ monocytes and macrophages because both the human and mouse data support that these are the dominant cell types which express IL-1β in heart failure. We implanted Ang II/PE pumps into control and IL-1β$^{flox/flox}$ Ccr2$^{creERT2}$ mice and treated these mice with continuous tamoxifen dosing throughout the duration of the experiment. We characterized FAP expression at day 7 by flow cytometry. Fibrosis was measured and echocardiography was performed at day 28 post Ang II/PE pump implantation. Briefly, we found that deletion of IL-1b from CCR2+ monocytes and monocyte-derived macrophages resulted in reduced abundance of FAP+ fibroblasts at day 7, decreased fibrosis at day 28, and improved systolic function compared to control mice. We have amended figure 6 and the main manuscript text to reflect these new experiments and additional analyses.

We have also added a description of these experiments to the manuscript main text as follows:

"***IL-1β derived from CCR2+ monocytes and macrophages is causally linked to fibrosis and diminished cardiac function.***
To determine whether IL-1β derived from CCR2$^{+}$ monocytes and macrophages is necessary for cardiac fibrosis, we generated mice that lack IL-1β in CCR2$^{+}$ monocytes and macrophages (IL-1β$^{flox/flox}$ Ccr2$^{creERT2}$). Control and IL-1β$^{flox/flox}$ Ccr2$^{creERT2}$ mice underwent sham surgery or received Ang II/PE eluting osmotic minipumps (**Fig. 6i**). To characterize early fibroblast activation, mice were sacrificed after 7 days of Ang II/PE infusion and hearts enzymatically digested for flow cytometry. Quantification of flow cytometry data revealed an increase in the proportion of FAP$^{+}$ fibroblasts in Ang II/PE treated animals compared to sham surgeries and importantly fewer FAP$^{+}$ fibroblasts in IL-1β$^{flox/flox}$ Ccr2$^{creERT2}$ mice compared to IL-1β$^{flox/flox}$ mice (**Fig. 6j**). Transthoracic echocardiography (TTE) was performed after 28 days of Ang II/PE infusion to characterize the impact of IL-1β deletion in CCR2$^{+}$ cells on cardiac function. TTE showed a significant decrease in E/e' and end systolic volume (ESV) with a significant improvement in fractional shortening (FS) an ejection fraction (EF) in IL-1β$^{flox/flox}$ Ccr2$^{creERT2}$ mice

compared to IL-1β$^{flox/flox}$ mice (**Fig. 6k, l**). Fibrosis was quantified after 28 days of Ang II/PE infusion by trichrome staining. Ang II/PE infusion resulted in diminished interstitial fibrosis in IL-1β$^{flox/flox}$ Ccr2$^{creERT2}$ mice compared to IL-1β$^{flox/flox}$ mice (**Fig. 6m**)."

Figure 6

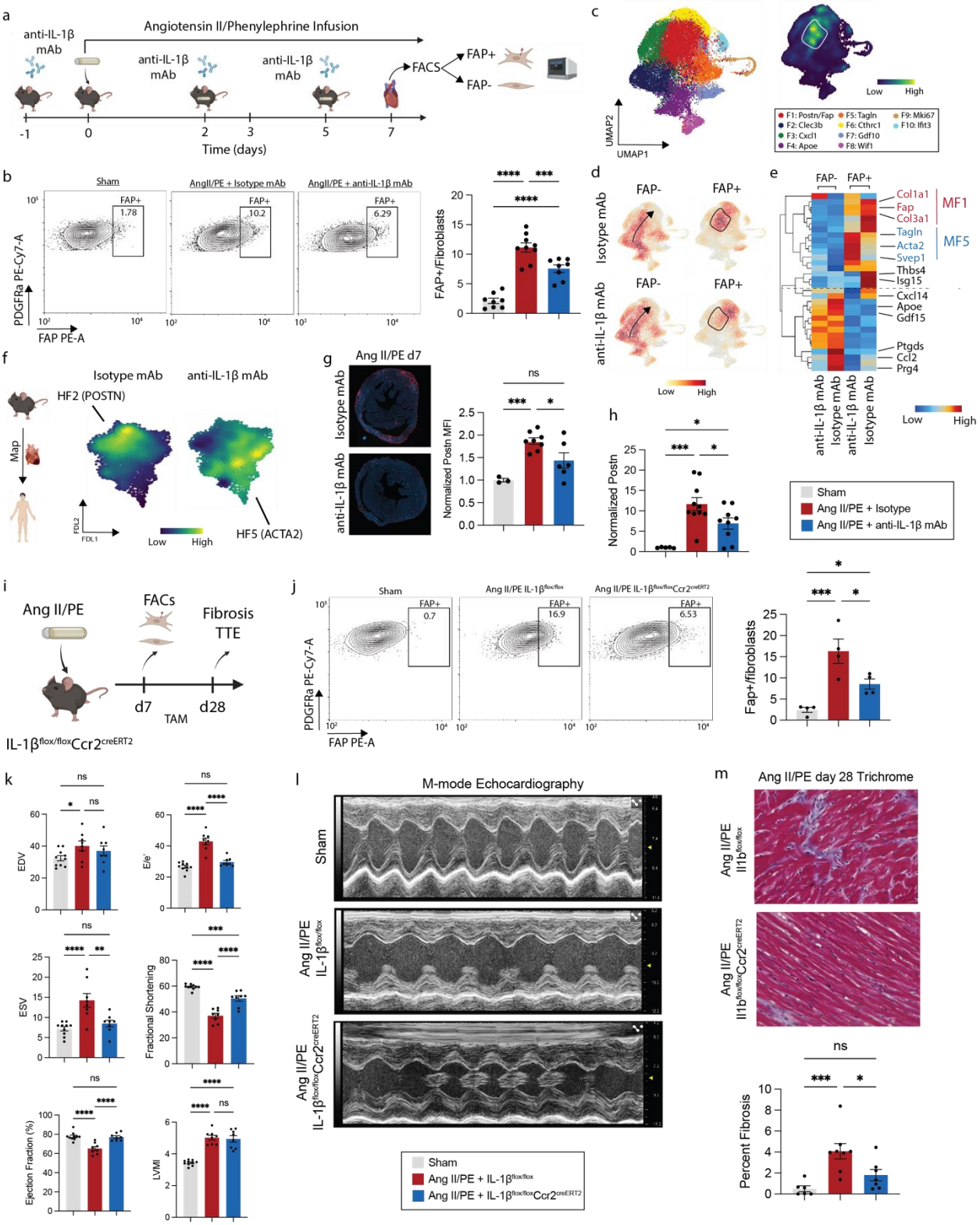
a
anti-IL-1β mAb
Angiotensin II/Phenylephrine Infusion
anti-IL-1β mAb
anti-IL-1β mAb
FACS
FAP+
FAP-
-1
0
2
3
5
7
Time (days)
b
Sham
AngII/PE + Isotype mAb
AngII/PE + anti-IL-1β mAb
FAP+ 1.78
FAP+ 10.2
FAP+ 6.29
PDGFRa PE-Cy7-A
FAP PE-A
FAP+/Fibroblasts
c
UMAP2
UMAP1
Low
High
F1: Postn/Fap
F2: Clec3b
F3: Cxcl1
F4: Apoe
F5: Tagln
F6: Cthrc1
F7: Gdf10
F8: Wif1
F9: Mki67
F10: Ifit3
d
FAP-
FAP+
Isotype mAb
anti-IL-1β mAb
Low
High
e
FAP-
FAP+
Col1a1
Fap
Col3a1
MF1
Tagln
Acta2
Svep1
MF5
Thbs4
Isg15
Cxcl14
Apoe
Gdf15
Ptgds
Ccl2
Prg4
anti-IL-1β mAb
Isotype mAb
anti-IL-1β mAb
Isotype mAb
Low
High
f
Isotype mAb
anti-IL-1β mAb
HF2 (POSTN)
Map
FDL2
FDL1
Low
High
HF5 (ACTA2)
g
Ang II/PE d7
Isotype mAb
anti-IL-1β mAb
Normalized Postn MFI
ns
h
Normalized Postn
Sham
Ang II/PE + Isotype
Ang II/PE + anti-IL-1β mAb
i
Ang II/PE
FACs
Fibrosis
TTE
d7
TAM
d28
IL-1β^flox/flox Ccr2^creERT2
j
Sham
Ang II/PE IL-1β^flox/flox
Ang II/PE IL-1β^flox/flox Ccr2^creERT2
FAP+ 0.7
FAP+ 16.9
FAP+ 6.53
PDGFRa PE-Cy7-A
FAP PE-A
Fap+/fibroblasts
k
EDV
E/e'
ESV
Fractional Shortening
Ejection Fraction (%)
LVMI
l
M-mode Echocardiography
Sham
Ang II/PE IL-1β^flox/flox
Ang II/PE IL-1β^flox/flox Ccr2^creERT2
Sham
Ang II/PE + IL-1β^flox/flox
Ang II/PE + IL-1β^flox/flox Ccr2^creERT2
m
Ang II/PE day 28 Trichrome
Ang II/PE Il1b^flox/flox
Ang II/PE Il1b^flox/flox Ccr2^creERT2
Percent Fibrosis

Point 2: The authors also proposed that fibroblasts expressing FAP diverge into distinct myofibroblasts and pro-fibrotic fibroblast populations. While this idea is novel it requires proper in vivo lineage tracing studies to validate the in-silico predictions.

To explicitly address this important point raised by the reviewer, we have generated $Fap^{creERT2}$ mice by knocking an inducible Cre recombinase into the endogenous FAP locus. We then generated $Fap^{CreERT2}Rosa26^{LSL\text{-}tdTomato}$ mice and performed in vivo fibroblast lineage tracing. These data are displayed in a new main figure (Figure 4).

Our human and mouse computational analyses predicted that FAP+ fibroblasts emerge early and may selectively contribute to Postn fibroblasts that are distinct from myofibroblasts. To test this hypothesis, $Fap^{CreERT2}Rosa26^{LSL\text{-}tdTomato}$ mice were subjected to the Ang II/PE injury model. Tamoxifen was given early after pump implantation (days 1-7, IP) at 60 mg/kg and mice were sacrificed at day 14 to characterize fibroblast lineages. We performed immunofluorescence and RNAscope in situ hybridization to stain for Postn (pro-fibrotic fibroblasts) and ACTA2 (myofibroblasts) and overlaid tdTomato signal (for Fap lineage labeled cells). We then specifically quantified cells within the myocardium interstitial areas that were $tdTomato^{+}Postn^{+}$ and $tdTomato^{+}Acta2^{+}$ and found that most $tdTomato^{+}$ cells expressed Postn but not Acta2. These results would suggest that FAP+ fibroblasts in cardiac injury predominantly contribute to the $Postn^{+}$ lineage but not the $Acta2^{+}$ myofibroblast lineage. We have created a new figure (Figure 4) integrating several orthogonal lines of evidence in human and mice using single cell RNA-sequencing, computational pseudotime trajectory analysis, multiomic RNA + ATAC sequencing, in vivo lineage tracing, and spatial transcriptomics to dissect cardiac fibroblast heterogeneity.

We added a description of these experiments to the manuscript main text as follows:

"***Distinct lineages of activated cardiac fibroblasts.***

To map fibroblast trajectories in AMI and heart failure, we undertook two approaches. First, we used scVelo with dynamical modeling to infer directionality in fibroblast cell state differentiation. Projection of the velocity vector field in a force directed layout suggested convergence toward the F2, F4, and F9 fibroblast states (**Fig. 4a**). Next, we used Palantir to predict fibroblast differentiation endpoints, which also identified F2, F4, and F9 as possible terminal states with low entropy values across a range of simulation parameters (**Fig. 4b**). To glean how fibroblasts might evolve over the time course of disease, we plotted donor and diseased fibroblast signatures (**Supplementary Fig. 7f**) versus pseudotime along each predicted lineage (F2, F4, F9). The donor fibroblast signature was most enriched early in pseudotime, while the diseased signature increased over pseudotime in each lineage. *FAP* expression transiently increases along the F2 and F4 lineages and progressively increases along the F9 lineage. Notably, the markers of each population increase over pseudotime in a lineage specific manner (**Fig. 4c**). To dissect putative regulators of the different trajectories, we identified differentially expressed genes and used the resultant gene list to perform a transcription factor enrichment analysis. This approach identified *FBN1, PPRX, FOSX1*, and *MEOX1* as the top transcription factors driving the F9 lineage (**Fig. 4d**). *MEOX1* was previously implicated in cardiac fibrosis[32]. We then used CellOracle to build a gene regulatory network of heart failure fibroblasts and identified enriched *RUNX1* connectivity across all 3 heart failure groups (**Fig. 4e**). Previously, we have shown that *RUNX1* expands in heart failure using RNAscope in situ hybridization in non-failing donors and heart failure myocardial samples interstitial cells[33]. Linear regression analysis of pseudobulk *RUNX1* and *POSTN* expression at the patient level shows a strong correlation (**Fig. 4f**). Gene expression density plots showed that *MEOX1* was co-expressed with *RUNX1* and

*POSTN* along the F9 lineage while *ACTA2* expression was restricted to a different cell state (F2) (**Fig. 4g**). Furthermore, *RUNX1* and *MEOX1* increased along the F9 lineage but not the F2 or F4 lineages (**Fig. 4d**). Using PathwayNet we found that *POSTN* and *RUNX1* are predicted to be connected via a transcriptional regulation network (**Supplementary Figure. 7g**). We validated that these populations are indeed distinct using RNAscope and immunofluorescence for POSTN and ACTA2 respectively from human infarct zone samples (**Fig. 4h**). Additionally, mouse spatial transcriptomics data collected at day 7 post-MI, indicated that *Acta2* and *Postn* expressed in different spatial distributions. *Postn* is enriched within the border zone, whereas *Acta2* is localized to the core of the infarct (**Fig. 4i**). To lineage trace $FAP^+$ fibroblasts, we generated $Fap^{creERT2}Rosa26^{tdTomato}$ mice (**Supplementary Figure. 20**, detailed in methods) and performed Ang II/PE mini-pump implantation (**Fig. 4j**). Using FAPi non-invasive PET imaging, we confirmed early enrichment of FAP at day 7 following AngII/PE infusion (**Fig. 4k**). Tamoxifen was administered to label $FAP^+$ fibroblasts on days 1-7 of Ang II/PE infusion and mice were sacrificed at day 14 (**Fig. 4j**). We then performed RNAscope in situ hybridization for *Postn* and immunofluorescence for ACTA2 and overlaid tdTomato signal (**Fig. 4l**). Quantification of $tdTomato^+Postn^+$ and $tdTomato^+ACTA2^+$ cells showed that $FAP^+$ cells contributed towards the Postn lineage and not the Acta2 myofibroblast lineage (**Fig. 4l**).”

Figure 4

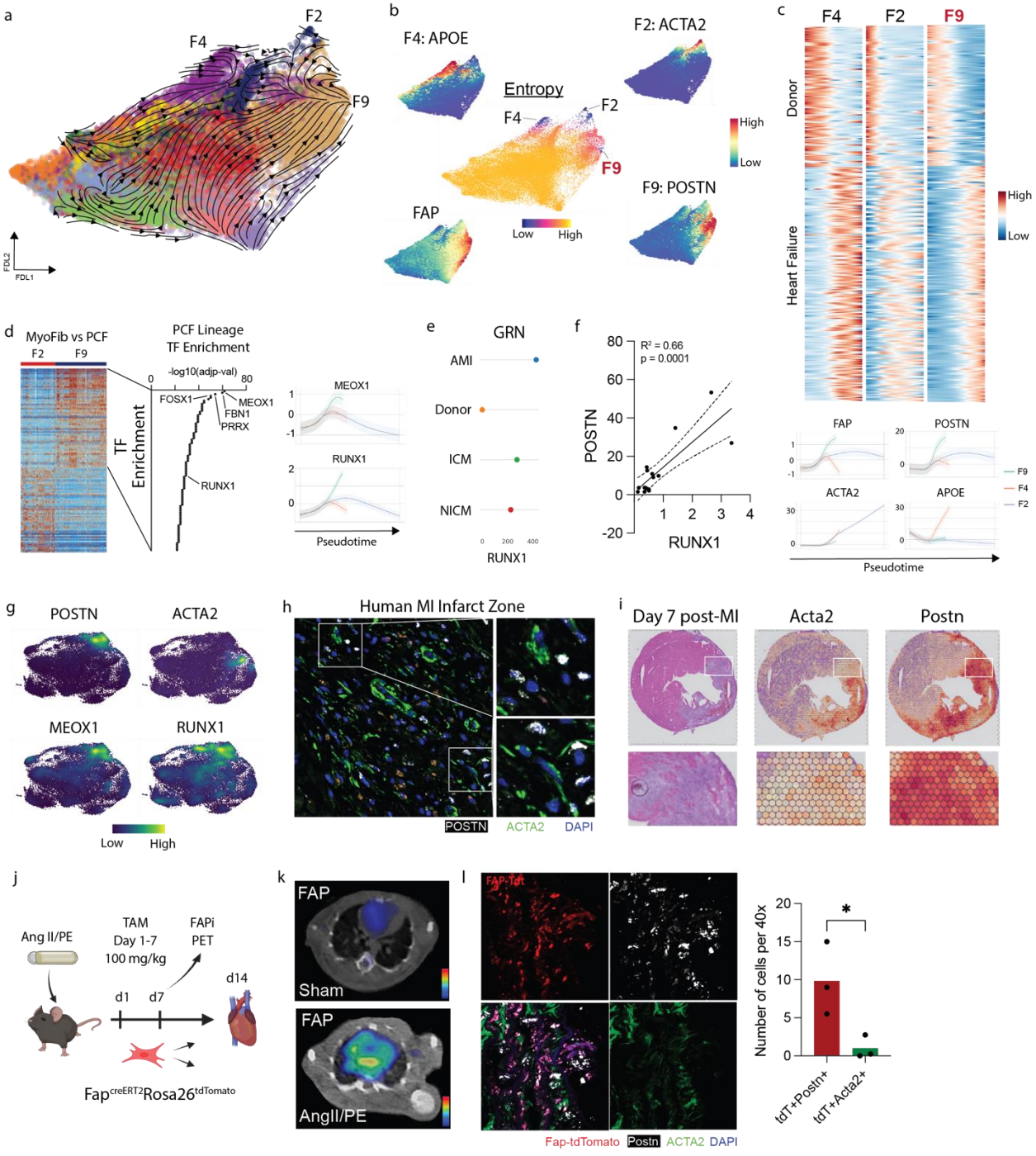
a
F2
F4
F9
FDL2
FDL1
b
F4: APOE
F2: ACTA2
Entropy
F4
F2
F9
High
Low
FAP
F9: POSTN
Low
High
c
F4
F2
F9
Donor
Heart Failure
High
Low
FAP
POSTN
ACTA2
APOE
F9
F4
F2
Pseudotime
d
MyoFib vs PCF
F2
F9
PCF Lineage
TF Enrichment
-log10(adjp-val)
0
80
FOSX1
MEOX1
FBN1
PRRX
RUNX1
TF Enrichment
MEOX1
RUNX1
Pseudotime
e
GRN
AMI
Donor
ICM
NICM
0
200
400
RUNX1
f
R² = 0.66
p = 0.0001
POSTN
RUNX1
g
POSTN
ACTA2
MEOX1
RUNX1
Low
High
h
Human MI Infarct Zone
POSTN
ACTA2
DAPI
i
Day 7 post-MI
Acta2
Postn
j
Ang II/PE
TAM
Day 1-7
100 mg/kg
FAPi
PET
d1
d7
d14
Fap^creERT2 Rosa26^tdTomato
k
FAP
Sham
FAP
AngII/PE
l
FAP-Tdt
Fap-tdTomato
Postn
ACTA2
DAPI
Number of cells per 40x
*
tdT+Postn+
tdT+Acta2+

Additionally, we have created a supplementary figure describing the construction of this new CRE, with the following addition to the methods section:

"**Gene Editing Design**
Analysis of genomic DNA sequence surrounding the target region, using the Benchling (www.benchling.com) guide RNA design tool, identified a gRNA sequence with a suitable target endonuclease site in *Fap* gene start site. Predicted off-target sites for the gRNA (crRNA2-AAGGTTAGTGCGTGCCGTCT) were identified using the specificity model developed and documented by Hsu and colleagues and embedded in the Benchling gRNA design tool. Design considerations for off-target editing were as follows. Higher off-target editing risk was considered when the "Score" is >2.0 with a canonical SpCas9 PAM (NGG), >50.0 with a chromosomally unlinked non-canonical PAM (NAG) or >20.0 with a linked non-canonical PAM yet in an annotated protein coding region. These "Score" thresholds were based on empirical targeted sequencing analysis of 20 different predicted off-target loci in 15 different mouse zygote gene editing experiments.

**Microinjection of gRNAs and plasmid donor DNA repair templates**
*Streptococcus pyogenes* Cas9 (SpCas9) V3 protein and gRNAs were purchased as part of the Alt-R CRISPR-Cas9 system using the crRNA:tracrRNA duplex format as the gRNA species (IDT, USA). Alt-R CRISPR-Cas9 crRNAs (Product# 1072532, IDT, USA) were synthesized using the gRNA sequences specified in the DESIGN section and hybridized with the Alt-R tracrRNA (Product# 1072534, IDT, USA) as per manufacturer's instructions. This gRNA duplex was used in all subsequent gene editing processes. The sequence of the double stranded DNA donor plasmid, that functions as the DNA repair template, was synthesized by Genscript. Features included asymmetric homology arm lengths of 1.6 kb and 2.0 kb, flanking the 2.2 kb insertion sequence. The final concentration of the gRNA, SpCas9 and donor components in the microinjection mixture was 50ng/ul, 100 ng/ul and 10 ng/ul, respectively. All animal work was approved by the Jackson Laboratory Animal Care and Use Committee and adhered to the standards of Guide for the Care and Use of Laboratory Animals set forth by the NIH. Microinjection was performed as described (PMID: 27210041) using C57BL/6J (Stock# 000664, The Jackson Laboratory, USA) donor female mice (3–4 weeks of age).

**Sequence characterization of Founder and N1 mice**
PCR primers flanking the gRNA target site, but outside the repair template homology arms, were used to amplify the region of interest from founder progeny. PCR amplicons were subjected to Sanger sequencing to identify founders with precise desired changes. Founders carrying desired mutations were bred with C57BL/6J mice (Stock #000664, The Jackson Laboratory, USA) to produce N1 progeny. N1 animals were confirmed by the same PCR-Sanger sequence analysis the founder population was subjected to. In contrast to founders, N1 animals are obligate heterozygotes, with one allele derived from an un-manipulated chromosome, enabling deconvolution of the two alleles in the mixed PCR amplicon. PCR primer sequences were as follows: Short Range PCR, Fap SR forward and Cre SR reverse; 5'-AGAACGCCCCCAAAATCTGT-3' and 5'- ATTCAACTTGCACCATGCCG-3', left homology arm PCR, Fap LHA forward and Cre SR reverse; 5'-GCTGATGGCTTTCTCTCGGA-3' and 5'-ATTCAACTTGCACCATGCCG-3', and right homology arm PCR, ERT RHA forward and Fap RHA reverse; 5'-CGGGCTCTACTTCATCGCAT-3' and 5'-CAGGTGACATGCTGAGGTGT-3'.
"

Supplementary Figure 20

a

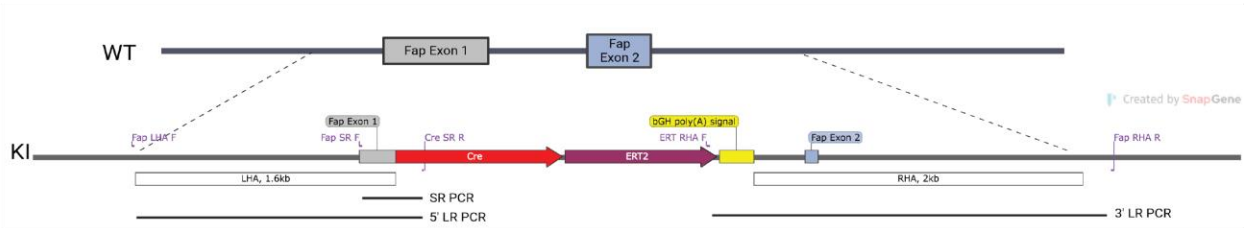


b


c

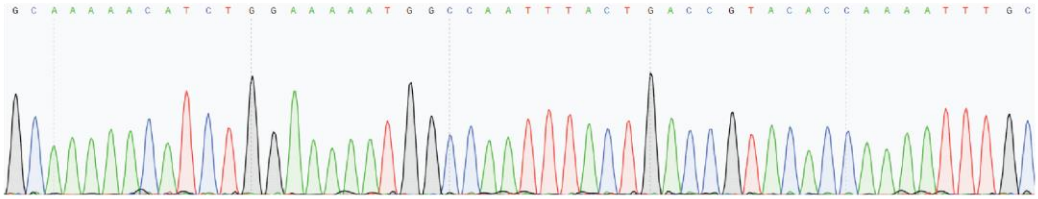

WT GCAAAAACATCTGGAAAAATGAAGGTTAGTGCGTGCCGTCTCGGGGACGACC
KI GCAAAAACATCTGGAAAAATGGCCAATTTACTGACCGTACACCAAAATTTGC
CRE M A N L L T V H Q N L

d

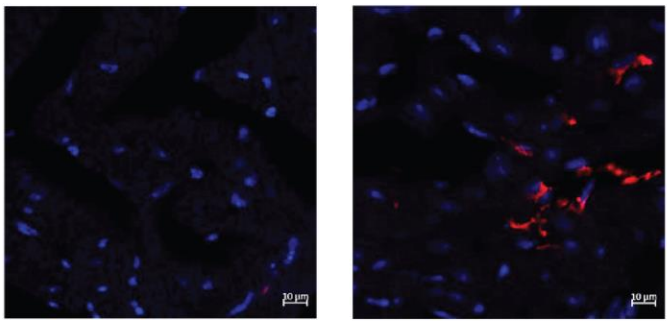

The authors further described that FAP+ fibroblasts treated with a neutralizing antibody against IL1b differentiated into a myofibroblast lineage that was not observed in isotype-treated control. However, this observation was not corroborated in their mouse model with fibroblast specific knockout of IL1R.

We thank the reviewer for addressing this important point. Mice treated with a neutralizing antibody against IL-β in the setting of Ang II/PE infusion showed depletion of $FAP^+$ and $POSTN^+$ fibroblasts. As outlined above, we now show that the $FAP^+$ cells selectively contribute to the POSTN lineage. To specifically address the reviewer's point, we performed flow cytometry to characterize fibroblast FAP expression at day 7 following Ang II/PE infusion in control and IL-$1R^{flox/flox}Dermo1^{Cre}$ mice as suggested by the reviewer. We found that that IL-$1R^{flox/flox}Dermo1^{Cre}$ mice had fewer $FAP^+$ fibroblast compared to control mice (Figure 5m). Furthermore, we also performed Ang II/PE pump implantation into control and IL-$1\beta^{flox/flox}$ $Ccr2^{creERT2}$ mice. Mice were treated with tamoxifen throughout the duration of the experiment. We measured $FAP^+$ fibroblasts by flow cytometry on day 7 following Ang II/PE pump implantation and found that the IL-$1\beta^{flox/flox}$ $Ccr2^{creERT2}$ mice had fewer $FAP^+$ fibroblasts compared to controls (Figure 6j). We also detected decreased fibrosis and improved systolic and diastolic function on day 28 compared to control mice (Figure 6k-m). To reflect these additional experiments, we have modified Figure 5-6 as shown below. We have also added the following to the main text of the manuscript:

"To determine whether IL-1β signaling to fibroblasts is necessary for cardiac fibrosis, we generated mice that lack the IL-1 receptor (*IL-1R*) in fibroblasts (IL-$1R^{flox/flox}Dermo1^{Cre}$ mice[34]). Control and IL-$1R^{flox/flox}Dermo1^{Cre}$ mice underwent sham surgery or received Ang II/PE eluting osmotic minipumps (**Fig. 5l**). To validate knockdown of the *IL-1R*, we sorted macrophages fibroblasts from IL-$1R^{flox/flox}$ and IL-$1R^{flox/flox}Dermo1^{Cre}$ mice 7 days after Ang II/PE infusion (**Supplementary Fig. 26a**) – using qPCR on sorted cells, we verify decreased *IL-1R* expression in fibroblasts but not macrophages (**Supplementary Fig. 26b**). To characterize early fibroblast activation, mice were sacrificed after 7 days of Ang II/PE infusion and hearts enzymatically digested for flow cytometry. Quantification of flow cytometry data revealed an increase in the proportion of $FAP^+$ fibroblasts in Ang II/PE treated animals compared to sham surgeries. Importantly, there were fewer $FAP^+$ fibroblasts in IL-$1R^{flox/flox}Dermo1^{Cre}$ mice compared to control mice (**Fig. 5m**). Fibrosis was quantified after 4 weeks of Ang II/PE infusion by trichrome staining. Ang II/PE infusion resulted in increased interstitial fibrosis in control mice compared to shams. Consistent with the conclusion that IL-1β signaling to fibroblasts promotes cardiac fibrosis, we observed reduced trichrome staining in Ang II/PE treated IL-$1R^{flox/flox}Dermo1^{Cre}$ mice compared to controls (**Fig. 5n**). Finally, we performed wheat germ agglutin (WGA) staining to quantify cardiomyocyte hypertrophy. We observed increased cardiomyocyte cross-sectional area in Ang II/PE treated controls compared to shams. However, there was a significant decrease in cardiomyocyte size in Ang II/PE treated IL-$1R^{flox/flox}Dermo1^{Cre}$ mice compared to controls (**Fig. 5o**)."

Figure 5

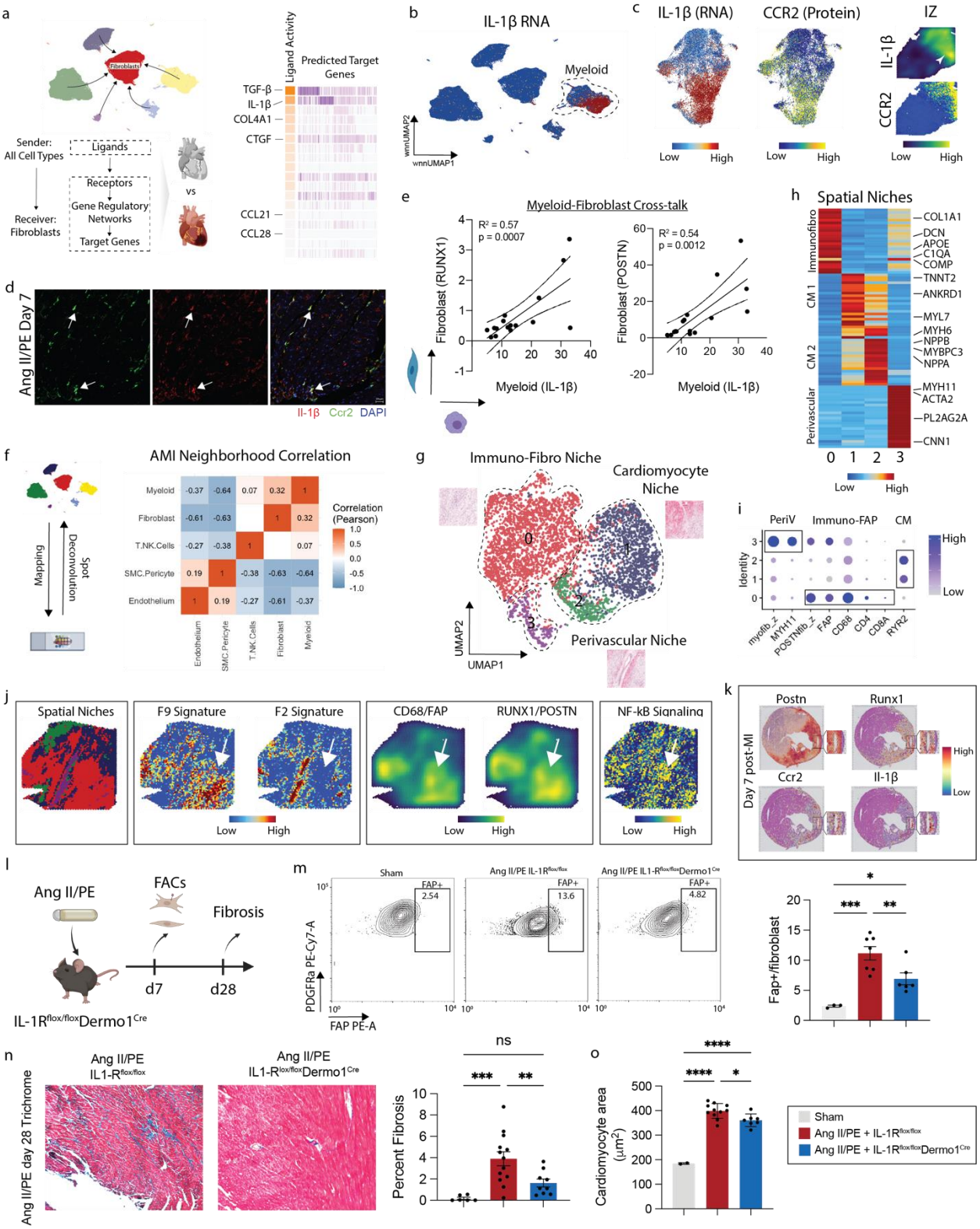
a
Fibroblasts
Sender: All Cell Types
Ligands
Receptors
Gene Regulatory Networks
Target Genes
Receiver: Fibroblasts
vs
Ligand Activity
Predicted Target Genes
TGF-β
IL-1β
COL4A1
CTGF
CCL21
CCL28
b
IL-1β RNA
Myeloid
wnnUMAP2
wnnUMAP1
c
IL-1β (RNA)
CCR2 (Protein)
IZ
IL-1β
CCR2
Low
High
d
Ang II/PE Day 7
Il-1β Ccr2 DAPI
e
Myeloid-Fibroblast Cross-talk
R² = 0.57
p = 0.0007
Fibroblast (RUNX1)
Myeloid (IL-1β)
R² = 0.54
p = 0.0012
Fibroblast (POSTN)
Myeloid (IL-1β)
h
Spatial Niches
Immunofibro
CM 1
CM 2
Perivascular
COL1A1
DCN
APOE
C1QA
COMP
TNNT2
ANKRD1
MYL7
MYH6
NPPB
MYBPC3
NPPA
MYH11
ACTA2
PL2AG2A
CNN1
0 1 2 3
Low
High
f
AMI Neighborhood Correlation
Mapping
Deconvolution
Spot
Myeloid
Fibroblast
T.NK.Cells
SMC.Pericyte
Endothelium
Correlation (Pearson)
g
Immuno-Fibro Niche
Cardiomyocyte Niche
Perivascular Niche
UMAP2
UMAP1
i
PeriV
Immuno-FAP
CM
Identity
myofib_z
MYH11
POSTNfib_z
FAP
CD68
CD4
CD8A
RYR2
High
Low
j
Spatial Niches
F9 Signature
F2 Signature
CD68/FAP
RUNX1/POSTN
NF-kB Signaling
Low
High
k
Postn
Runx1
Ccr2
Il-1β
Day 7 post-MI
High
Low
l
Ang II/PE
FACs
Fibrosis
d7
d28
IL-1R^flox/flox Dermo1^Cre
m
Sham
Ang II/PE IL-1R^flox/flox
Ang II/PE IL1-R^flox/flox Dermo1^Cre
FAP+
2.54
13.6
4.82
PDGFRa PE-Cy7-A
FAP PE-A
Fap+/fibroblast
n
Ang II/PE day 28 Trichrome
Ang II/PE IL1-R^flox/flox
Ang II/PE IL1-R^lox/lox Dermo1^Cre
Percent Fibrosis
ns
o
Cardiomyocyte area (μm²)
Sham
Ang II/PE + IL-1R^flox/flox
Ang II/PE + IL-1R^flox/flox Dermo1^Cre

While I appreciate that the authors attempted to use a fibroblast specific knockout of IL1R (Il1rfl/fl Dermo1-Cre) to demonstrate that IL1b signaling to fibroblast is necessary for cardiac fibrosis, the only readout was reduced trichrome staining.

To address this point, we performed flow cytometry on cardiac fibroblasts on day 7 following Ang II/PE infusion in control and IL-1R$^{flox/flox}$Dermo1$^{Cre}$ mice. We found that that IL-1R$^{flox/flox}$Dermo1$^{Cre}$ mice had fewer FAP+ fibroblast compared to control mice. To reflect these additional experiments, we have modified Figure 5 and revised the main text as shown above.

While I applaud the authors' computational efforts to characterize an interesting axis of myeloid-fibroblast cross talk in human cardiac disease, this manuscript lacks sufficient quantitative in vivo evidence to support their claims.

We thank the reviewer for this very important comment. Considering the very relevant suggestions made by the reviewer, we have expanded the work in the manuscript with additional human data, computational analysis, and novel mouse models to better characterize immune-fibroblast crosstalk in the failing human heart. Below, we outline the novel elements of the work herein and how it relates to and advances prior work in the field. Points 3-4 highlight our revisions that provide additional in vivo evidence that support our conclusions.

1. We added extensive new human data for a total of 22 CITE-seq from fresh hearts and 23 Multiome (RNA/ATAC) from frozen hearts. Both these data elements are novel and there are currently no studies which have profiled RNA, protein, and ATAC from failing human hearts. Importantly, the CITE-seq was performed in fresh explanted hearts from non-failing donors, acutely infarcted tissues (within a week of MI), and chronically failing hearts. These data offer an unprecedented opportunity to characterize cells from diseased human hearts and identify cell states at high granularity. We believe that this data can be of use to the broader field to identify new hypothesis, annotate existing datasets at higher resolution, leverage the ever-growing computational models to gain deeper insights from these data, and interpret newly generated human and mouse omics data in the context of these high-resolution state annotations. To facilitate these applications, we will be working with the human cell atlas to share out data in a user-friendly portal as well as the Seurat team to build an Azimuth reference so future studies can seamlessly map their data onto this reference for imputation of cell states and surface protein information.

2. An important consideration for translational studies for new targets is the applicability of experimental findings to human disease. Here in, we have utilized published data and generated additional single cell data from the 3 most widely used in vivo models of cardiac injury (MI, Ang II/PE infusion, and TAC) and compared this to newly generated single cell RNA sequencing data from human cell culture systems of fibroblast activation. Using integrated cell mapping, we show that the in vivo models are better surrogates for the populations identified in human hearts as compared to the cell culture systems. These findings are useful for the field as they can leverage our human data to compare how in vivo and in vitro perturbations may affect the corresponding human heart cell states which can have tremendous translation value.

3. Using the human CITE-seq data, we identify transcriptionally distinct myofibroblast and POSTN cell states which have previously largely considered a single population. Recent studies have leveraged immunomodulator approaches like CAR T cells to target activated fibroblasts marked by fibroblast activator protein (FAP) to target cardiac

fibrosis which highlights the therapeutic potential of this cell state. Importantly, to deplete these cells or modify their cell state transitions, it is critical to understand the precise markers of this population in humans as well as the lineages they go down in the injured heart. Given the plastic nature of fibroblasts and the dearth of genetic tools to study FAP+ fibroblasts, there is no data on how these fibroblasts evolve in the injured heart as well as their molecular markers in human tissue. Using an array of orthogonal techniques: single cell RNA-sequencing, immunofluorescence, and in vivo lineage tracing with a novel Fap-cre mouse, we show that these populations are distinct transcriptional states and come from different lineages in the failing heart. These are very important findings and tools for future studies targeting activated fibroblasts.

4. We further leverage the human multi-omic data in additional to integration with published spatial transcriptomics data to identify IL-1β as a potential therapeutic target to hinder macrophage fibroblast crosstalk. Within the human data, show that CCR2 monocytes and macrophages are producing the IL-1β which is predicted to signal to activated fibroblasts and drive fibrosis in heart failure. We generated mice lacking the IL-1R on fibroblasts and showed that in Ang II/PE infusion there is decreased fibroblast activation and less fibrosis compared to controls. Additionally, we use a monoclonal anti-IL-1β neutralizing antibody to show that IL-1β suppression reshapes the early activation landscape of fibroblasts. To mechanistically implicate CCR2 monocytes and macrophages as the causal cell state in driving fibrosis, we generated mice lacking the IL-1β ligand in CCR2 cells showed that in Ang II/PE infusion there is decreased fibroblast activation, less fibrosis, and improved systolic and diastolic function compared to controls. Our findings highlight the potential for targeting IL-1β in patients with heart failure, a finding that is consistent with secondary analysis of the CANTOS clinical trial (PMID 28845751).

REVIEWER #2

Amrute et al. use multi-omics data and relevant mouse models to elucidate immune-fibroblast crosstalk in the context of heart failure. They find a subset of CCR2+ macrophages that signal to fibroblast via IL-1b and rewire their gene regulatory network and differentiation trajectory towards a pro-fibrotic fibroblast phenotype. Il1b deficient mice or treatment with anti-IL1b alleviates fibrosis and reprograms fibroblasts. The manuscript is well written and interesting but is very abundant in computational predictions with only some validation.

Major critiques:
• The first part of the paper essentially reports fibroblasts clusters during cardiac inflammation/fibrosis with the value of presenting human data in comparison with mouse models, to show reasonable alignment. The data at this point is purely in silico with poor validating value on what the different fibroblast clusters represent, beyond correlation with disease. Is there any other more rigorous metric to demonstrate this alignment?

We thank the reviewer for point out this very important point. As stated above, we characterize distinct fibroblast cell states early in the manuscript in failing human hearts and show concordance between human and in vivo mouse models of cardiac injury included diseased associated cell states. As a first step, we leveraged a published mouse MI spatial transcriptomics dataset to overlay the signatures for the different human fibroblast cell states in space. This approach served as an orthogonal approach to the single cell mapping and further shows that distinct fibroblast states are selectively distributed within the infarct, border, and remotes zones. We have modified Figure 3 to reflect these additional analyses and added the following to the main text of the manuscript: "Additionally, we leveraged a published mouse MI spatial transcriptomics data collected 7 days following MI and overlaid signatures of human cardiac fibroblast cell states to serve as an orthogonal approach. Notably, we find selective enrichment of F2 and F9 fibroblasts within the infarct and border zones, respectively (**Fig. 3i**)."

Figure 3

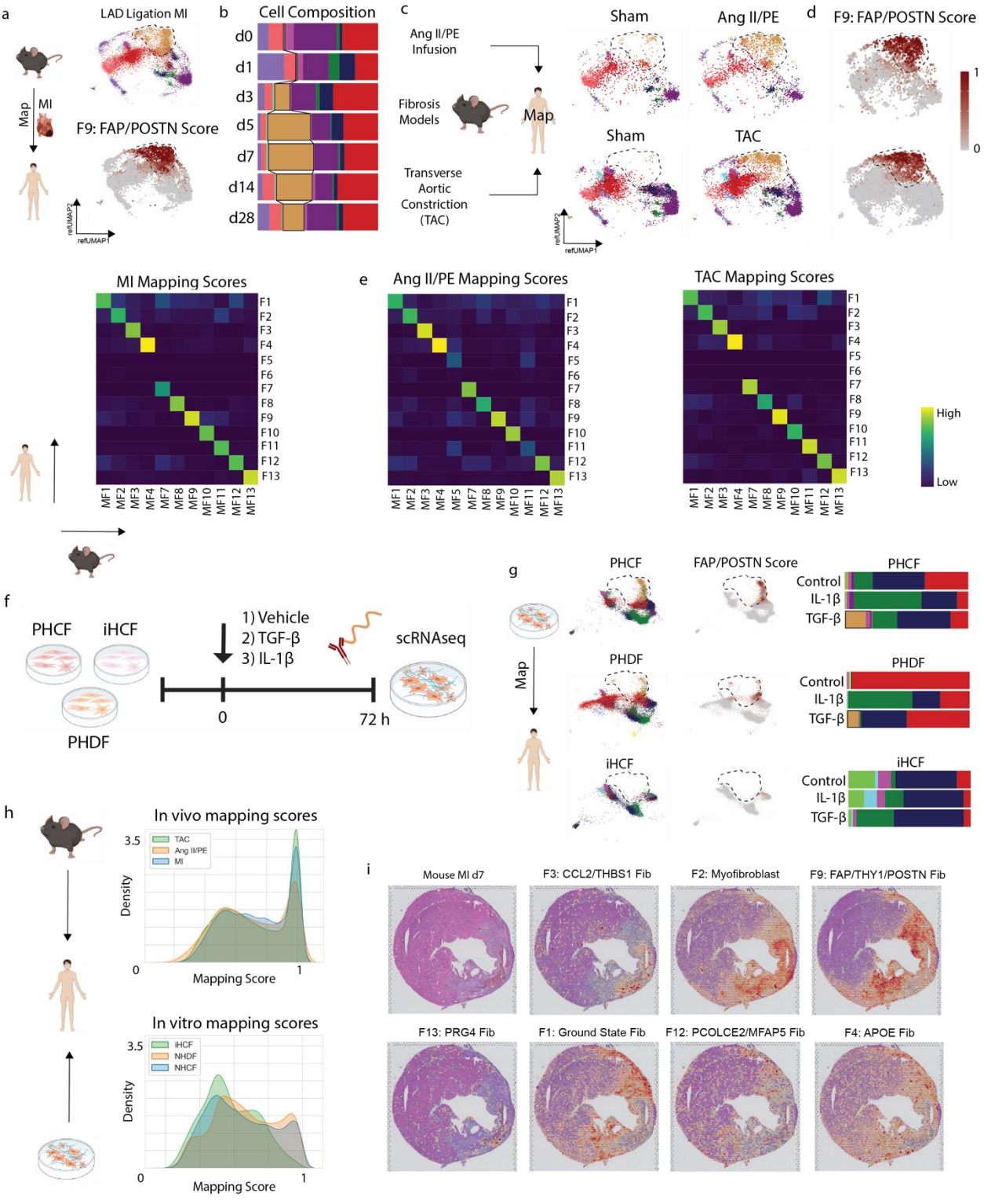
a
LAD Ligation MI
Map
MI
F9: FAP/POSTN Score
refUMAP2
refUMAP1
b
Cell Composition
d0
d1
d3
d5
d7
d14
d28
c
Ang II/PE Infusion
Fibrosis Models
Transverse Aortic Constriction (TAC)
Map
Sham
Ang II/PE
Sham
TAC
d
F9: FAP/POSTN Score
1
0
MI Mapping Scores
e
Ang II/PE Mapping Scores
TAC Mapping Scores
F1
F2
F3
F4
F5
F6
F7
F8
F9
F10
F11
F12
F13
MF1
MF2
MF3
MF4
MF5
MF7
MF8
MF9
MF10
MF11
MF12
MF13
High
Low
f
PHCF
iHCF
PHDF
1) Vehicle
2) TGF-β
3) IL-1β
0
72 h
scRNAseq
g
PHCF
FAP/POSTN Score
PHCF
Control
IL-1β
TGF-β
Map
PHDF
PHDF
iHCF
iHCF
h
In vivo mapping scores
TAC
Ang II/PE
MI
Density
3.5
0
1
Mapping Score
In vitro mapping scores
iHCF
NHDF
NHCF
i
Mouse MI d7
F3: CCL2/THBS1 Fib
F2: Myofibroblast
F9: FAP/THY1/POSTN Fib
F13: PRG4 Fib
F1: Ground State Fib
F12: PCOLCE2/MFAP5 Fib
F4: APOE Fib

To further address this issue, we have generated a novel inducible Cre mouse line to trace the lineage of FAP+ fibroblasts and performed additional in vivo lineage tracing experiments and computational analyses in a new main figure (Figure 4). We generated a $Fap^{creERT2}$ mice by knocking an inducible Cre recombinase into the endogenous FAP locus. We then generated $Fap^{CreERT2}Rosa26^{LSL\text{-}tdTomato}$ mice and performed in vivo fibroblast lineage tracing. These data are displayed in a new main figure (Figure 4).

Our human and mouse computational analyses predicted that FAP+ fibroblasts emerge early and may selectively contribute to Postn fibroblasts that are distinct from myofibroblasts. To test this hypothesis, $Fap^{CreERT2}Rosa26^{LSL\text{-}tdTomato}$ mice were subjected to the Ang II/PE injury model. Tamoxifen was given early after pump implantation (days 1-7, IP) at 60 mg/kg and mice were sacrificed at day 14 to characterize fibroblast lineages. We performed immunofluorescence and RNAscope in situ hybridization to stain for Postn (pro-fibrotic fibroblasts) and ACTA2 (myofibroblasts) and overlaid tdTomato signal (for Fap lineage labeled cells). We then specifically quantified cells within the myocardium interstitial areas that were $tdTomato^{+}Postn^{+}$ and $tdTomato^{+}Acta2^{+}$ and found that most $tdTomato^{+}$ cells expressed Postn but not Acta2. These results would suggest that FAP+ fibroblasts in cardiac injury predominantly contribute to the $Postn^{+}$ lineage but not the $Acta2^{+}$ myofibroblast lineage. We have created a new figure (Figure 4) integrating several orthogonal lines of evidence in human and mice using single cell RNA-sequencing, computational pseudotime trajectory analysis, multiomic RNA + ATAC sequencing, in vivo lineage tracing, and spatial transcriptomics to dissect cardiac fibroblast heterogeneity.

We have also added a separate section to the manuscript main text as follows:

"***Distinct lineages of activated cardiac fibroblasts.***

To map fibroblast trajectories in AMI and heart failure, we undertook two approaches. First, we used scVelo with dynamical modeling to infer directionality in fibroblast cell state differentiation. Projection of the velocity vector field in a force directed layout suggested convergence toward the F2, F4, and F9 fibroblast states (**Fig. 4a**). Next, we used Palantir to predict fibroblast differentiation endpoints, which also identified F2, F4, and F9 as possible terminal states with low entropy values across a range of simulation parameters (**Fig. 4b**). To glean how fibroblasts might evolve over the time course of disease, we plotted donor and diseased fibroblast signatures (**Supplementary Fig. 7f**) versus pseudotime along each predicted lineage (F2, F4, F9). The donor fibroblast signature was most enriched early in pseudotime, while the diseased signature increased over pseudotime in each lineage. *FAP* expression transiently increases along the F2 and F4 lineages and progressively increases along the F9 lineage. Notably, the markers of each population increase over pseudotime in a lineage specific manner (**Fig. 4c**). To dissect putative regulators of the different trajectories, we identified differentially expressed genes and used the resultant gene list to perform a transcription factor enrichment analysis. This approach identified *FBN1, PPRX, FOSX1*, and *MEOX1* as the top transcription factors driving the F9 lineage (**Fig. 4d**). *MEOX1 was previously implicated in cardiac fibrosis*[32]. We then used CellOracle to build a gene regulatory network of heart failure fibroblasts and identified enriched *RUNX1* connectivity across all 3 heart failure groups (**Fig. 4e**). Previously, we have shown that *RUNX1* expands in heart failure using RNAscope in situ hybridization in non-failing donors and heart failure myocardial samples interstitial cells[33]. Linear regression analysis of pseudobulk *RUNX1* and *POSTN* expression at the patient level shows a strong correlation (**Fig. 4f**). Gene expression density plots showed that *MEOX1* was co-expressed with *RUNX1* and *POSTN* along the F9 lineage while *ACTA2* expression was restricted to a different cell state (F2) (**Fig. 4g**). Furthermore, *RUNX1* and *MEOX1* increased along the F9 lineage but not the F2

or F4 lineages (**Fig. 4d**). Using PathwayNet we found that *POSTN* and *RUNX1* are predicted to be connected via a transcriptional regulation network (**Supplementary Figure. 7g**). We validated that these populations are indeed distinct using RNAscope and immunofluorescence for POSTN and ACTA2 respectively from human infarct zone samples (**Fig. 4h**). Additionally, mouse spatial transcriptomics data collected at day 7 post-MI, indicated that *Acta2* and *Postn* expressed in different spatial distributions. *Postn* is enriched within the border zone, whereas *Acta2* is localized to the core of the infarct (**Fig. 4i**). To lineage trace $FAP^+$ fibroblasts, we generated $Fap^{creERT2}Rosa26^{tdTomato}$ mice (**Supplementary Figure. 20**, detailed in methods) and performed Ang II/PE mini-pump implantation (**Fig. 4j**). Using FAPi non-invasive PET imaging, we confirmed early enrichment of FAP at d7 following AngII/PE infusion (**Fig. 4k**). Tamoxifen was administered to label $FAP^+$ fibroblasts on days 1-7 of Ang II/PE infusion and mice were sacrificed at day 14 (**Fig. 4j**). We then performed RNAscope in situ hybridization for *Postn* and immunofluorescence for ACTA2 and overlaid tdTomato signal (**Fig. 4l**). Quantification of $tdTomato^+Postn^+$ and $tdTomato^+ACTA2^+$ cells showed that $FAP^+$ cells contributed towards the Postn lineage and not the Acta2 myofibroblast lineage (**Fig. 4l**)."

Figure 4

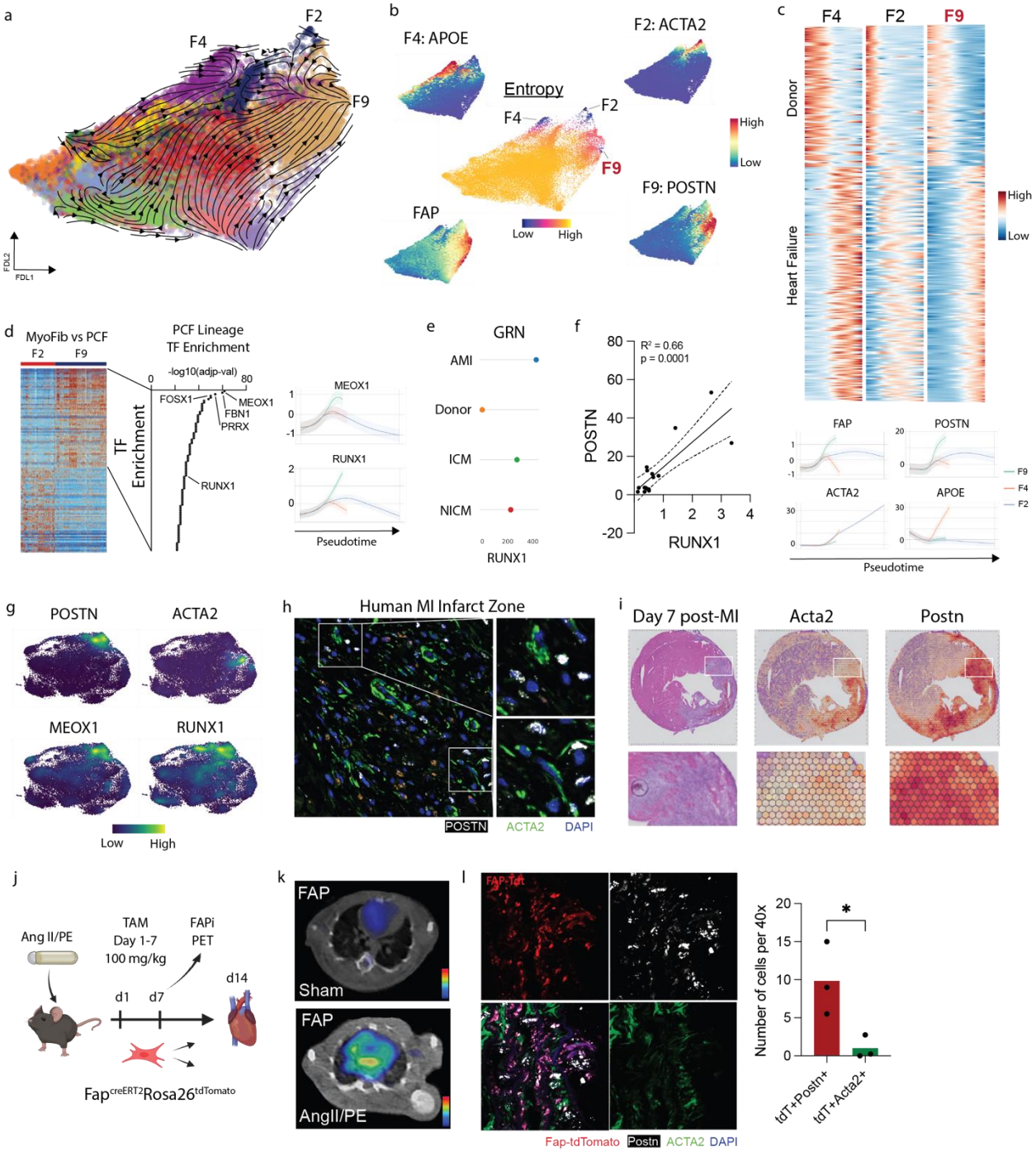
a
F2
F4
F9
FDL2
FDL1
b
F4: APOE
F2: ACTA2
Entropy
F4
F2
F9
High
Low
FAP
F9: POSTN
Low
High
c
F4
F2
F9
Donor
Heart Failure
High
Low
FAP
POSTN
ACTA2
APOE
F9
F4
F2
Pseudotime
d
MyoFib vs PCF
F2
F9
PCF Lineage
TF Enrichment
-log10(adjp-val)
0
80
FOSX1
MEOX1
FBN1
PRRX
RUNX1
TF Enrichment
MEOX1
RUNX1
Pseudotime
e
GRN
AMI
Donor
ICM
NICM
0
200
400
RUNX1
f
R² = 0.66
p = 0.0001
POSTN
RUNX1
g
POSTN
ACTA2
MEOX1
RUNX1
Low
High
h
Human MI Infarct Zone
POSTN
ACTA2
DAPI
i
Day 7 post-MI
Acta2
Postn
j
Ang II/PE
TAM
Day 1-7
100 mg/kg
FAPi
PET
d1
d7
d14
Fap^creERT2 Rosa26^tdTomato
k
FAP
Sham
FAP
AngII/PE
l
FAP-Tdt
Fap-tdTomato
Postn
ACTA2
DAPI
Number of cells per 40x
*
tdT+Postn+
tdT+Acta2+

Additionally, we have created a supplementary figure describing the construction of this new CRE, with the following addition to the methods section:

"**Gene Editing Design**
Analysis of genomic DNA sequence surrounding the target region, using the Benchling (www.benchling.com) guide RNA design tool, identified a gRNA sequence with a suitable target endonuclease site in *Fap* gene start site. Predicted off-target sites for the gRNA (crRNA2-AAGGTTAGTGCGTGCCGTCT) were identified using the specificity model developed and documented by Hsu and colleagues and embedded in the Benchling gRNA design tool. Design considerations for off-target editing were as follows. Higher off-target editing risk was considered when the "Score" is >2.0 with a canonical SpCas9 PAM (NGG), >50.0 with a chromosomally unlinked non-canonical PAM (NAG) or >20.0 with a linked non-canonical PAM yet in an annotated protein coding region. These "Score" thresholds were based on empirical targeted sequencing analysis of 20 different predicted off-target loci in 15 different mouse zygote gene editing experiments.

**Microinjection of gRNAs and plasmid donor DNA repair templates**
*Streptococcus pyogenes* Cas9 (SpCas9) V3 protein and gRNAs were purchased as part of the Alt-R CRISPR-Cas9 system using the crRNA:tracrRNA duplex format as the gRNA species (IDT, USA). Alt-R CRISPR-Cas9 crRNAs (Product# 1072532, IDT, USA) were synthesized using the gRNA sequences specified in the DESIGN section and hybridized with the Alt-R tracrRNA (Product# 1072534, IDT, USA) as per manufacturer's instructions. This gRNA duplex was used in all subsequent gene editing processes. The sequence of the double stranded DNA donor plasmid, that functions as the DNA repair template, was synthesized by Genscript. Features included asymmetric homology arm lengths of 1.6 kb and 2.0 kb, flanking the 2.2 kb insertion sequence. The final concentration of the gRNA, SpCas9 and donor components in the microinjection mixture was 50ng/ul, 100 ng/ul and 10 ng/ul, respectively. All animal work was approved by the Jackson Laboratory Animal Care and Use Committee and adhered to the standards of Guide for the Care and Use of Laboratory Animals set forth by the NIH. Microinjection was performed as described (PMID: 27210041) using C57BL/6J (Stock# 000664, The Jackson Laboratory, USA) donor female mice (3–4 weeks of age).

**Sequence characterization of Founder and N1 mice**
PCR primers flanking the gRNA target site, but outside the repair template homology arms, were used to amplify the region of interest from founder progeny. PCR amplicons were subjected to Sanger sequencing to identify founders with precise desired changes. Founders carrying desired mutations were bred with C57BL/6J mice (Stock #000664, The Jackson Laboratory, USA) to produce N1 progeny. N1 animals were confirmed by the same PCR-Sanger sequence analysis the founder population was subjected to. In contrast to founders, N1 animals are obligate heterozygotes, with one allele derived from an un-manipulated chromosome, enabling deconvolution of the two alleles in the mixed PCR amplicon. PCR primer sequences were as follows: Short Range PCR, Fap SR forward and Cre SR reverse; 5'-AGAACGCCCCCAAAATCTGT-3' and 5'- ATTCAACTTGCACCATGCCG-3', left homology arm PCR, Fap LHA forward and Cre SR reverse; 5'-GCTGATGGCTTTCTCTCGGA-3' and 5'-ATTCAACTTGCACCATGCCG-3', and right homology arm PCR, ERT RHA forward and Fap RHA reverse; 5'-CGGGCTCTACTTCATCGCAT-3' and 5'-CAGGTGACATGCTGAGGTGT-3'.
"

Supplementary Figure 20

a

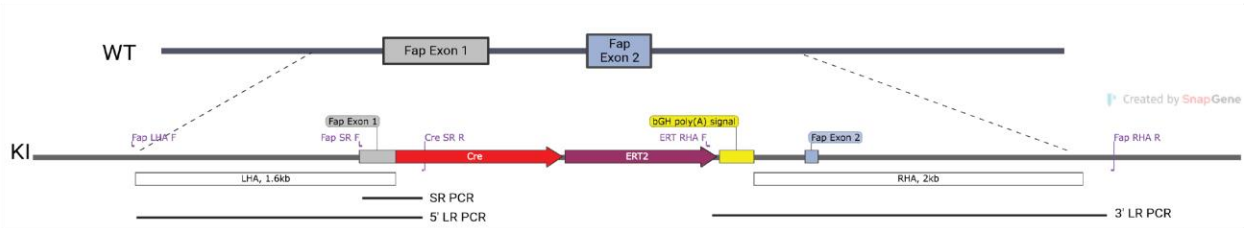


b


c

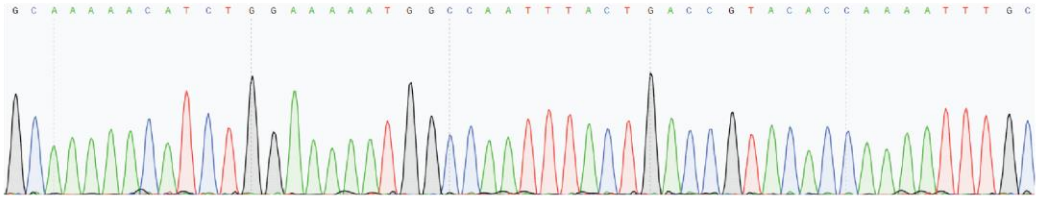

WT GCAAAAACATCTGGAAAAATGAAGGTTAGTGCGTGCCGTCTCGGGGACGACC
KI GCAAAAACATCTGGAAAAATGGCCAATTTACTGACCGTACACCAAAATTTGC
CRE M A N L L T V H Q N L

d

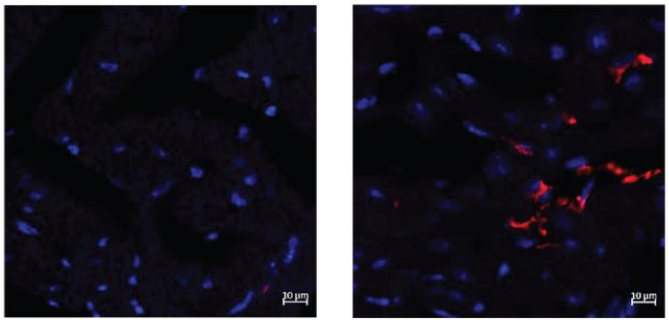

• The role of RUNX1 in the regulation of FAP+ pro-fibrotic fibroblast is predicted, not tested by any experimental approach. Sometimes, this is not clearly stated in the document like in lines 573-575: “We identify a macrophage subset in humans which signals to fibroblasts via IL-1 β and modulates fibroblast activation, lineage specification via a RUNX1 orchestrated gene regulatory network”.

We thank the reviewer for this comment. To clarify such discrepancies, we have amended the manuscript to highlight this as a computational prediction. “We identify a macrophage subset in humans which signals to fibroblasts via IL-1β and modulates fibroblast activation, lineage specification via predicted a *RUNX1* orchestrated gene regulatory network, and cardiac fibrosis.”

• About the expansion of myeloid cells and fibroblast mentioned in lines 184-187, there is not reference to any figure supporting this statement.

We thank the reviewer for pointing this out. We have referenced the appropriate figure panel. (**Fig. 1g**).

• In the second section of the Results, relative to “Expansion of pathologic fibroblast subsets in acute MI and chronic heart failure”, the authors categorize fibroblasts as perivascular or interstitial to justify their focus on the F9 subset because “Given the fibrosis associated transcriptional signature of F9 fibroblasts and their localization within the infarct and fibrotic regions of the myocardium” (226-228). However, this categorization is just based in few images of spatial transcriptomics, with no distance quantification and without showing any data on vessels localization for comparison (lanes 208-210 and 222-225, Supplementary Figure 4D).

To address this important comment, we have performed extensive additional analyses with the spatial transcriptomics data from human and mouse, and utilized coronary artery adventitial fibroblast scRNA-seq.

As the reviewer points out, the panels shown in Supplementary Fig. 4b – d are descriptive examples showing the F2 fibroblast cluster is enriched in locations adjacent to blood vessels whereas the F9 cluster is enriched within interstitial areas. To characterize the spatial localization of fibroblast cell states, we performed 3 orthogonal analyses: (1) fibroblast cell state co-localization analysis, (2) cell compartment correlation analysis between fibroblast cell sates and other major cell types, and (3) fibroblast cell state spatial localization with cell types using spatial distance. We have amended the main figure 2 and created a new Supplementary Figure 10 to reflect these analyses:

(1) We used the fibroblast cell state marker genes (Supplementary Figure 6) and created gene set scores for each fibroblast cell states in an integrated spatial transcriptomics dataset across 31 samples from 23 patients (14 control, 12 infarct zone, 3 border zone, 6 remote zone, and 6 fibrotic zone) from Supplementary Figure 9. To visualize how the fibroblast cell states vary by spatially, we constructed two heatmaps: one grouped by spatial niche (Supplementary Figure 10a) and the other grouped by sample region (Figure 2i). Our analysis showed that different fibroblast cell states were enriched across myocardial sampling locations with F2, F3, F4, F8, and F9 most enriched in the infarct zone and different populations enriched within the border and remote zone. Some fibroblast cell states like F1, F3, F4, and F12 were present across tissue areas. The heatmap of fibroblast cell state gene scores by spatial niche (Supplementary Figure 10

a) further highlighted that different fibroblast cell states are enriched across distinct spatial niches – as the reviewer importantly highlights not every fibroblast cell state is in a different location as some states share niches while others do not. These results are consistent with the transcriptional and spatial plasticity within human cardiac fibroblasts.

(2) To characterize spatial localization of fibroblast cell states in the context of other cell types, we performed an integrated cell compartment correlation analysis (CCCA) across all samples based on the probability of cells located in the same spatial spot (utilizing the spatial transcriptomics data and the single nucleus RNA-seq reference): we first did CCCA with fibroblast cell states and other cell types (Supplementary Figure 10b) and then CCCA with fibroblast cell states, myeloid cell states, and other cell types (Supplementary Figure 10c). The generated heatmaps highlight that distinct fibroblast cell states are spatially associated with different cell types. For instance, F2 is more spatially associated with VSMCs, endothelial cells, and pericytes while F9 is more associated with myeloid cells (Supplementary Figure 10b, c).

(3) Given the stronger localization of F2 with perivascular niches and F9 with interstitial fibrosis, we calculated a distance matrix based on spatial image coordinates and constructed a minimum spanning tree representing the spatial cellular proximity using the SColoc function within CellTrek toolkit. This analysis showed through an orthogonal approach (spatial distance) that F2 fibroblasts are associated with perivascular niches while F9 fibroblasts are more associated with macrophages and F4 fibroblasts (Supplementary Figure 10d).

An important limitation of current spatial transcriptomic techniques is limited resolution, thereby precluding single cell mapping. Furthermore, methods like Curio seeker offer higher resolution insights but lack the read depth. To obviate these limitations and to dissect perivascular (vascular, adventitial) fibroblasts from interstitial fibroblasts, we utilized human coronary artery single cell data – these vessels travel through the myocardium and are surrounded by adventitial and perivascular fibroblasts. We specifically selected out the fibroblast populations and reference mapped them to our human cardiac fibroblasts to address which populations are more perivascular: notably, we found that the F2 and F11 fibroblasts were most enriched in the adventitia, whereas F9 fibroblasts were largely absent (Figure 2j, k).

We have amended Figure 2 and created a new Supplementary Figure 10 highlighting these new analyses. We have also amended the methods section for experimental and computational analysis details and included these new findings in the results section as follows:

"To characterize the spatial localization of transcriptionally distinct fibroblast cell states, we built an integrated spatial transcriptomics dataset across 31 samples from 23 patients (14 control, 12 infarct zone, 3 border zone, 6 remote zone, and 6 fibrotic zone) (**Supplementary Fig. 9**) and performed 3 orthogonal analyses: (1) fibroblast cell state co-localization analysis: we created fibroblast cell state gene set scores and constructed heatmaps to characterize how different fibroblast cell states localize across myocardial regions and relative to each other. This analysis showed that different fibroblast cell states were enriched across myocardial sampling locations including the infarct zone (F2, F3, F4, F8, F9), border zone (F5, F6, F7, F10, F13), and remote zone (F11). Some fibroblast cell states (F1, F3, F4, F12) were present across tissue compartments. The heatmap of fibroblast cell state gene scores by spatial niche (**Fig. 2i**, **Supplementary Fig. 10a**) further highlighted that different fibroblast cell states are enriched across distinct spatial niches. (2) To characterize spatial localization of fibroblast cell states in the context of other cell types, we performed an integrated cell compartment correlation analysis (CCCA) across all samples based on the probability of cells located in the same spatial spot (utilizing the spatial transcriptomics data and the single nucleus RNA-seq reference). We

performed CCCA between fibroblast cell states and other major cell types (**Supplementary Fig. 10b**) as well as with myeloid cell states (**Supplementary Fig. 10c**). The generated heatmaps highlight that distinct fibroblast cell states partition into spatially restricted niches. For example, F2 fibroblasts localize with VSMCs, endothelial cells, and pericytes, while F9 fibroblasts localize with myeloid cells (**Supplementary Fig. 10b, c**). (3) Given the stronger localization of F2 fibroblasts with perivascular niches and F9 fibroblasts with interstitial fibrosis, we calculated a distance matrix based on spatial image coordinates and constructed a minimum spanning tree representing the spatial cellular proximity using the SColoc function within CellTrek toolkit. This analysis showed through an orthogonal approach (spatial distance) that F2 fibroblasts are associated with perivascular niches while F9 fibroblasts are more associated with immune cells and F4 fibroblasts (**Supplementary Fig. 10d**). To further dissect the precise cell states contributing to perivascular (vascular, adventitial) fibroblasts versus interstitial fibroblasts, we utilized human coronary artery single cell data[31]. These vessels travel through the myocardium and are surrounded by adventitial and perivascular fibroblasts. We reference mapped the fibroblast populations to our human cardiac fibroblasts to identify perivascular fibroblasts within our heart dataset. We found that the F2 and F11 fibroblasts were most enriched in the adventitia, whereas F9 fibroblasts were largely absent (**Fig. 2j, k**).”

Figure 2

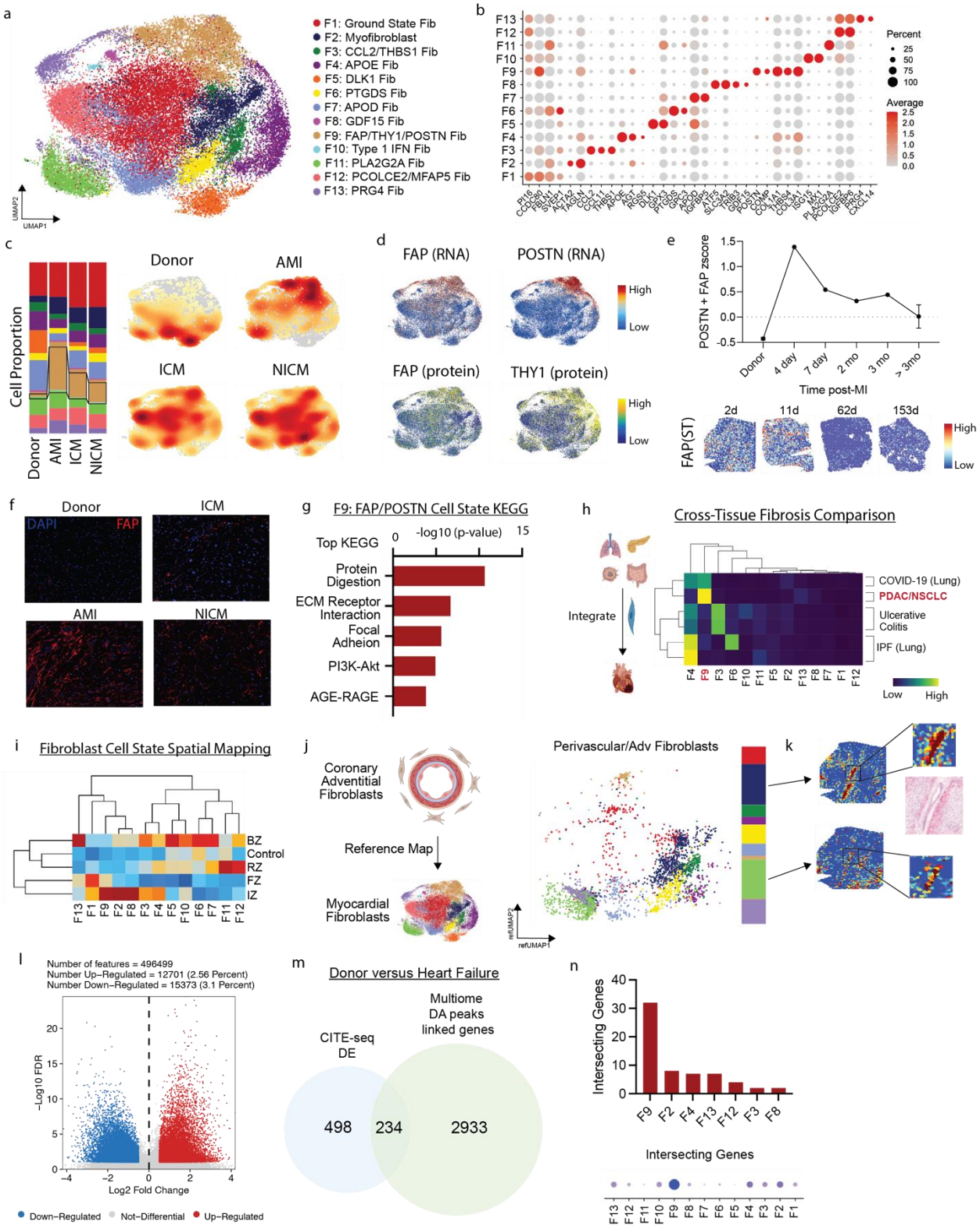
a
F1: Ground State Fib
F2: Myofibroblast
F3: CCL2/THBS1 Fib
F4: APOE Fib
F5: DLK1 Fib
F6: PTGDS Fib
F7: APOD Fib
F8: GDF15 Fib
F9: FAP/THY1/POSTN Fib
F10: Type 1 IFN Fib
F11: PLA2G2A Fib
F12: PCOLCE2/MFAP5 Fib
F13: PRG4 Fib
UMAP1
UMAP2
b
Percent
Average
c
Donor
AMI
ICM
NICM
Cell Proportion
d
FAP (RNA)
POSTN (RNA)
FAP (protein)
THY1 (protein)
High
Low
e
POSTN + FAP zscore
Donor
4 day
7 day
2 mo
3 mo
>3mo
Time post-MI
2d
11d
62d
153d
FAP(ST)
f
DAPI
FAP
g
F9: FAP/POSTN Cell State KEGG
Top KEGG
-log10 (p-value)
Protein Digestion
ECM Receptor Interaction
Focal Adheion
PI3K-Akt
AGE-RAGE
h
Cross-Tissue Fibrosis Comparison
Integrate
COVID-19 (Lung)
PDAC/NSCLC
Ulcerative Colitis
IPF (Lung)
Low
High
i
Fibroblast Cell State Spatial Mapping
BZ
Control
RZ
FZ
IZ
j
Coronary Adventitial Fibroblasts
Reference Map
Myocardial Fibroblasts
Perivascular/Adv Fibroblasts
k
l
Number of features = 496499
Number Up-Regulated = 12701 (2.56 Percent)
Number Down-Regulated = 15373 (3.1 Percent)
-Log10 FDR
Log2 Fold Change
Down-Regulated
Not-Differential
Up-Regulated
m
Donor versus Heart Failure
CITE-seq DE
Multiome DA peaks linked genes
498
234
2933
n
Intersecting Genes

Supplementary Figure 10

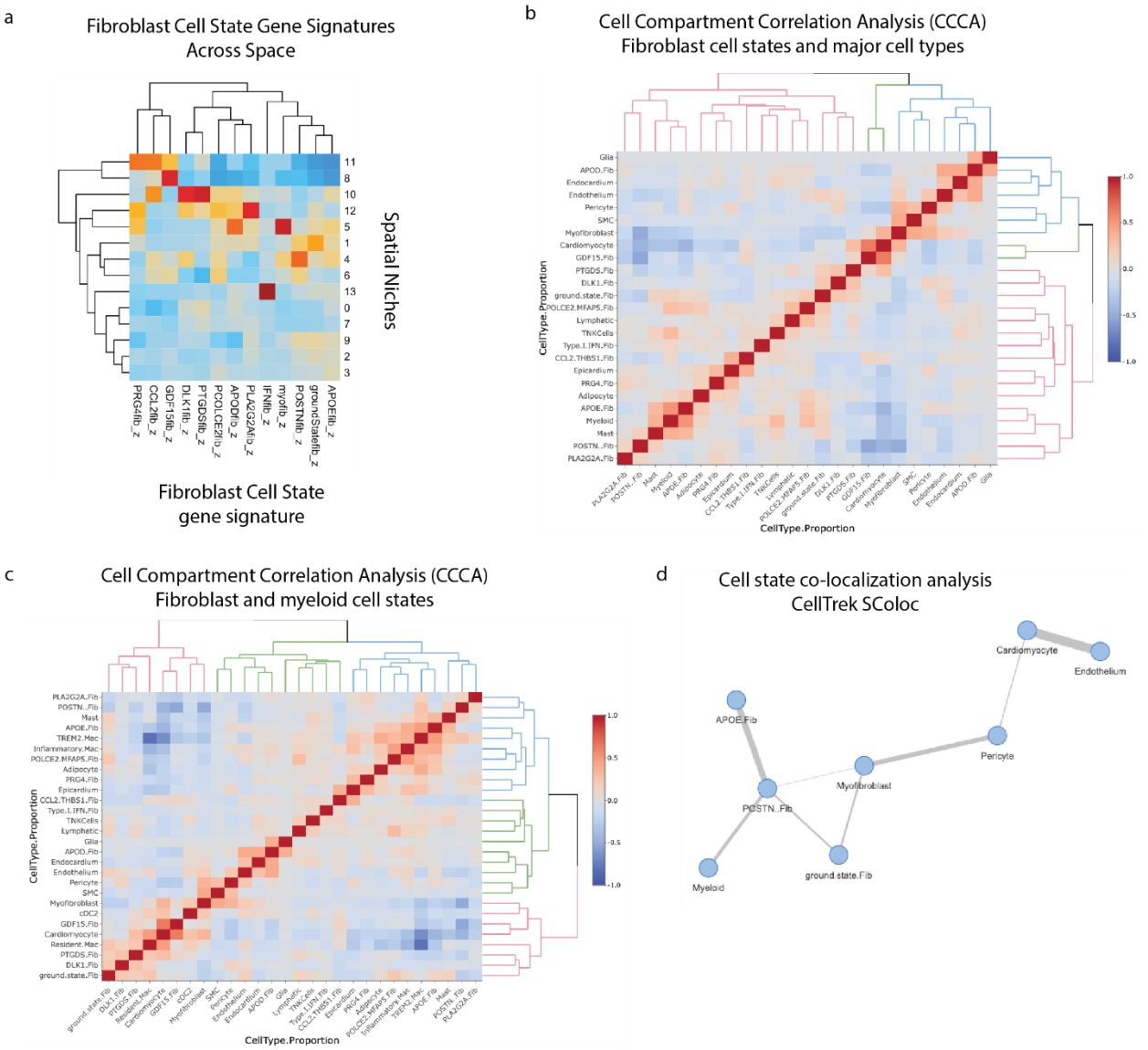

• In Figure 5, the effect of anti-IL1b treatment is moderate and substantial number of FAP+ fibroblasts still exist in AngII/PE group compared to Sham group. Are there other pathways that can activate fibroblasts? Or the effect of the antibody is not strong? Do Il1r f/f Dermo1-Cre mice show a strong reduction of FAP+ fibroblast population compared to the control mice group? Along this line, it´d be relevant to show whether treatment with anti-IL1b improves cardiac function, not only fibrosis as shown in Fig.4p.

We thank the reviewer for this important comment. It is certainly feasible for other pathways (TGF-β, SPP1) to activate fibroblasts. Additionally, neutralizing antibody treatment is imperfect, and does not fully suppress IL-1β signaling. To address the point the reviewer made "Do Il1r f/f Dermo1-Cre mice show a strong reduction of FAP+ fibroblast population compared to the control mice group?", we performed flow cytometry to characterize fibroblast activation at day 7 following Ang II/PE infusion in control and IL-1R$^{flox/flox}$Dermo1$^{Cre}$ mice as suggested by the reviewer and found that that IL-1R$^{flox/flox}$Dermo1$^{Cre}$ mice had fewer FAP+ fibroblast compared to control hearts. Additionally, we performed wheat germ agglutin (WGA) staining to quantify cardiomyocyte hypertrophy to dissect the impact of blocking IL-1 signaling to fibroblasts on neighboring cardiomyocytes. To reflect these additional experiments, we have modified Figure 5 as shown below. We have also added the following to the main text of the manuscript:

"To determine whether IL-1β signaling to fibroblasts is necessary for cardiac fibrosis, we generated mice that lack the IL-1 receptor (*IL-1R*) in fibroblasts (IL-1R$^{flox/flox}$Dermo1$^{Cre}$ mice[34]). Control and IL-1R$^{flox/flox}$Dermo1$^{Cre}$ mice underwent sham surgery or received Ang II/PE eluting osmotic minipumps (**Fig. 5l**). To validate knockdown of the *IL-1R*, we sorted macrophages fibroblasts from IL-1R$^{flox/flox}$ and IL-1R$^{flox/flox}$Dermo1$^{Cre}$ mice 7 days after Ang II/PE infusion (**Supplementary Fig. 26a**) – using qPCR on sorted cells, we verify decreased *IL-1R* expression in fibroblasts but not macrophages (**Supplementary Fig. 26b**). To characterize early fibroblast activation, mice were sacrificed after 7 days of Ang II/PE infusion and hearts enzymatically digested for flow cytometry. Quantification of flow cytometry data revealed an increase in the proportion of FAP$^{+}$ fibroblasts in Ang II/PE treated animals compared to sham surgeries. Importantly, there were fewer FAP$^{+}$ fibroblasts in IL-1R$^{flox/flox}$Dermo1$^{Cre}$ mice compared to control mice (**Fig. 5m**). Fibrosis was quantified after 4 weeks of AngII/PE infusion by trichrome staining. Ang II/PE infusion resulted in increased interstitial fibrosis in control mice compared to shams. Consistent with the conclusion that IL-1β signaling to fibroblasts promotes cardiac fibrosis, we observed reduced trichrome staining in Ang II/PE treated IL-1R$^{flox/flox}$Dermo1$^{Cre}$ mice compared to controls (**Fig. 5n**). Finally, we performed wheat germ agglutin (WGA) staining to quantify cardiomyocyte hypertrophy. We observed increased cardiomyocyte cross-sectional area in Ang II/PE treated controls compared to shams. However, there was a significant decrease in cardiomyocyte size in Ang II/PE treated IL-1R$^{flox/flox}$Dermo1$^{Cre}$ mice compared to controls (**Fig. 5o**). "

Figure 5

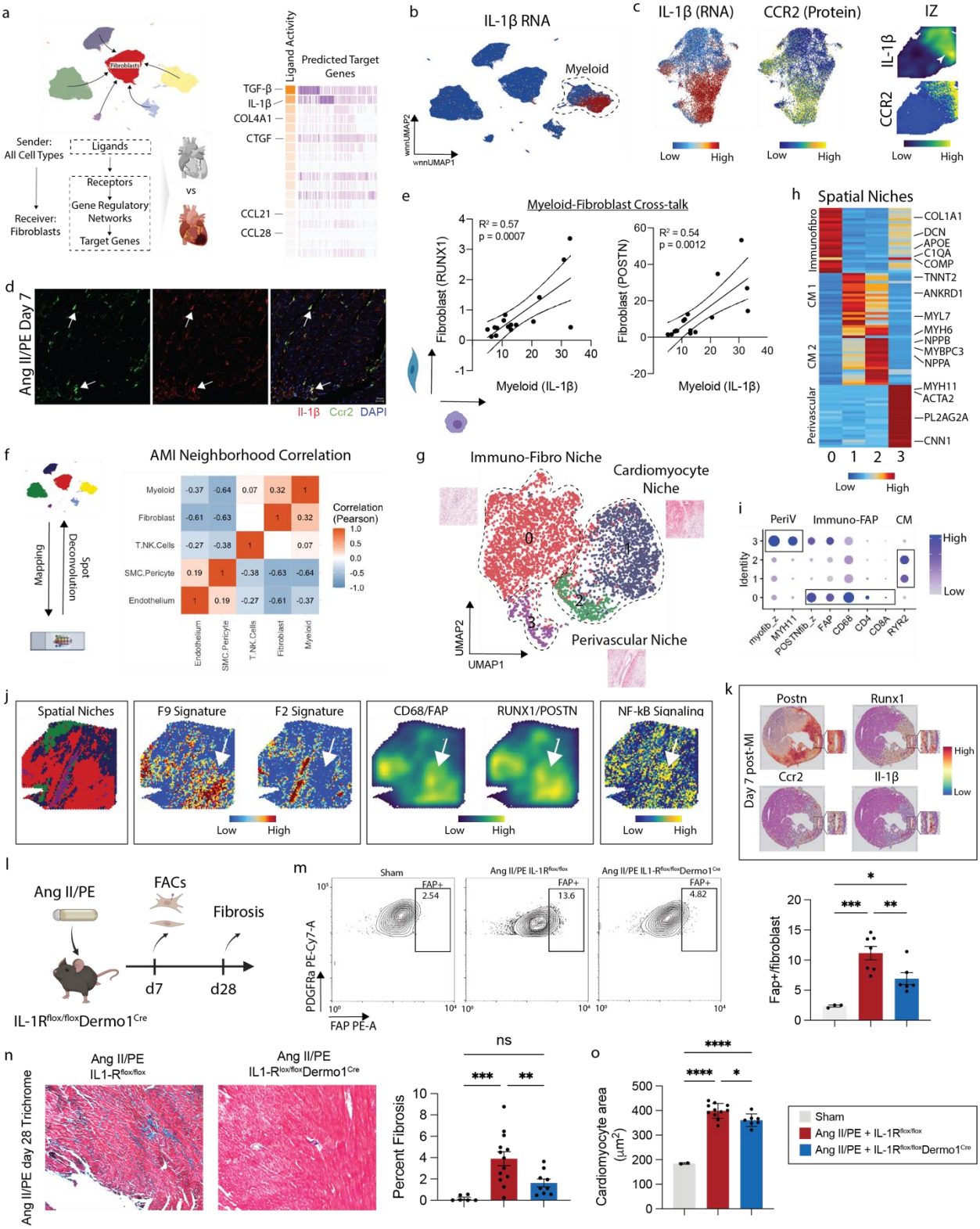
a
Fibroblasts
Sender: All Cell Types
Ligands
Receptors
Gene Regulatory Networks
Target Genes
Receiver: Fibroblasts
vs
Ligand Activity
Predicted Target Genes
TGF-β
IL-1β
COL4A1
CTGF
CCL21
CCL28
b
IL-1β RNA
Myeloid
wnnUMAP2
wnnUMAP1
c
IL-1β (RNA)
CCR2 (Protein)
IZ
IL-1β
CCR2
Low
High
d
Ang II/PE Day 7
Il-1β Ccr2 DAPI
e
Myeloid-Fibroblast Cross-talk
R² = 0.57
p = 0.0007
Fibroblast (RUNX1)
Myeloid (IL-1β)
R² = 0.54
p = 0.0012
Fibroblast (POSTN)
Myeloid (IL-1β)
h
Spatial Niches
Immunofibro
CM 1
CM 2
Perivascular
COL1A1
DCN
APOE
C1QA
COMP
TNNT2
ANKRD1
MYL7
MYH6
NPPB
MYBPC3
NPPA
MYH11
ACTA2
PL2AG2A
CNN1
0 1 2 3
Low
High
f
AMI Neighborhood Correlation
Mapping
Deconvolution
Spot
Myeloid
Fibroblast
T.NK.Cells
SMC.Pericyte
Endothelium
Correlation (Pearson)
g
Immuno-Fibro Niche
Cardiomyocyte Niche
Perivascular Niche
UMAP2
UMAP1
i
PeriV
Immuno-FAP
CM
Identity
myofib_z
MYH11
POSTNfib_z
FAP
CD68
CD4
CD8A
RYR2
High
Low
j
Spatial Niches
F9 Signature
F2 Signature
CD68/FAP
RUNX1/POSTN
NF-kB Signaling
Low
High
k
Postn
Runx1
Ccr2
Il-1β
Day 7 post-MI
High
Low
l
Ang II/PE
FACs
Fibrosis
d7
d28
IL-1R^flox/flox Dermo1^Cre
m
Sham
Ang II/PE IL-1R^flox/flox
Ang II/PE IL-1R^flox/flox Dermo1^Cre
FAP+
2.54
13.6
4.82
PDGFRa PE-Cy7-A
FAP PE-A
Fap+/fibroblast
n
Ang II/PE day 28 Trichrome
Ang II/PE IL1-R^flox/flox
Ang II/PE IL1-R^lox/lox Dermo1^Cre
ns
Percent Fibrosis
o
Cardiomyocyte area (μm²)
Sham
Ang II/PE + IL-1R^flox/flox
Ang II/PE + IL-1R^flox/flox Dermo1^Cre

To address the comment made by the reviewer “Along this line, it´d be relevant to show whether treatment with anti-IL1b improves cardiac function, not only fibrosis as shown in Fig.4p.”: To mechanistically investigate the impact of targeting IL-1β on cardiac function, we generated IL-1β $^{flox/flox}$ Ccr2$^{creERT2}$ mice to specifically knockout IL-1β in monocytes and monocyte derived macrophages. We focused specifically on CCR2 monocytes and macrophages because both the human and mouse data support that these are the dominant cell types which produce IL-1β in heart failure. We then performed Ang II/PE pump implantation with continuous tamoxifen dosing throughout the duration of the experiment and characterized early Fap activation at day 7 by flow cytometry, fibrosis, and systolic and diastolic function with echocardiography at 28 days post Ang II/PE pump implantation. Briefly, we found that the IL-1β $^{flox/flox}$ Ccr2$^{creERT2}$ mice had fewer FAP+ fibroblasts at day 7, decreased fibrosis, and improved systolic and diastolic function compared to IL-1β $^{flox/flox}$ mice. We have amended figure 6 and the main manuscript text to reflect these new experiments and additional analysis.

“***IL-1β derived from CCR2+ monocytes and macrophages is causally linked to fibrosis and diminished cardiac function.***
To determine whether IL-1β derived from CCR2$^{+}$ monocytes and macrophages is necessary for cardiac fibrosis, we generated mice that lack IL-1β in CCR$^{2+}$ monocytes and macrophages (IL-1β$^{flox/flox}$ Ccr2$^{creERT2}$). Control and IL-1β$^{flox/flox}$ Ccr2$^{creERT2}$ mice underwent sham surgery or received Ang II/PE eluting osmotic minipumps (**Fig. 6i**). To characterize early fibroblast activation, mice were sacrificed after 7 days of Ang II/PE infusion and hearts enzymatically digested for flow cytometry. Quantification of flow cytometry data revealed an increase in the proportion of FAP$^{+}$ fibroblasts in Ang II/PE treated animals compared to sham surgeries and importantly fewer FAP$^{+}$ fibroblasts in IL-1β$^{flox/flox}$ Ccr2$^{creERT2}$ mice compared to IL-1β$^{flox/flox}$ mice (**Fig. 6j**). Transthoracic echocardiography (TTE) was performed after 28 days of Ang II/PE infusion to characterize the impact of IL-1β deletion in CCR2+ cells on cardiac function. TTE showed a significant decrease in E/e’ and end systolic volume (ESV) with a significant improvement in fractional shortening (FS) an ejection fraction (EF) in IL-1β$^{flox/flox}$ Ccr2$^{creERT2}$ mice compared to IL-1β$^{flox/flox}$ mice (**Fig. 6k, l**). Fibrosis was quantified after 28 days of Ang II/PE infusion by trichrome staining. Ang II/PE infusion resulted in deminished interstitial fibrosis in IL-1β$^{flox/flox}$ Ccr2$^{creERT2}$ mice compared to IL-1β$^{flox/flox}$ mice (**Fig. 6m**).”

Figure 6

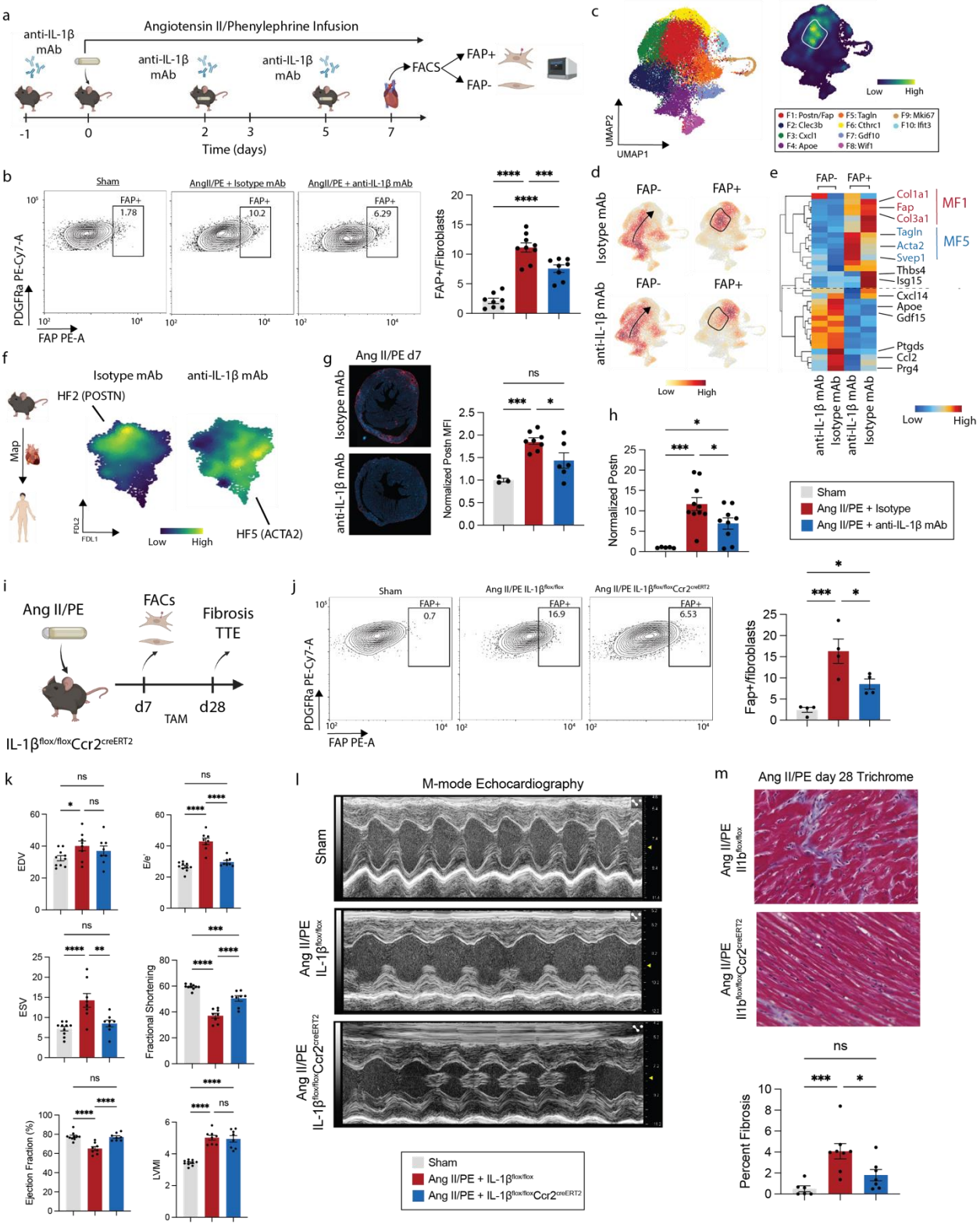
a
anti-IL-1β mAb
Angiotensin II/Phenylephrine Infusion
anti-IL-1β mAb
anti-IL-1β mAb
FACS
FAP+
FAP-
-1
0
2
3
5
7
Time (days)
b
Sham
AngII/PE + Isotype mAb
AngII/PE + anti-IL-1β mAb
FAP+ 1.78
FAP+ 10.2
FAP+ 6.29
PDGFRa PE-Cy7-A
FAP PE-A
FAP+/Fibroblasts
c
UMAP2
UMAP1
Low
High
F1: Postn/Fap
F2: Clec3b
F3: Cxcl1
F4: Apoe
F5: Tagln
F6: Cthrc1
F7: Gdf10
F8: Wif1
F9: Mki67
F10: Ifit3
d
FAP-
FAP+
Isotype mAb
anti-IL-1β mAb
Low
High
e
FAP-
FAP+
Col1a1
Fap
Col3a1
MF1
Tagln
Acta2
Svep1
MF5
Thbs4
Isg15
Cxcl14
Apoe
Gdf15
Ptgds
Ccl2
Prg4
anti-IL-1β mAb
Isotype mAb
anti-IL-1β mAb
Isotype mAb
Low
High
Sham
Ang II/PE + Isotype
Ang II/PE + anti-IL-1β mAb
f
Isotype mAb
anti-IL-1β mAb
HF2 (POSTN)
Map
FDL2
FDL1
Low
High
HF5 (ACTA2)
g
Ang II/PE d7
Isotype mAb
anti-IL-1β mAb
Normalized Postn MFI
h
Normalized Postn
i
Ang II/PE
FACs
Fibrosis
TTE
d7
TAM
d28
IL-1β^flox/flox Ccr2^creERT2
j
Sham
Ang II/PE IL-1β^flox/flox
Ang II/PE IL-1β^flox/flox Ccr2^creERT2
FAP+ 0.7
FAP+ 16.9
FAP+ 6.53
PDGFRa PE-Cy7-A
FAP PE-A
Fap+/fibroblasts
k
EDV
E/e'
ESV
Fractional Shortening
Ejection Fraction (%)
LVMI
l
M-mode Echocardiography
Sham
Ang II/PE IL-1β^flox/flox
Ang II/PE IL-1β^flox/flox Ccr2^creERT2
Sham
Ang II/PE + IL-1β^flox/flox
Ang II/PE + IL-1β^flox/flox Ccr2^creERT2
m
Ang II/PE day 28 Trichrome
Ang II/PE Il1b^flox/flox
Ang II/PE Il1b^flox/flox Ccr2^creERT2
Percent Fibrosis

• Fig4A: can the rationale and methodological approach behind the nichenet search explained better? which is the dataset used for this? which cell types are considered in this search? The call for TGFb and IL1b seem more of a biased call than an actual search.

We thank the reviewer for this comment. The goal of the ligand receptor analysis was to un-biasedly identify signaling between all cell types and fibroblasts enriched in heart failure versus the donor samples. We used NicheNet to predict ligand-receptor pairs that are both differentially expressed and active between heart failure and donor. The idea of using all cell type as senders and fibroblasts as receivers was to perform an un-biased screen of any cell type which may be signaling to and activating fibroblasts. From this analysis, ligand-receptor pairs were ranked based on ligand activity in any sender and receptor and downstream activity in the fibroblasts. TGF-β and IL-1β were among the top ranked ligands. To identify which cell type is expressing the IL-1 receptor and IL-1β ligand, we plotted these respective genes in the global UMAP (Figure 5, Supplementary Figure 28). We found IL-1R to be enriched within the fibroblasts and the IL-1β ligand was specific to CCR2 monocytes and macrophages. We have added the above to the methods section to better explain the approach. Additional details can be found on the official NicheNet paper (PMID 31819264). We have added the following to the methods section:

"We used nichenetr (v1.1.0) default pipeline to predict ligand-receptor pairs that are both differentially expressed and active between heart failure and donor. The idea of using all cell type as senders and fibroblasts as receivers was to perform an un-biased screen of any cell type which may be signaling to and activating fibroblasts. From this analysis, ligand-receptor pairs were ranked based on ligand activity in any sender and receptor and downstream activity in the fibroblasts. The regulatory potential from top 20 ligands on their predicted targets in fibroblasts was represented in a heatmap. To further capture the disease altered signaling from myeloid cells to fibroblasts, we extended the analysis to draw information from the differential expression of the ligand-receptor pairs across HF groups (HF vs healthy) by using the differential NicheNet pipeline. Circos plot was created to visualize the interaction between ligands from myeloid cells and receptors from fibroblast cells."

• Related to the above, Fig4i: the correlation between POSTN/RUNX1 with NFKB is interesting but again no specific for IL1b, is the cytokine actually expressed at these sites enriched in F9 fibroblasts? beyond in silico predictions, the paper generally lacks from direct validation e.g. by immunofluroesence, genetic models (reporters, loss of function), etc. to confirm predictions. For example, can the authors show that Il1b+ macrophages associate physically with Meox+ or Postn+ or FAP+ fibroblasts? This point is particularly relevant since it is clear that F9 fibroblasts are predicted to be in large areas of the myocardium (Fig.S16), so it's unclear the specificity and resolution of the transcriptional profiling performed by spatial seq.

We thank the reviewer for this very important point. The current generation of spatial transcriptomics tools used in this manuscript are from the Visium platform which has a limited resolution of 55 μm making it challenging to acquire single cell level resolution. To show that IL-1$\beta$ is co-expressed within areas of high Postn, Ccr2, and Runx1 we leveraged mouse MI spatial data and have added this additional analysis in Figure 5k.

• The production of Il1b by macrophages as causal to fibroblast reprogramming and fibrosis is predicted, not demonstrated. It would be necessary to genetically disrupt Il1b expression specifically by macrophages.

We thank the reviewer for the comment. To mechanistically investigate the impact of targeting IL-1β on cardiac function, we generated IL-1β$^{flox/flox}$ Ccr2$^{creERT2}$ mice to specifically knockout IL-1β in CCR2+ monocytes and monocyte-derived macrophages. We focused specifically on CCR2+ monocytes and macrophages because both the human and mouse data support that these are the dominant cell types which express IL-1β in heart failure. We implanted Ang II/PE pumps into control and IL-1β$^{flox/flox}$ Ccr2$^{creERT2}$ mice and treated these mice with continuous tamoxifen dosing throughout the duration of the experiment. We characterized FAP expression at day 7 by flow cytometry. Fibrosis was measured and echocardiography was performed at day 28 post Ang II/PE pump implantation. Briefly, we found that deletion of IL-1b from CCR2+ monocytes and monocyte-derived macrophages resulted in reduced abundance of FAP+ fibroblasts at day 7, decreased fibrosis at day 28, and improved systolic function compared to control mice. We have amended figure 6 and the main manuscript text to reflect these new experiments and additional analyses.

We have also added a description of these experiments to the manuscript main text as follows:

"***IL-1β derived from CCR2+ monocytes and macrophages is causally linked to fibrosis and diminished cardiac function.***
To determine whether IL-1β derived from CCR2$^{+}$ monocytes and macrophages is necessary for cardiac fibrosis, we generated mice that lack IL-1β in CCR$^{2+}$ monocytes and macrophages (IL-1β$^{flox/flox}$ Ccr2$^{creERT2}$). Control and IL-1β$^{flox/flox}$ Ccr2$^{creERT2}$ mice underwent sham surgery or received Ang II/PE eluting osmotic minipumps (**Fig. 6i**). To characterize early fibroblast activation, mice were sacrificed after 7 days of Ang II/PE infusion and hearts enzymatically digested for flow cytometry. Quantification of flow cytometry data revealed an increase in the proportion of FAP$^{+}$ fibroblasts in Ang II/PE treated animals compared to sham surgeries and importantly fewer FAP$^{+}$ fibroblasts in IL-1β$^{flox/flox}$ Ccr2$^{creERT2}$ mice compared to IL-1β$^{flox/flox}$ mice (**Fig. 6j**). Transthoracic echocardiography (TTE) was performed after 28 days of Ang II/PE infusion to characterize the impact of IL-1β deletion in CCR2+ cells on cardiac function. TTE showed a significant decrease in E/e' and end systolic volume (ESV) with a significant improvement in fractional shortening (FS) an ejection fraction (EF) in IL-1β$^{flox/flox}$ Ccr2$^{creERT2}$ mice compared to IL-1β$^{flox/flox}$ mice (**Fig. 6k, l**). Fibrosis was quantified after 28 days of Ang II/PE infusion by trichrome staining. Ang II/PE infusion resulted in deminished interstitial fibrosis in IL-1β$^{flox/flox}$ Ccr2$^{creERT2}$ mice compared to IL-1β$^{flox/flox}$ mice (**Fig. 6m**)."

Figure 6

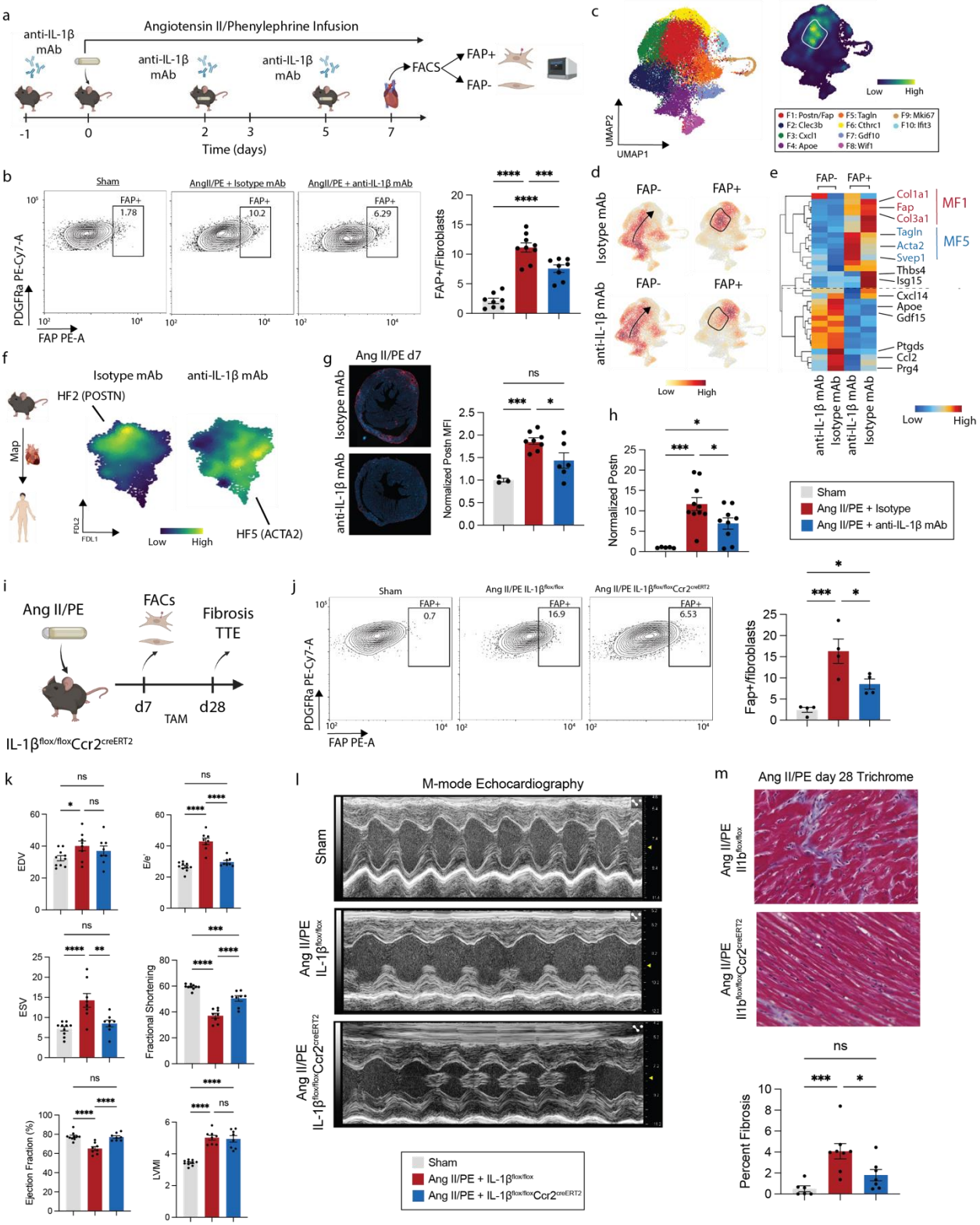
a
anti-IL-1β mAb
Angiotensin II/Phenylephrine Infusion
anti-IL-1β mAb
anti-IL-1β mAb
FACS
FAP+
FAP-
-1
0
2
3
5
7
Time (days)
b
Sham
AngII/PE + Isotype mAb
AngII/PE + anti-IL-1β mAb
FAP+ 1.78
FAP+ 10.2
FAP+ 6.29
PDGFRa PE-Cy7-A
FAP PE-A
FAP+/Fibroblasts
c
UMAP2
UMAP1
Low
High
F1: Postn/Fap
F2: Clec3b
F3: Cxcl1
F4: Apoe
F5: Tagln
F6: Cthrc1
F7: Gdf10
F8: Wif1
F9: Mki67
F10: Ifit3
d
FAP-
FAP+
Isotype mAb
anti-IL-1β mAb
Low
High
e
FAP-
FAP+
Col1a1
Fap
Col3a1
MF1
Tagln
Acta2
Svep1
MF5
Thbs4
Isg15
Cxcl14
Apoe
Gdf15
Ptgds
Ccl2
Prg4
anti-IL-1β mAb
Isotype mAb
anti-IL-1β mAb
Isotype mAb
Low
High
Sham
Ang II/PE + Isotype
Ang II/PE + anti-IL-1β mAb
f
Isotype mAb
anti-IL-1β mAb
HF2 (POSTN)
Map
FDL2
FDL1
Low
High
HF5 (ACTA2)
g
Ang II/PE d7
Isotype mAb
anti-IL-1β mAb
Normalized Postn MFI
h
Normalized Postn
i
Ang II/PE
FACs
Fibrosis
TTE
d7
TAM
d28
IL-1β^flox/flox Ccr2^creERT2
j
Sham
Ang II/PE IL-1β^flox/flox
Ang II/PE IL-1β^flox/flox Ccr2^creERT2
FAP+ 0.7
FAP+ 16.9
FAP+ 6.53
PDGFRa PE-Cy7-A
FAP PE-A
Fap+/fibroblasts
k
EDV
E/e'
ESV
Fractional Shortening
Ejection Fraction (%)
LVMI
l
M-mode Echocardiography
Sham
Ang II/PE IL-1β^flox/flox
Ang II/PE IL-1β^flox/flox Ccr2^creERT2
Sham
Ang II/PE + IL-1β^flox/flox
Ang II/PE + IL-1β^flox/flox Ccr2^creERT2
m
Ang II/PE day 28 Trichrome
Ang II/PE Il1b^flox/flox
Ang II/PE Il1b^flox/flox Ccr2^creERT2
Percent Fibrosis

• Fig4A: can the rationale and methodological approach behind the nichenet search explained better? which is the dataset used for this? which cell types are considered in this search? The call for TGFb and IL1b seem more of a biased call than an actual search.

We thank the reviewer for this comment. The goal of the nichenet search analysis was to un-biasedly identify ligand-receptor pairs whose interaction is enriched in heart failure relative to donor specifically using fibroblasts as the receivers and all cell types as the senders to allow for an un-biased screen. From this analysis, ligand-receptor pairs were ranked based on ligand activity in any sender cell type and receptor and downstream activity in the fibroblasts. Using this approach, IL-1β and TGF-β were the top hits. To identify which cell types are expressing IL-1β, we plotted this gene in the global UMAP and identified CCR2 monocytes and macrophages as the dominant source (Fig. 5b, c). Additionally, we also plotted the expression of IL-1R which was enriched within endocardium, fibroblasts, and a subset of endothelial cells. Within fibroblasts, IL-1R was highest in the POSTN population (Supplementary Figure 28). To better clarify the NicheNet framework, we have amended the methods section to read below. Additional details of this method can be found in the original paper describing the algorithm (PMID 31819264).

"We used nichenetr (v1.1.0) default pipeline to predict ligand-receptor pairs that are both differentially expressed and active between heart failure and donor. The rationale for using all cell type as senders and fibroblasts as receivers was to perform an un-biased screen of any cell type which may be signaling to and activating fibroblasts. From this analysis, ligand-receptor pairs were ranked based on ligand activity in any sender and receptor and downstream activity in the fibroblasts. The regulatory potential from top 20 ligands on their predicted targets in fibroblasts was represented in a heatmap. To further capture the disease altered signaling from myeloid cells to fibroblasts, we extended the analysis to draw information from the differential expression of the ligand-receptor pairs across HF groups (HF vs healthy) by using the differential NicheNet pipeline. Circos plot was created to visualize the interaction between ligands from myeloid cells and receptors from fibroblast cells."

• Fig.5B: the cytometry plots reveal a continuum of fibroblasts in FAP expression, unlike what one would expect, and the minor shifts are interpreted as IL1b regulating "fibroblast specification". This unclear separation was then used to sort FAPpos vs FAPneg cells for scRNAseq. It is unclear to me why this approach was followed rather than direct sequencing of all fibroblasts in the anti-IL1b treated and untreated groups to build a fibroblast map with all states.

We thank the reviewer for this comment. To validate the gating procedure, we used a negative control with no FAP antibody to set our gates (Supplementary Figure 18). We agree that FACS did not reveal two distinct populations and instead showed a continuum. These data are consistent with the concept that FAP expression increases during cardiac fibroblast differentiation (Fig 2c). It is important to note, that while separate FAP- and FAP+ fibroblast libraries were generated, all fibroblasts were sequenced and analyzed together. Sequencing revealed that the sorted FAP+ and FAP- populations are indeed transcriptionally different. As an internal validation, the FAP+ population expressed markedly higher levels of Fap mRNA than the FAP- population (Fig. 6c-e).

• Minor:
• The predictions shown in Fig.5k-l merging mouse and human data are shallow and only predictive and not quantified in any way. More conclusive experiments in the mouse during actual transcriptomics of the compared groups would be needed to make a relevant point.

We thank the reviewer for the comment. To validate this prediction, we carried out a genetic deletion of IL-1β in monocytes and macrophages to more conclusively test the effect of targeting IL-1$\beta$ in vivo. To mechanistically investigate the impact of targeting IL-1β on cardiac function, we generated IL-1β $^{flox/flox}$ Ccr2$^{creERT2}$ mice to specifically knockout IL-1β in CCR2+ monocytes and monocyte derived macrophages. We focused specifically on CCR2 monocytes and macrophages because both the human and mouse data support that these are the dominant cell types which produce IL-1β in heart failure. We then performed Ang II/PE pump implantation with continuous tamoxifen dosing throughout the duration of the experiment and measured Fap expression at day 7 by flow cytometry. We also measured fibrosis and systolic and diastolic function with echocardiography at 28 days post Ang II/PE pump implantation. Briefly, we found that the IL-1β $^{flox/flox}$ Ccr2$^{creERT2}$ mice had fewer FAP+ fibroblasts at day 7, decreased fibrosis, and improved systolic and diastolic function compared to controls. We have amended figure 6 and the main manuscript text to reflect these new experiments and additional analysis.

• page 6: there is no defined perivascular or interstitial spatial niches that I can tell in Fig.S4. How are these discriminated or described?

To address this important comment, we have performed extensive additional analyses with the spatial transcriptomics data from human and mouse, and utilized coronary artery adventitial fibroblast scRNA-seq.

As the reviewer points out, the panels shown in Supplementary Fig. 4b – d are descriptive examples showing the F2 fibroblast cluster is enriched in locations adjacent to blood vessels whereas the F9 cluster is enriched within interstitial areas. To characterize the spatial localization of fibroblast cell states, we performed 3 orthogonal analyses: (1) fibroblast cell state co-localization analysis, (2) cell compartment correlation analysis between fibroblast cell sates and other major cell types, and (3) fibroblast cell state spatial localization with cell types using spatial distance. We have amended the main figure 2 and created a new Supplementary Figure 10 to reflect these analyses:

(1) We used the fibroblast cell state marker genes (Supplementary Figure 3) and created gene set scores for each fibroblast cell states in an integrated spatial transcriptomics dataset across 31 samples from 23 patients (14 control, 12 infarct zone, 3 border zone, 6 remote zone, and 6 fibrotic zone) from Supplementary Figure 16. To visualize how the fibroblast cell states vary spatially, we constructed two heatmaps: one grouped by spatial niche (Supplementary Figure 210a) and the other grouped by sample region (Figure 2i). Our analysis showed that different fibroblast cell states were enriched across myocardial sampling locations with F2, F3, F4, F8, and F9 most enriched in the infarct zone and different populations enriched within the border and remote zone. Some fibroblast cell states like F1, F3, F4, and F12 were present across tissue areas. The heatmap of fibroblast cell state gene scores by spatial niche (Supplementary Figure 10a) further highlighted that different fibroblast cell states are enriched across distinct spatial niches – as the reviewer importantly highlights not every fibroblast cell state is in a different location as some states share niches while others do not. These results are consistent with the transcriptional and spatial plasticity within human cardiac fibroblasts.

(2) To characterize spatial localization of fibroblast cell states in the context of other cell types, we performed an integrated cell compartment correlation analysis (CCCA) across all samples based on the probability of cells located in the same spatial spot (utilizing the spatial transcriptomics data and the single nucleus RNA-seq reference): we first did CCCA with fibroblast cell states and other cell types (Supplementary Figure 10b) and then CCCA with fibroblast cell states, myeloid cell states, and other cell types (Supplementary Figure 10c). The generated heatmaps highlight that distinct fibroblast cell states are spatially associated with different cell types. For instance, F2 is more spatially associated with VSMCs, endothelial cells, and pericytes while F9 is more associated with myeloid cells (Supplementary Figure 10b, c).
(3) Given the stronger localization of F2 with perivascular niches and F9 with interstitial fibrosis, we calculated a distance matrix based on spatial image coordinates and constructed a minimum spanning tree representing the spatial cellular proximity using the SColoc function within CellTrek toolkit. This analysis showed through an orthogonal approach (spatial distance) that F2 fibroblasts are associated with perivascular niches while F9 fibroblasts are more associated with macrophages and F4 fibroblasts (Supplementary Figure 10d).

An important limitation of current spatial transcriptomic techniques is limited resolution, thereby precluding single cell mapping. Furthermore, methods like Curio seeker offer higher resolution insights but lack the read depth. To obviate these limitations and to dissect perivascular (vascular, adventitial) fibroblasts from interstitial fibroblasts, we utilized human coronary artery single cell data – these vessels travel through the myocardium and are surrounded by adventitial and perivascular fibroblasts. We specifically selected out the fibroblast populations and reference mapped them to our human cardiac fibroblasts to address which populations are more perivascular: notably, we found that the F2 and F11 fibroblasts were most enriched in the adventitia, whereas F9 fibroblasts were largely absent (Figure 2j, k).

We have amended Figure 2 and created a new Supplementary Figure 10 highlighting these new analyses. We have also amended the methods section for experimental and computational analysis details and included these new findings in the results section as follows:

“To characterize the spatial localization of transcriptionally distinct fibroblast cell states, we built an integrated spatial transcriptomics dataset across 31 samples from 23 patients (14 control, 12 infarct zone, 3 border zone, 6 remote zone, and 6 fibrotic zone) (**Supplementary Fig. 9**) and performed 3 orthogonal analyses: (1) fibroblast cell state co-localization analysis: we created fibroblast cell state gene set scores and constructed heatmaps to characterize how different fibroblast cell states localize across myocardial regions and relative to each other. This analysis showed that different fibroblast cell states were enriched across myocardial sampling locations including the infarct zone (F2, F3, F4, F8, F9), border zone (F5, F6, F7, F10, F13), and remote zone (F11). Some fibroblast cell states (F1, F3, F4, F12) were present across tissue compartments. The heatmap of fibroblast cell state gene scores by spatial niche (**Fig. 2i**, **Supplementary Fig. 10a**) further highlighted that different fibroblast cell states are enriched across distinct spatial niches. (2) To characterize spatial localization of fibroblast cell states in the context of other cell types, we performed an integrated cell compartment correlation analysis (CCCA) across all samples based on the probability of cells located in the same spatial spot (utilizing the spatial transcriptomics data and the single nucleus RNA-seq reference). We performed CCCA between fibroblast cell states and other major cell types (**Supplementary Fig. 10b**) as well as with myeloid cell states (**Supplementary Fig. 10c**). The generated heatmaps highlight that distinct fibroblast cell states partition into spatially restricted niches. For example, F2 fibroblasts localize with VSMCs, endothelial cells, and pericytes, while F9 fibroblasts localize

with myeloid cells (**Supplementary Fig. 10b, c**). (3) Given the stronger localization of F2 fibroblasts with perivascular niches and F9 fibroblasts with interstitial fibrosis, we calculated a distance matrix based on spatial image coordinates and constructed a minimum spanning tree representing the spatial cellular proximity using the SColoc function within CellTrek toolkit. This analysis showed through an orthogonal approach (spatial distance) that F2 fibroblasts are associated with perivascular niches while F9 fibroblasts are more associated with immune cells and F4 fibroblasts (**Supplementary Fig. 10d**). To further dissect the precise cell states contributing to perivascular (vascular, adventitial) fibroblasts versus interstitial fibroblasts, we utilized human coronary artery single cell data[31]. These vessels travel through the myocardium and are surrounded by adventitial and perivascular fibroblasts. We reference mapped the fibroblast populations to our human cardiac fibroblasts to identify perivascular fibroblasts within our heart dataset. We found that the F2 and F11 fibroblasts were most enriched in the adventitia, whereas F9 fibroblasts were largely absent (**Fig. 2j, k**).”

Figure 2

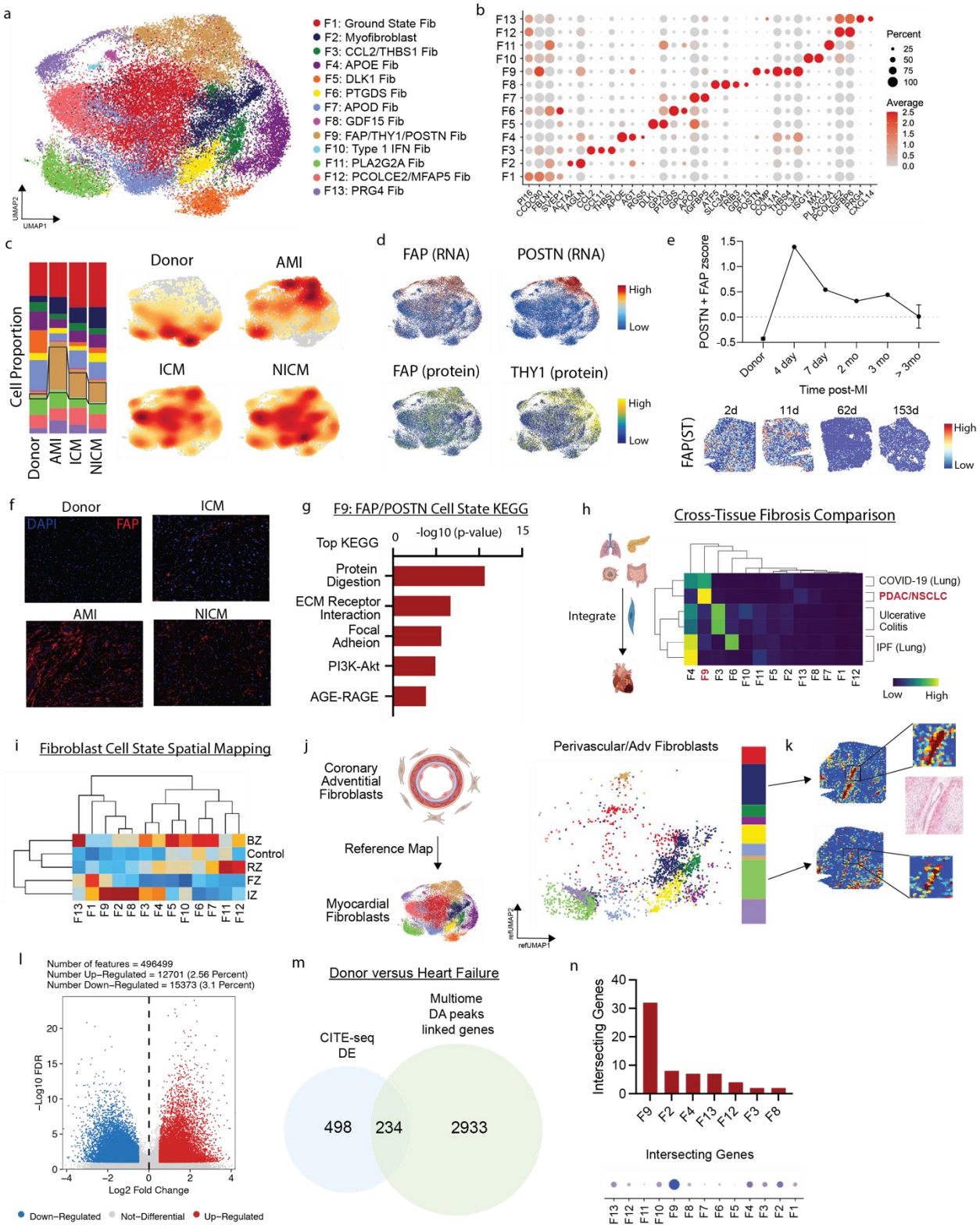
a
F1: Ground State Fib
F2: Myofibroblast
F3: CCL2/THBS1 Fib
F4: APOE Fib
F5: DLK1 Fib
F6: PTGDS Fib
F7: APOD Fib
F8: GDF15 Fib
F9: FAP/THY1/POSTN Fib
F10: Type 1 IFN Fib
F11: PLA2G2A Fib
F12: PCOLCE2/MFAP5 Fib
F13: PRG4 Fib
UMAP1
UMAP2
b
Percent
Average
c
Donor
AMI
ICM
NICM
Cell Proportion
d
FAP (RNA)
POSTN (RNA)
FAP (protein)
THY1 (protein)
High
Low
e
POSTN + FAP zscore
Donor
4 day
7 day
2 mo
3 mo
>3mo
Time post-MI
2d
11d
62d
153d
FAP(ST)
f
DAPI
FAP
g
F9: FAP/POSTN Cell State KEGG
Top KEGG
-log10 (p-value)
Protein Digestion
ECM Receptor Interaction
Focal Adheion
PI3K-Akt
AGE-RAGE
h
Cross-Tissue Fibrosis Comparison
Integrate
COVID-19 (Lung)
PDAC/NSCLC
Ulcerative Colitis
IPF (Lung)
Low
High
i
Fibroblast Cell State Spatial Mapping
BZ
Control
RZ
FZ
IZ
j
Coronary Adventitial Fibroblasts
Reference Map
Myocardial Fibroblasts
Perivascular/Adv Fibroblasts
k
l
Number of features = 496499
Number Up-Regulated = 12701 (2.56 Percent)
Number Down-Regulated = 15373 (3.1 Percent)
-Log10 FDR
Log2 Fold Change
Down-Regulated
Not-Differential
Up-Regulated
m
Donor versus Heart Failure
Multiome DA peaks linked genes
CITE-seq DE
498
234
2933
n
Intersecting Genes

Supplementary Figure 10

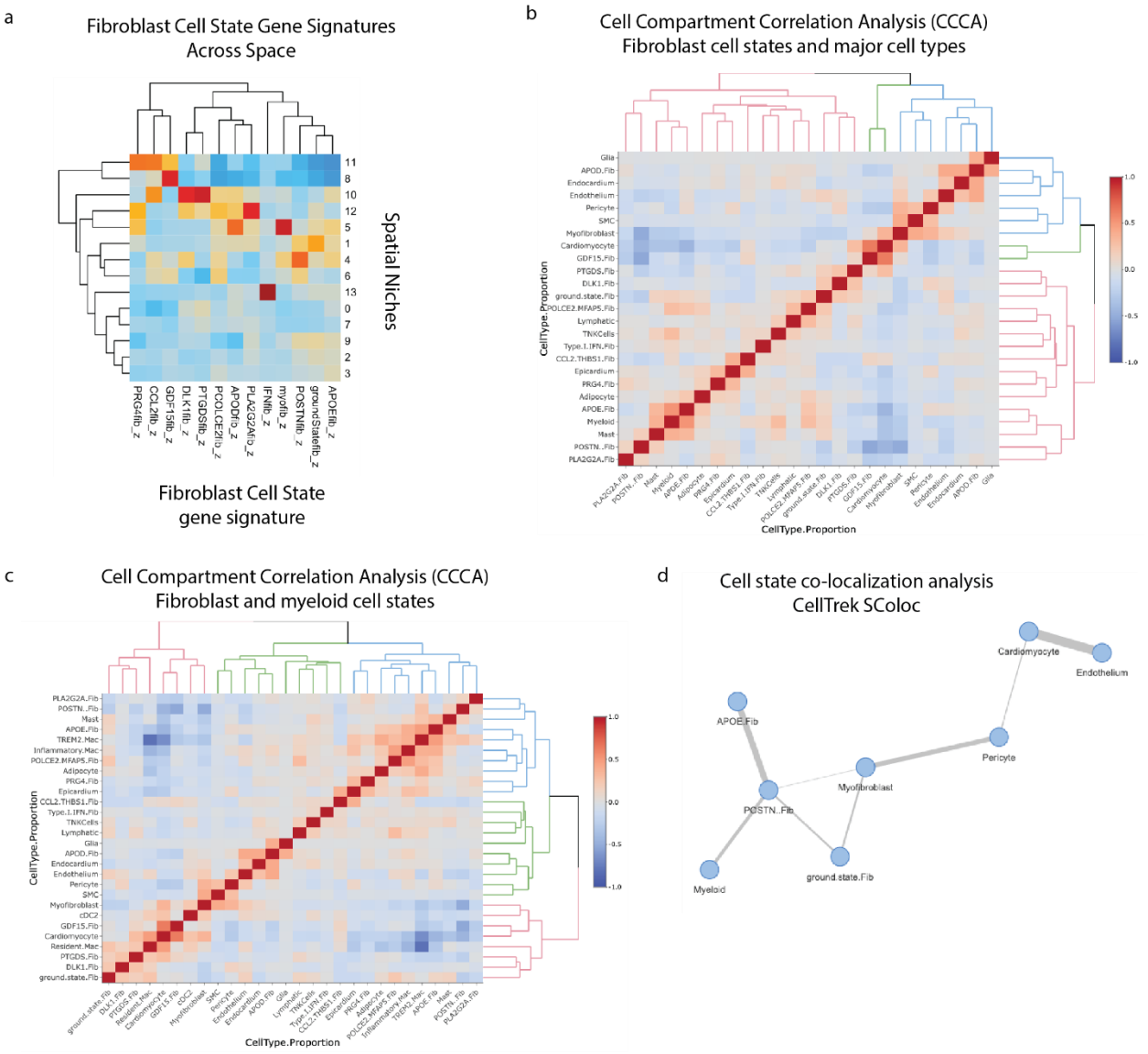

• The Fig. 2n call in page 8 seems to be incorrect in the actual figure. Related to this, the choice of ENRA to examine openness of the locus and association with HF is a bit random, what about RUNX1 and MEOX1?

We thank the reviewer for this important comment. Initially, we had a limited number of samples in the Multiome dataset which precluded a robust un-biased analysis. However, we have added many new Multiome donor and HF samples for a total of 23. Using this expanded dataset, we performed an un-biased analysis between donor and HF chromatin accessibility, leveraged the multi-omic RNA/ATAC element via peak-2-gene linkage to identify key genes whose RNA and chromatin changes in HF. We have performed this additional analysis and amended figure 2 to reflect these changes and have added the following to the main text:

"We first computed the differential accessibility in fibroblasts between non-failing donors and failing hearts (**Fig. 2l**). We found 15,373 features up and 12,701 features down in heart failure. Using the peak to gene links, we identified nearby genes linked to these differentially accessible peaks based on a high correlation between gene accessibility and expression within the same nuclei – we found 3,167 unique genes linked to differentially accessible peaks (**Fig. 2m**). We overlapped this gene list with the pseudobulk RNA differential expression gene list between donor and heart failure and found 234 overlapping genes (**Fig. 2m**). We then used intersecting genes (those which are increased in heart failure at the RNA and chromatin level) and looked for enrichment in different fibroblast cell states – we found that the F9 fibroblast had the greatest enrichment of this gene set and a gene set score of the intersecting genes as a dot plot shows greatest expression within F9 (**Fig. 2n**)."

• The data regarding the immune-fibroblast niche and T-cell is rather descriptive and preliminary. How do you connect this data to your main story of macrophage–fibroblast crosstalk? How do T-cells affect the fibroblast phenotype if at all? I would suggest leaving these data out of the paper.

We thank the reviewer for the comment. Given the unbiased nature of the spatial co-localization analysis, we wanted to report all the relevant findings. But as the reviewer points out this data is largely descriptive and preliminary – as per the suggestion, we have removed the T-cell niche analysis out of the paper.

• Likewise, in Fig.5G the use of the new tool CellOracle to predict perturbations in Runx1KO fibroblasts is interesting but speculative and out of place in this paper. what is the intention of adding it and how does it link with anti-Il1b treatment?

We thank the reviewer for the comment. The purpose of including this analysis was to show the potential application of using this dataset for new hypothesis generation within the field for future targeted mechanistic experiments. We agree that this result is highly predictive and as the reviewer suggests, we have removed it from the paper.

• Misspelling: line 183: aobserved

Thank you for the correction, we have made the relevant change.

• typo: line 442 should be Fig5C, not 5A, right?

Thank you for the correction, we have made the relevant change.

• it´s impossible for me read the heading of some panels, eg. Fig.3C

Thank you for the correction, we have made the relevant change.

• IL-1, IL-B and IL-1B are mixed throughout the document. Please choose one for consistency

Thank you for the correction, we have made the relevant change to read IL-1β.

REVIEWER #3

This interesting study examines populations of human and mouse cardiac cells, with an emphasis on subpopulations of fibroblasts, during the heart's response to injury. The findings are potentially very impactful and the datasets will be useful to the field. Inclusion of human data is a strength. An enormous amount of data is analyzed—a strength, because of the efforts to reconcile with previous research, and a weakness, because following what was done is extremely challenging. Parsing observation from interpretation is tough with the limited description of the different analyses performed. The authors should make a stronger effort to clearly describe what has been done in each of the comparative analyses in the main text, perhaps paring down some of the extensive analyses to explain in sufficient detail those that would need to be repeated by future investigators wishing to examine these subpopulations of cells. Additional characterization of the effect of Il1 beta on cardiac phenotypes would strengthen the paper.

Thank you for the positive feedback. In response to the outlined suggestions, we have focused and strengthened the informatics analysis and provided in vivo validation data related to the $FAP^+$ fibroblast lineage and role of IL-1β signaling on fibrosis and cardiac phenotypes.

Other feedback:

The legend says that Figure 1D is "RNA and protein" data, whereas the results say the clusters were based on differential gene expression. Please clarify in main text how these clusters were defined.

We thank the reviewer for point this discrepancy out. We have outlined the details of the clustering analysis in the methods as follows: "Weighted nearest neighbor clustering[44] (WNN) was performed with the significant RNA PCs and dsb normalized proteins (minus isotype controls) directly without PCA as previously outlined with the FindMultiModalNeighbors function in Seurat. Subsequently, a uniform manifold approximation (UMAP) embedding was constructed and FindClusters was used to un-biasedly cluster cells using the SLM modularity optimization algorithm. Clustering was performed for a suite of different resolutions (0.1-0.8 at 0.1 intervals) and differential gene and protein expression using the FindAllMarkers function and a Wilcoxon Rank Sum test with a logFC cut-off of 0.25 and a min.pct cut-off of 0.1. Clusters were annotated using canonical gene and protein markers and subsequent violin plots (RNA) and heatmaps (protein) were created to assess clean separation of clusters into distinct cell types. Previously identified canonical marker genes were also plotted on the UMAP object to further validate cluster annotations. In Supplementary Figure 2 a and b, we display the top differentially expressed genes and marker proteins."

What data are the basis for this claim: "Accumulation of fibroblasts was seen across pathological conditions beginning 1 week after acute MI"? Is this a temporal analysis based on a subset of patients with different times out from MI? What markers were used for fibroblasts in this conclusion?

We thank the reviewer for the comment. We apologize for the ambiguous nature of the sentence and have corrected it to read: "In the HF cohort we saw expansion of cardiac fibroblast relative to donor." To capture broad timeline post myocardial infarction, the acute MI and ICM samples were obtained from patients with different times out from MI – the following times were included (Figure 1a): 4 days, 7 days, 2 months, 3 months, 4 months, 19 months, 41 months, 99

months, 187 months, and 15 years. The temporal analysis of fibroblast states time post MI is presented in figure 2e and shown below.

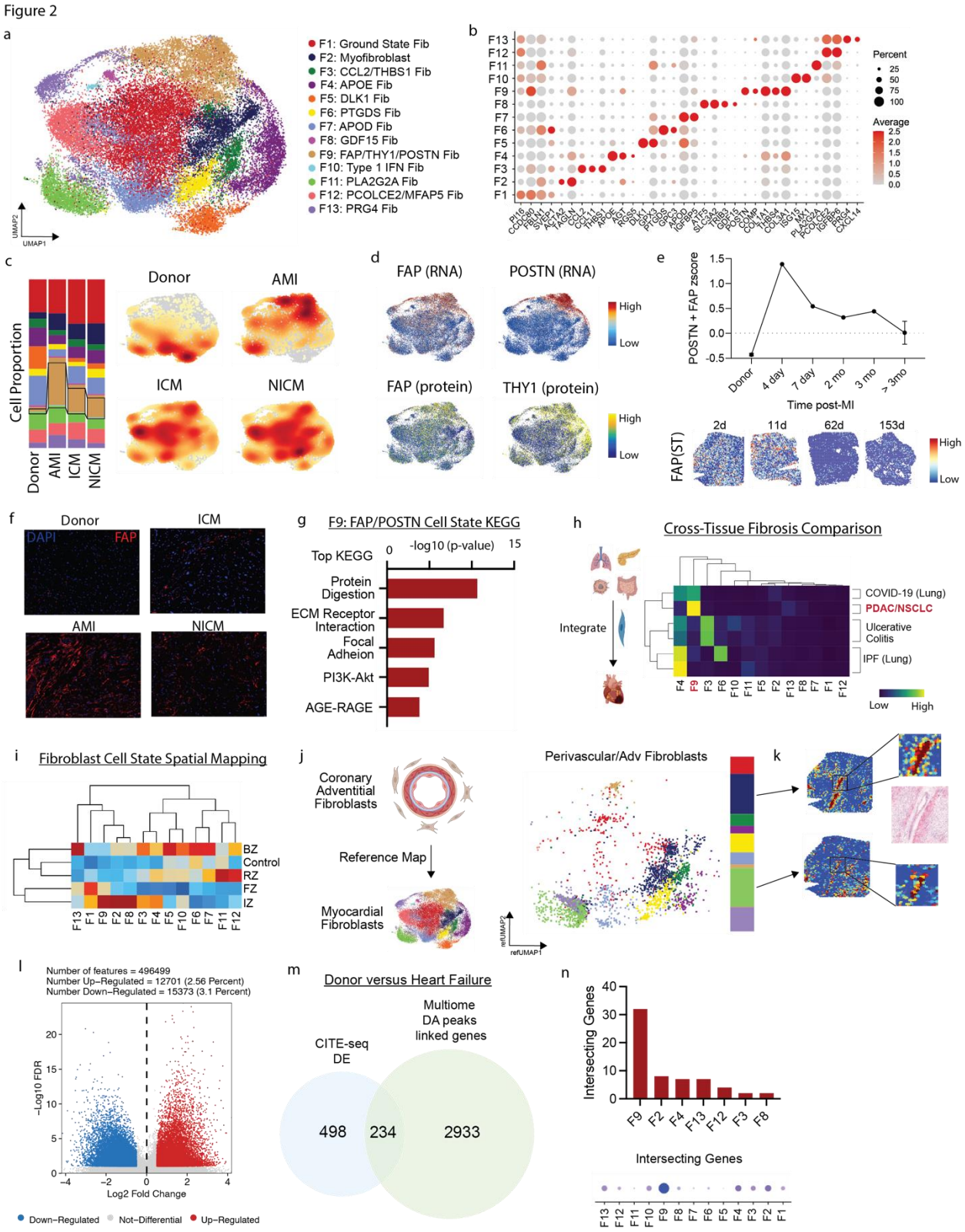

Please list in the figure which ‘canonical markers’ were used to determine cell populations in Figure 1I.

We thank the reviewer for the comment. In figure 1i, we reference mapped the integrated Multiome dataset onto a large comprehensive single nucleus RNA sequencing reference atlas (Supplementary Figure 13) to annotate nuclei. The reference object was annotated using canonical markers as follows: differential expression testing using the FindAllMarkers function was used to find marker genes for different clusters. Previously published gene sets (PMID 35959412) were used to annotate the clusters. To expand the precise gene markers of the different cell populations, we have performed differential expression testing on both the reference object and the Multiome object and generated a heatmap of the top10 marker genes in the different cell types. We have amended Supplementary Figure 13 to include the heatmap for the reference object and added the heatmap of marker genes for the Multiome dataset in Supplementary Figure 22. To further support the cell type clustering, we used previously defined marker genes (PMID 35959412, PMID 375853573) to create gene set scores and overlaid the signature on the UMAP embedding and created a dot plot of gene set signatures to support the clustering (Supplementary Figure 22) and attached below.

Supplementary Figure 4

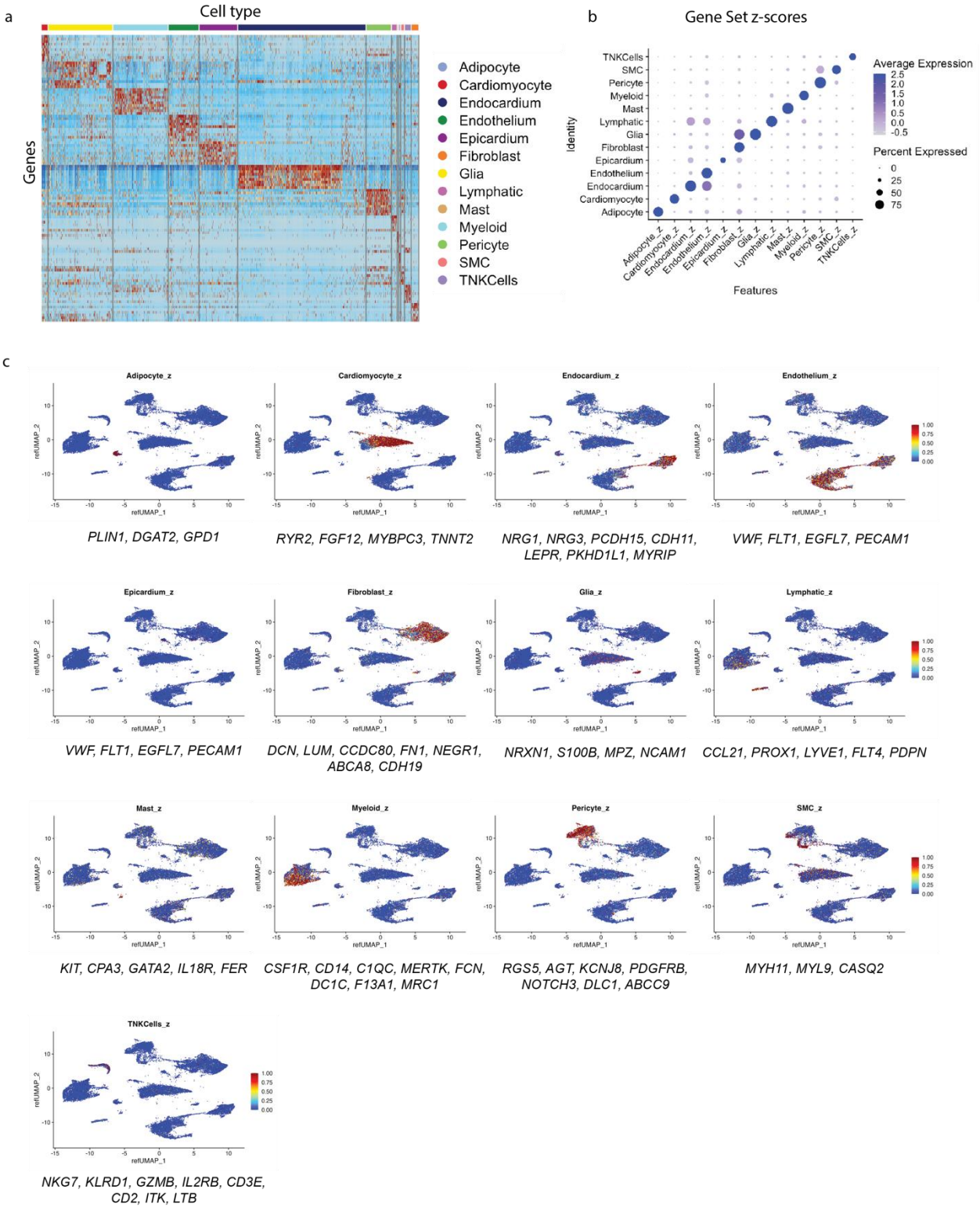

RNA and ATAC data should be split out and analyzed in parallel, in addition to the combined method in Figure 1. Are the accessibility changes around the same canonical genes sufficient to retrieve the same clusters using only the ATAC data? What differences in clustering exist when these datasets are not combined?

We thank the reviewer for the suggestion. To strengthen and allow for more robust analyses using the Multiome (RNA + ATAC) data, we increased the number of samples from n = 9 to n = 23 including donors, acute myocardial infarction, ischemic cardiomyopathy, and non-ischemic cardiomyopathy. We have integrated all 23 samples and analyzed the RNA and ATAC separately as suggested by the reviewer and then also together using the ArchR addCombinedDims function.

Using our integrated single nucleus RNA sequence reference atlas (Supplementary Figure 13a) we reference mapped the Multiome RNA data to annotate clusters as shown in Figure 1i. As suggested by the reviewer, we then performed clustering using the ATAC-seq information from the same nuclei and have made a new Supplementary Figure comparing the clustering from RNA, ATAC, and joint. We have expanded the methods section to describe the various modality and joint approaches as follows: “In ArchR the addIterativeLSI function was used on the RNA and ATAC modalities respectively with default paameters followed by harmony integration to get modality specific clustering and dimensional reductions. To generate a joint RNA/ATAC embedding, the ArchR addCombinedDims function was used and this combined embedding was used for subsequent UMAP construction and clustering. To compare how the ATAC derived cell clustering compares to the RNA and joint embedding, we generated a confusion matrix.”

We have also expanded the main text of the manuscript to include the following “We found that for the major cell types, the RNA annotations map to unique ATAC clusters in cardiomyocytes, myeloid, fibroblasts, endothelium, pericytes, T and NK Cells, and endocardium. This was not observed for cell types with lower abundance such as adipocytes, epicardial cells, lymphatics, smooth muscle cells, mast cells, and glia. Together, this suggests that the ability of ATAC-seq data alone to discriminate between rarer cell types within a large dataset is limited highlights the utility of paired RNA and ATAC information from the same nuclei.”

The above analysis is reflected in a new Supplementary Figure 23 and shown below.

Supplementary Figure 5

a

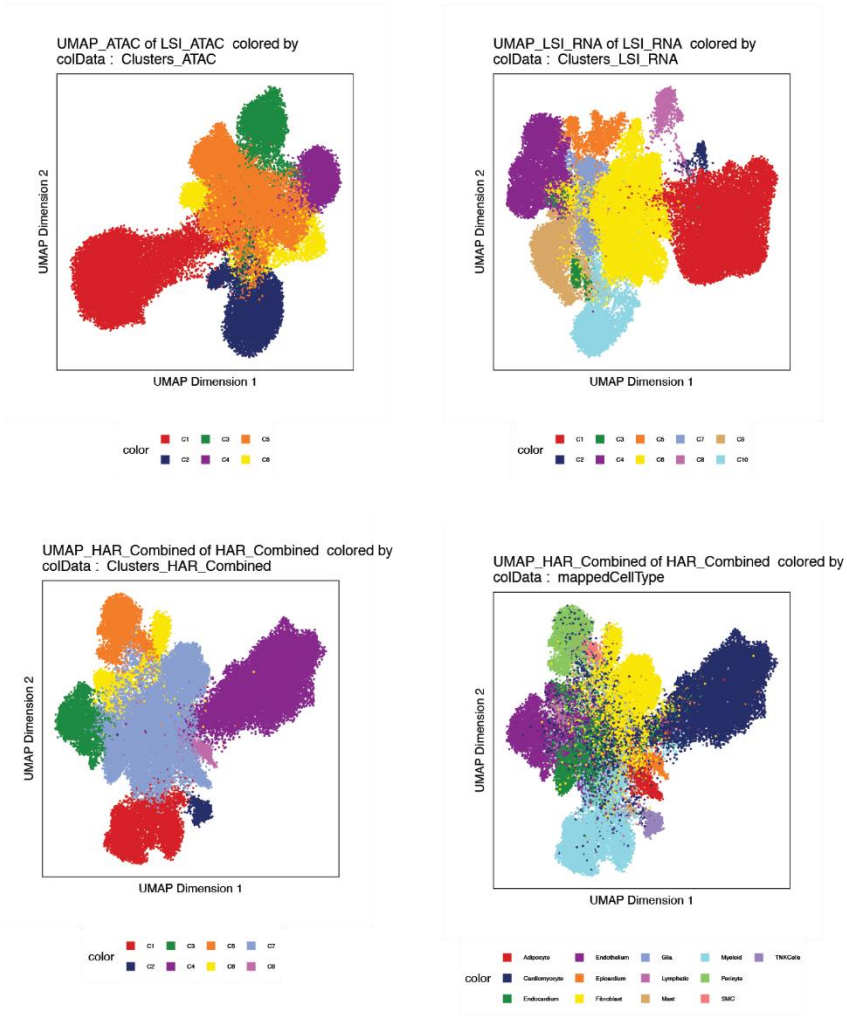


b

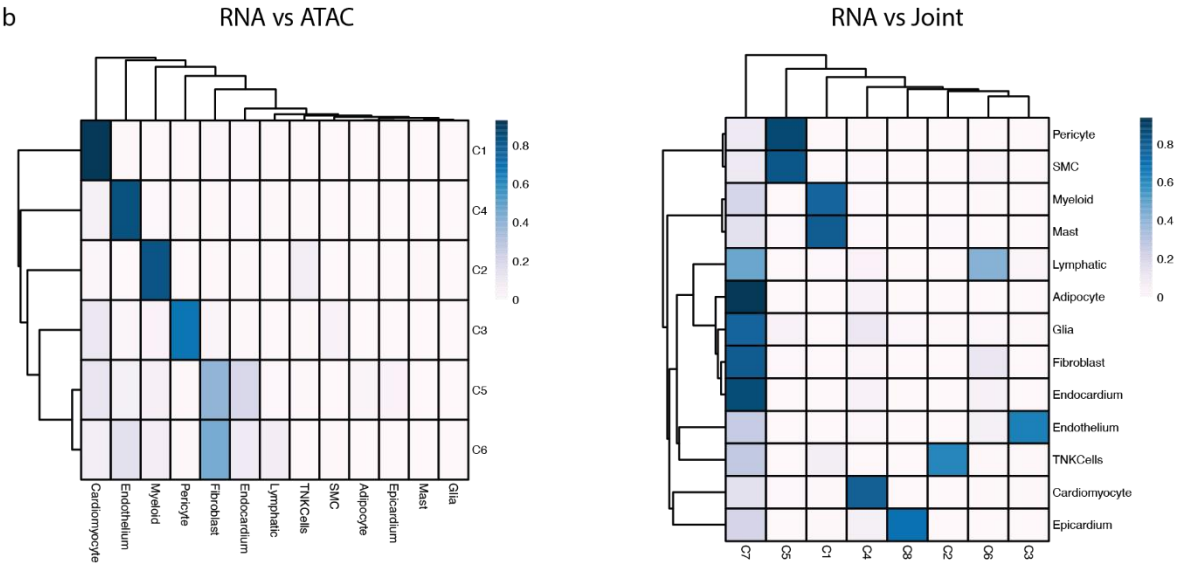

Expanding on the last point, a strength of snRNA and ATAC with Multiome is that, in principle, the experiment can reveal whether the accessibility changes and expression changes are happening in the same cell. What is the observation in the present study? Also, the investigators are missing a chance to dig deeper into how the accessibility and expression data identify the same or different features of these populations of cells. What subpopulations of cells are identified only with RNA or only with ATAC?

We thank the reviewer for this very important suggestion. To address the reviewers first comment "a strength of snRNA and ATAC with Multiome is that, in principle, the experiment can reveal whether the accessibility changes and expression changes are happening in the same cell. What is the observation in the present study? From the same nuclei, we compared the RNA expression of a given gene and the accessibility to correlate the gene accessibility-expression from the same nuclei. We have computed the Pearson correlation coefficient for all genes between expression and accessibility in the same nuclei and generated a new panel (Figure 1l). Additionally, we calculated the number of linked nearby putative enhancers for each gene based on the prior peak to gene linkage analysis (previously described PMID 34390642). Finally, we plotted the Gene Expression-accessibility Pearson correlation coefficient versus the number of linked enhancers for each gene. As described (PMID 34390642), we defined genes predictive of chromatin (GPCs) as genes with a Pearson correlation coefficient in the top 10 percentile and linked to at least 10 (cis regulatory elements) CREs. Some of these GPCs comprised of transcription factors and given a strong correlation between accessibility and expression, the accessibility in these TFs likely precedes cell state changes in development, homeostasis, and disease.

We have also amended Figure 1 and the main text with the following: "We next leveraged the Multiome RNA and ATAC to compute a Pearson correlation score between gene expression and accessibility (GE-GA) from each nucleus for every gene (**Fig. 1l**). We found that the GE-GA correlation was variable based on the gene suggesting that accessibility and expression may not always correlate at a given time and may be a function of the biology of the gene. We then utilized a prior method to compute the number of linked enhancers to each gene using the peak 2 gene linkage matrix[28]. Next, we defined genes predictive of chromatin (GPCs) as genes with a Pearson correlation coefficient in the top 10 percentile and linked to at least 10 (cis regulatory elements) CREs (**Fig. 1m**). Some of these GPCs comprised of transcription factors and given a high GE-GA correlation, the accessibility in these transcription factors may precede changes in gene expression and cell state."

We have expanded the methods to include "We have computed the Pearson correlation coefficient for all genes between the gene expression and accessibility vectors. The ArchR peak 2 gene linkage function was used to identify putative CREs for each gene [28]. GPCs were defined as genes with GE-GA correlation in the top 10 percentile and linked to at least 10 CREs[28]." We cited the original paper (PMID 34390642) describing the strategy for technical details and have also provided our code in the GitHub repository."
Analysis shown in amended figure below (specifically Figure 1l, m):

Figure 1

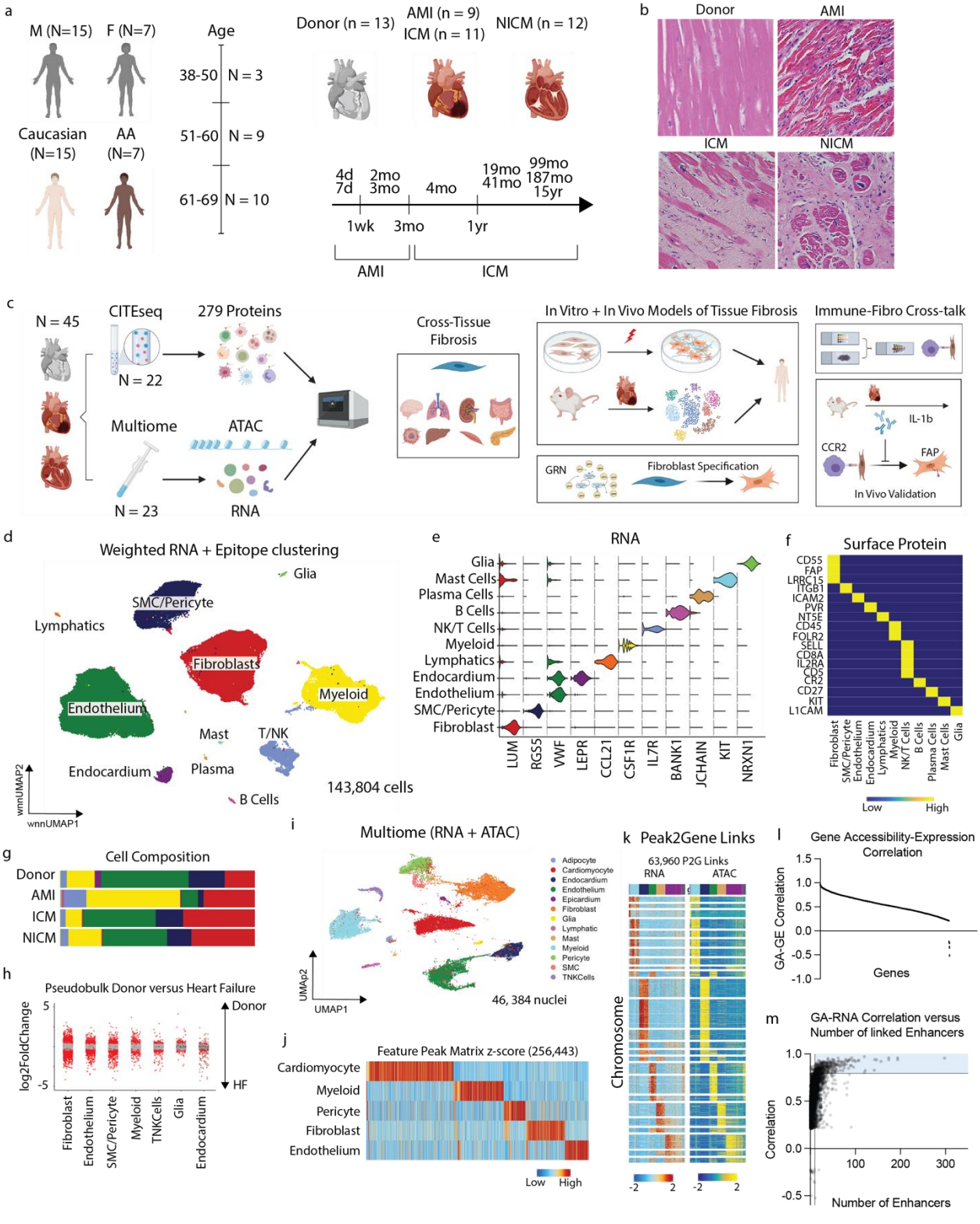
a
M (N=15)
F (N=7)
Age
38-50 N = 3
51-60 N = 9
61-69 N = 10
Caucasian (N=15)
AA (N=7)
Donor (n = 13)
AMI (n = 9)
ICM (n = 11)
NICM (n = 12)
4d
7d
2mo
3mo
4mo
19mo
41mo
99mo
187mo
15yr
1wk
3mo
1yr
AMI
ICM
b
Donor
AMI
ICM
NICM
c
N = 45
CITEseq
279 Proteins
N = 22
Multiome
ATAC
RNA
N = 23
Cross-Tissue Fibrosis
In Vitro + In Vivo Models of Tissue Fibrosis
GRN
Fibroblast Specification
Immune-Fibro Cross-talk
IL-1b
CCR2
FAP
In Vivo Validation
d
Weighted RNA + Epitope clustering
Glia
SMC/Pericyte
Lymphatics
Fibroblasts
Myeloid
Endothelium
Mast
T/NK
Endocardium
Plasma
B Cells
143,804 cells
wnnUMAP2
wnnUMAP1
e
RNA
Glia
Mast Cells
Plasma Cells
B Cells
NK/T Cells
Myeloid
Lymphatics
Endocardium
Endothelium
SMC/Pericyte
Fibroblast
LUM
RGS5
VWF
LEPR
CCL21
CSF1R
IL7R
BANK1
JCHAIN
KIT
NRXN1
f
Surface Protein
CD55
FAP
LRRC15
ITGB1
ICAM2
PVR
NT5E
CD45
FOLR2
SELL
CD8A
IL2RA
CD5
CR2
CD27
KIT
L1CAM
Fibroblast
SMC/Pericyte
Endothelium
Endocardium
Lymphatics
Myeloid
NK/T Cells
B Cells
Plasma Cells
Mast Cells
Glia
Low
High
g
Cell Composition
Donor
AMI
ICM
NICM
h
Pseudobulk Donor versus Heart Failure
log2FoldChange
5
-5
Donor
HF
Fibroblast
Endothelium
SMC/Pericyte
Myeloid
TNKCells
Glia
Endocardium
i
Multiome (RNA + ATAC)
Adipocyte
Cardiomyocyte
Endocardium
Endothelium
Epicardium
Fibroblast
Glia
Lymphatic
Mast
Myeloid
Pericyte
SMC
TNKCells
UMAp2
UMAP1
46, 384 nuclei
j
Feature Peak Matrix z-score (256,443)
Cardiomyocyte
Myeloid
Pericyte
Fibroblast
Endothelium
Low
High
k Peak2Gene Links
63,960 P2G Links
RNA
ATAC
Chromosome
-2
2
-2
2
l
Gene Accessibility-Expression Correlation
GA-GE Correlation
1.5
1.0
0.5
0.0
-0.5
-1.0
Genes
m
GA-RNA Correlation versus Number of linked Enhancers
Correlation
1.0
0.5
0.0
-0.5
100
200
300
Number of Enhancers

Regarding this sentence: “Using RNA derived annotations, we called peaks and found feature marker peaks for the major cell types (Fig. 1J).” What is a ‘feature marker peak’? Unclear what is shown in this figure and how it was generated. Likewise Figure 1K needs a better description to understand what is going on.

We thank the reviewer for the comment and have amended the manuscript as follows: “We used MACS2 to call peaks within ArchR and performed differential accessibility enrichment across cell types to identify cell type specific peaks (**Fig. 1j**). We then used ArchR to calculate peak to gene links, visualized by constructing a heatmap of the peak-to-gene links split by the two modalities (**Fig. 1k**).” We have further expanded on the methods section to explain how these two panels were generated: “ArchR was used to construct pseudobulk replicates across ATAC clusters and peaks were called using MACS2. The ArchR getMarkerFeatures function was used to identify peaks that are unique to each cell type. The addPeak2GeneLinks function from ArchR was then used to calculate peak to gene links using gene expression and accessibility from the same nucleus with a correlation cut-off of 0.3. To visualize the correspondence between the p2g links, a heatmap was constructed which shows ATAC and RNA z-scores with rows clustered using k-means clustering through the ArchR package plotPeak2GeneHeatmap.”

Are the ‘classical’ fibroblast markers used for ground state clustering in Figure 2a the genes Pl16, CCDC80 and FBLN1 from Figure 2B? Please be explicit.

We thank the reviewer for the comment. The markers used for ground state clustering were indeed Pl16, CCDC80 and FBLN1 from Fig. 2b. This population was noted to have pan-fibroblast genes shared across the other fibroblast cell states. We have amended the sentence in the main text to include these 3 genes as the reviewer suggests.

The description in the results and the figure legend are insufficient to understand what the authors observe in the figure and how they come to this conclusion: “Spatial transcriptomics data from human heart indicated that fibroblast populations were located within defined perivascular and interstitial spatial niches (Supplementary Fig. 4B – D).” On the basis of what observation was ‘were located in defined…niches’ determined? What would the alternative look like (i.e. what is a control showing the absence of defined localization)?

Regarding this statement: “F2 and F9 fibroblasts resided within distinct regions of the myocardium (Supplementary Fig. 4D)”; what this figure appears to show is F2 expression in perivascular and F9 in interstitial sections, but not the opposite analysis, which would be required to make this conclusion. Please clarify. These data are intriguing and hint that the investigators may have uncovered different populations involved in perivascular vs interstitial fibrosis.

We thank the reviewer for these important comments and agree with the assertion that we have uncovered different populations involved in interstitial and perivascular fibrosis. To address the points raised, we have performed extensive additional analyses with the spatial transcriptomics data from human and mouse, and utilized coronary artery adventitial fibroblast scRNA-seq.

As the reviewer points out, the panels shown in Supplementary Fig. 4b – d are descriptive examples showing the F2 fibroblast cluster is enriched in locations adjacent to blood vessels whereas the F9 cluster is enriched within interstitial areas. To characterize the spatial localization of fibroblast cell states, we performed 3 orthogonal analyses: (1) fibroblast cell state co-localization analysis, (2) cell compartment correlation analysis between fibroblast cell sates

and other major cell types, and (3) fibroblast cell state spatial localization with cell types using spatial distance. We have amended the main figure 2 and created a new Supplementary Figure 10 to reflect these analyses:

(1) We used the fibroblast cell state marker genes (Supplementary Figure 3) and created gene set scores for each fibroblast cell states in an integrated spatial transcriptomics dataset across 31 samples from 23 patients (14 control, 12 infarct zone, 3 border zone, 6 remote zone, and 6 fibrotic zone) from Supplementary Figure 16. To visualize how the fibroblast cell states vary by spatially, we constructed two heatmaps: one grouped by spatial niche (Supplementary Figure 10a) and the other grouped by sample region (Figure 2i). Our analysis showed that different fibroblast cell states were enriched across myocardial sampling locations with F2, F3, F4, F8, and F9 most enriched in the infarct zone and different populations enriched within the border and remote zone. Some fibroblast cell states like F1, F3, F4, and F12 were present across tissue areas. The heatmap of fibroblast cell state gene scores by spatial niche (Supplementary Figure 10 a) further highlighted that different fibroblast cell states are enriched across distinct spatial niches – as the reviewer importantly highlights not every fibroblast cell state is in a different location as some states share niches while others do not. These results are consistent with the transcriptional and spatial plasticity within human cardiac fibroblasts.
(2) To characterize spatial localization of fibroblast cell states in the context of other cell types, we performed an integrated cell compartment correlation analysis (CCCA) across all samples based on the probability of cells located in the same spatial spot (utilizing the spatial transcriptomics data and the single nucleus RNA-seq reference): we first did CCCA with fibroblast cell states and other cell types (Supplementary Figure 10b) and then CCCA with fibroblast cell states, myeloid cell states, and other cell types (Supplementary Figure 10c). The generated heatmaps highlight that distinct fibroblast cell states are spatially associated with different cell types. For instance, F2 is more spatially associated with VSMCs, endothelial cells, and pericytes while F9 is more associated with myeloid cells (Supplementary Figure 10b, c).
(3) Given the stronger localization of F2 with perivascular niches and F9 with interstitial fibrosis, we calculated a distance matrix based on spatial image coordinates and constructed a minimum spanning tree representing the spatial cellular proximity using the SColoc function within CellTrek toolkit. This analysis showed through an orthogonal approach (spatial distance) that F2 fibroblasts are associated with perivascular niches while F9 fibroblasts are more associated with macrophages and F4 fibroblasts (Supplementary Figure 10d).

An important limitation of current spatial transcriptomic techniques is limited resolution, thereby precluding single cell mapping. Furthermore, methods like Curio seeker offer higher resolution insights but lack the read depth. To obviate these limitations and to dissect perivascular (vascular, adventitial) fibroblasts from interstitial fibroblasts, we utilized human coronary artery single cell data – these vessels travel through the myocardium and are surrounded by adventitial and perivascular fibroblasts. We specifically selected out the fibroblast populations and reference mapped them to our human cardiac fibroblasts to address which populations are more perivascular: notably, we found that the F2 and F11 fibroblasts were most enriched in the adventitia, whereas F9 fibroblasts were largely absent (Figure 2j, k).

We have amended Figure 2 and created a new Supplementary Figure 10 highlighting these new analyses. We have also amended the methods section for experimental and computational analysis details and included these new findings in the results section as follows:

“To characterize the spatial localization of transcriptionally distinct fibroblast cell states, we built an integrated spatial transcriptomics dataset across 31 samples from 23 patients (14 control, 12 infarct zone, 3 border zone, 6 remote zone, and 6 fibrotic zone) (**Supplementary Fig. 9**) and performed 3 orthogonal analyses: (1) fibroblast cell state co-localization analysis: we created fibroblast cell state gene set scores and constructed heatmaps to characterize how different fibroblast cell states localize across myocardial regions and relative to each other. This analysis showed that different fibroblast cell states were enriched across myocardial sampling locations including the infarct zone (F2, F3, F4, F8, F9), border zone (F5, F6, F7, F10, F13), and remote zone (F11). Some fibroblast cell states (F1, F3, F4, F12) were present across tissue compartments. The heatmap of fibroblast cell state gene scores by spatial niche (**Fig. 2i**, **Supplementary Fig. 10a**) further highlighted that different fibroblast cell states are enriched across distinct spatial niches. (2) To characterize spatial localization of fibroblast cell states in the context of other cell types, we performed an integrated cell compartment correlation analysis (CCCA) across all samples based on the probability of cells located in the same spatial spot (utilizing the spatial transcriptomics data and the single nucleus RNA-seq reference). We performed CCCA between fibroblast cell states and other major cell types (**Supplementary Fig. 10b**) as well as with myeloid cell states (**Supplementary Fig. 10c**). The generated heatmaps highlight that distinct fibroblast cell states partition into spatially restricted niches. For example, F2 fibroblasts localize with VSMCs, endothelial cells, and pericytes, while F9 fibroblasts localize with myeloid cells (**Supplementary Fig. 10b, c**). (3) Given the stronger localization of F2 fibroblasts with perivascular niches and F9 fibroblasts with interstitial fibrosis, we calculated a distance matrix based on spatial image coordinates and constructed a minimum spanning tree representing the spatial cellular proximity using the SColoc function within CellTrek toolkit. This analysis showed through an orthogonal approach (spatial distance) that F2 fibroblasts are associated with perivascular niches while F9 fibroblasts are more associated with immune cells and F4 fibroblasts (**Supplementary Fig. 10d**). To further dissect the precise cell states contributing to perivascular (vascular, adventitial) fibroblasts versus interstitial fibroblasts, we utilized human coronary artery single cell data[31]. These vessels travel through the myocardium and are surrounded by adventitial and perivascular fibroblasts. We reference mapped the fibroblast populations to our human cardiac fibroblasts to identify perivascular fibroblasts within our heart dataset. We found that the F2 and F11 fibroblasts were most enriched in the adventitia, whereas F9 fibroblasts were largely absent (**Fig. 2j, k**).”

Amended figure 2 and new Supplementary Figure 10.

Figure 2

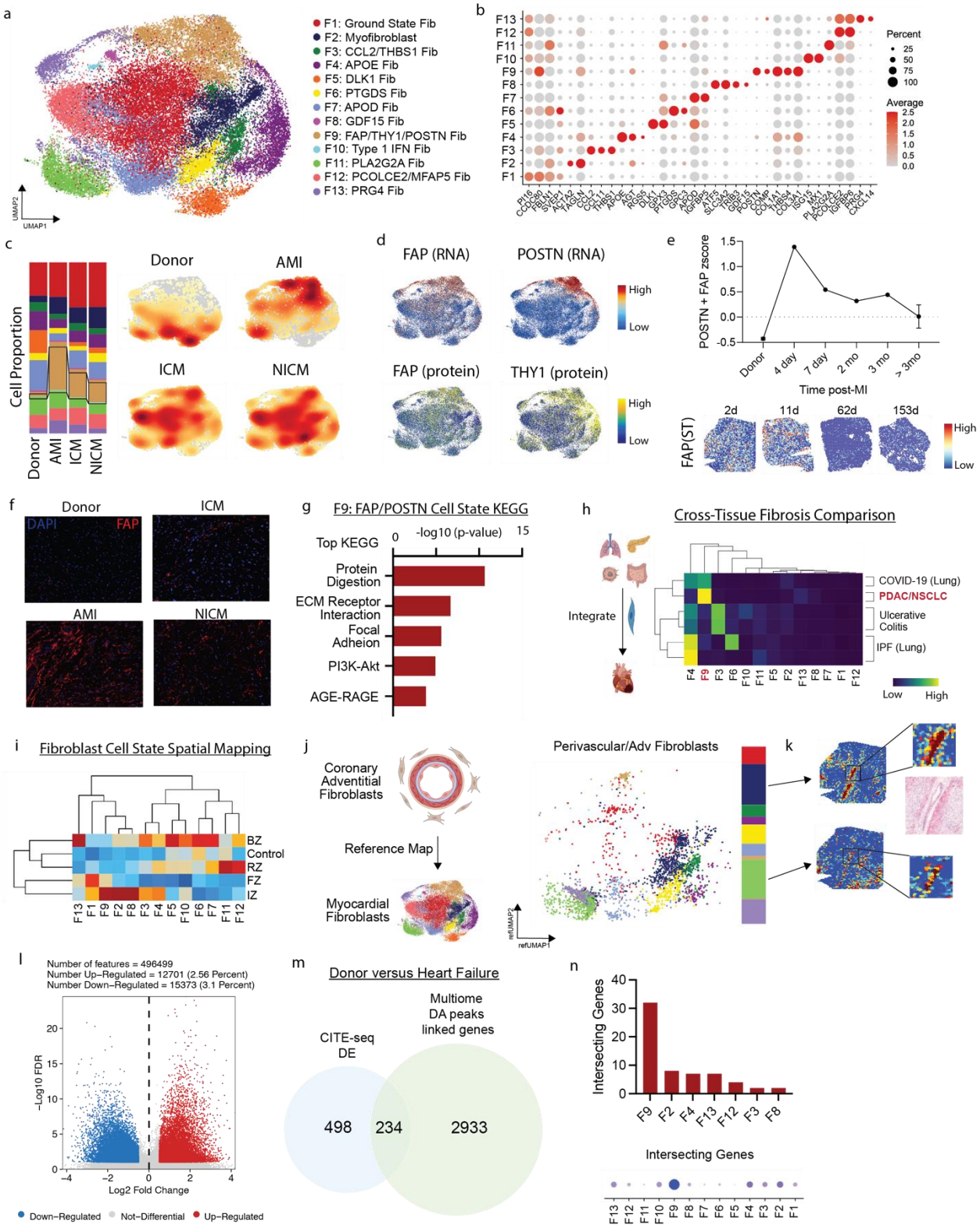
a
F1: Ground State Fib
F2: Myofibroblast
F3: CCL2/THBS1 Fib
F4: APOE Fib
F5: DLK1 Fib
F6: PTGDS Fib
F7: APOD Fib
F8: GDF15 Fib
F9: FAP/THY1/POSTN Fib
F10: Type 1 IFN Fib
F11: PLA2G2A Fib
F12: PCOLCE2/MFAP5 Fib
F13: PRG4 Fib
UMAP1
UMAP2
b
Percent
Average
c
Donor
AMI
ICM
NICM
Cell Proportion
d
FAP (RNA)
POSTN (RNA)
FAP (protein)
THY1 (protein)
High
Low
e
POSTN + FAP zscore
Donor
4 day
7 day
2 mo
3 mo
>3mo
Time post-MI
2d
11d
62d
153d
FAP(ST)
f
DAPI
FAP
g
F9: FAP/POSTN Cell State KEGG
Top KEGG
-log10 (p-value)
Protein Digestion
ECM Receptor Interaction
Focal Adheion
PI3K-Akt
AGE-RAGE
h
Cross-Tissue Fibrosis Comparison
Integrate
COVID-19 (Lung)
PDAC/NSCLC
Ulcerative Colitis
IPF (Lung)
Low
High
i
Fibroblast Cell State Spatial Mapping
BZ
Control
RZ
FZ
IZ
j
Coronary Adventitial Fibroblasts
Reference Map
Myocardial Fibroblasts
Perivascular/Adv Fibroblasts
k
l
Number of features = 496499
Number Up-Regulated = 12701 (2.56 Percent)
Number Down-Regulated = 15373 (3.1 Percent)
-Log10 FDR
Log2 Fold Change
Down-Regulated
Not-Differential
Up-Regulated
m
Donor versus Heart Failure
Multiome DA peaks linked genes
CITE-seq DE
498
234
2933
n
Intersecting Genes

Supplementary Figure 10

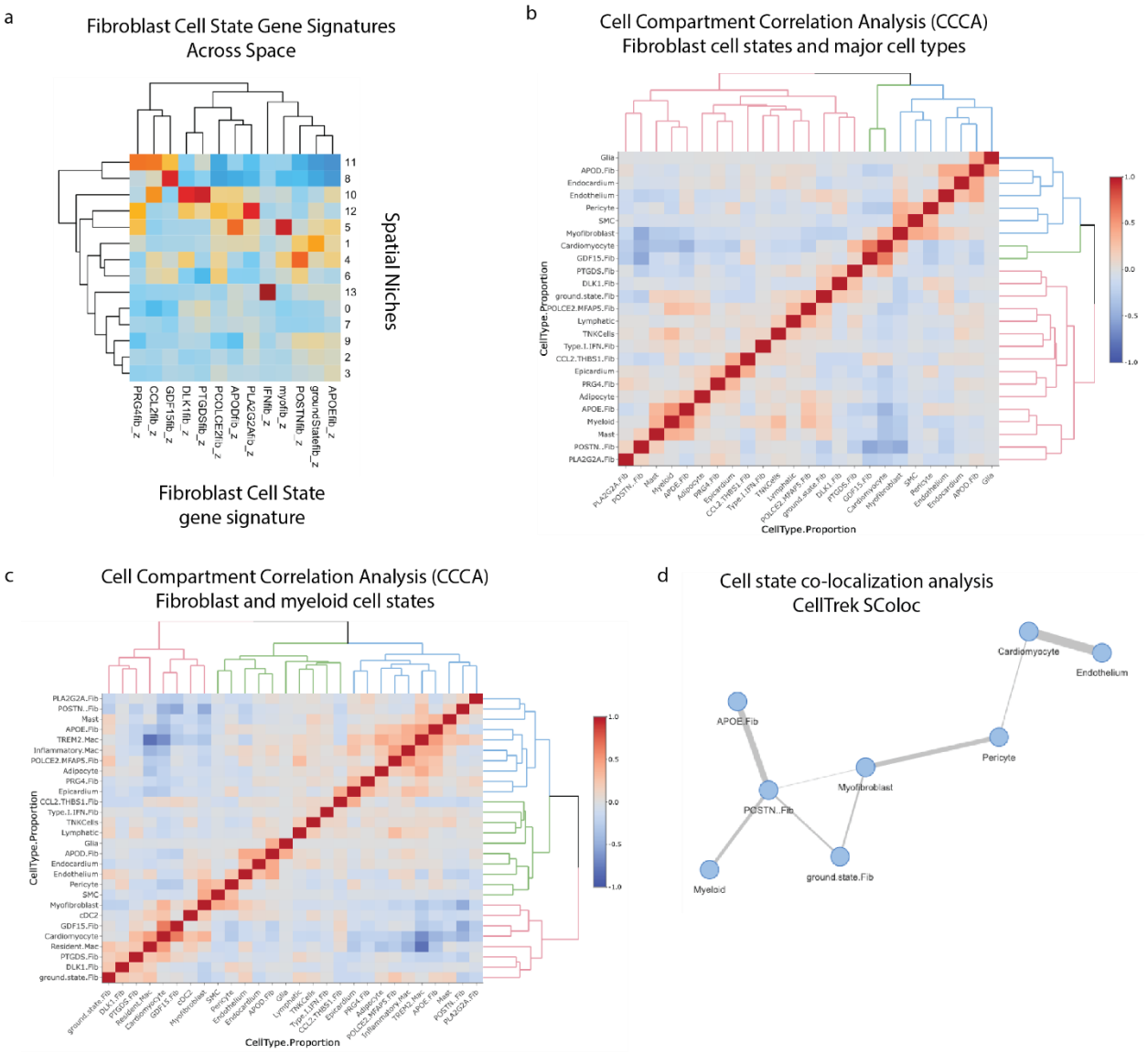

Please specify in each of the panels of Figure 2 whether RNA, ATAC or both are used for clustering and analyses. Legend says CITED, so this is protein information too? Please clarify in results and legend text.

We thank the reviewer for point this point. We have amended the figure legend and clarified the results section. To clarify, the manuscript results section now reads "Gene expression was used for unbiased clustering, harmony integration to correct for batch effects, and subsequent DGE identified 13 distinct fibroblast cell states…".

Related to the last point: many bulk RNA seq or PCR based measurements of gene activation in hearts and isolated fibroblasts show activation of acta2 and postn, whereas these authors demonstrate these genes are not active in the same cells (Figure 2B), an important observation.

We thank the reviewer for point out this very important element of the data presented in the manuscript. As outlined above, we used various spatial transcriptomic techniques to show that these populations represent transcriptionally distinct states, and they occupy different spatial neighborhoods. To further explore and dissect this point made by the reviewer, we have generated $Fap^{creERT2}$ mice by knocking an inducible Cre recombinase into the endogenous FAP locus. We then generated $Fap^{CreERT2}Rosa26^{LSL\text{-}tdTomato}$ mice and performed in vivo fibroblast lineage tracing. These data are displayed in a new main figure (Figure 4).

Our human and mouse computational analyses predicted that FAP+ fibroblasts emerge early and may selectively contribute to Postn fibroblasts that are distinct from myofibroblasts. To test this hypothesis, $Fap^{CreERT2}Rosa26^{LSL\text{-}tdTomato}$ mice were subjected to the Ang II/PE injury model. Tamoxifen was given early after pump implantation (days 1-7, IP) at 60 mg/kg and mice were sacrificed at day 14 to characterize fibroblast lineages. We performed immunofluorescence and RNAscope in situ hybridization to stain for Postn (pro-fibrotic fibroblasts) and ACTA2 (myofibroblasts) and overlaid tdTomato signal (for Fap lineage labeled cells). We then specifically quantified cells within the myocardium interstitial areas that were $tdTomato^{+}Postn^{+}$ and $tdTomato^{+}Acta2^{+}$ and found that most $tdTomato^{+}$ cells expressed Postn but not Acta2. These results would suggest that FAP+ fibroblasts in cardiac injury predominantly contribute to the $Postn^{+}$ lineage but not the $Acta2^{+}$ myofibroblast lineage. We have created a new figure (Figure 4) integrating several orthogonal lines of evidence in human and mice using single cell RNA-sequencing, computational pseudotime trajectory analysis, multiomic RNA + ATAC sequencing, in vivo lineage tracing, and spatial transcriptomics to dissect cardiac fibroblast heterogeneity.

We added a description of these experiments to the manuscript main text as follows:

"***Distinct lineages of activated cardiac fibroblasts.***

To map fibroblast trajectories in AMI and heart failure, we undertook two approaches. First, we used scVelo with dynamical modeling to infer directionality in fibroblast cell state differentiation. Projection of the velocity vector field in a force directed layout suggested convergence toward the F2, F4, and F9 fibroblast states (**Fig. 4a**). Next, we used Palantir to predict fibroblast differentiation endpoints, which also identified F2, F4, and F9 as possible terminal states with low entropy values across a range of simulation parameters (**Fig. 4b**). To glean how fibroblasts might evolve over the time course of disease, we plotted donor and diseased fibroblast signatures (**Supplementary Fig. 7f**) versus pseudotime along each predicted lineage (F2, F4, F9). The donor fibroblast signature was most enriched early in pseudotime, while the diseased signature increased over pseudotime in each lineage. *FAP* expression transiently increases

along the F2 and F4 lineages and progressively increases along the F9 lineage. Notably, the markers of each population increase over pseudotime in a lineage specific manner (**Fig. 4c**). To dissect putative regulators of the different trajectories, we identified differentially expressed genes and used the resultant gene list to perform a transcription factor enrichment analysis. This approach identified *FBN1, PPRX, FOSX1*, and *MEOX1* as the top transcription factors driving the F9 lineage (**Fig. 4d**). *MEOX1 was previously implicated in cardiac fibrosis*[32]. We then used CellOracle to build a gene regulatory network of heart failure fibroblasts and identified enriched *RUNX1* connectivity across all 3 heart failure groups (**Fig. 4e**). Previously, we have shown that *RUNX1* expands in heart failure using RNAscope in situ hybridization in non-failing donors and heart failure myocardial samples interstitial cells[33]. Linear regression analysis of pseudobulk *RUNX1* and *POSTN* expression at the patient level shows a strong correlation (**Fig. 4f**). Gene expression density plots showed that *MEOX1* was co-expressed with *RUNX1* and *POSTN* along the F9 lineage while *ACTA2* expression was restricted to a different cell state (F2) (**Fig. 4g**). Furthermore, *RUNX1* and *MEOX1* increased along the F9 lineage but not the F2 or F4 lineages (**Fig. 4d**). Using PathwayNet we found that *POSTN* and *RUNX1* are predicted to be connected via a transcriptional regulation network (**Supplementary Figure. 7g**). We validated that these populations are indeed distinct using RNAscope and immunofluorescence for POSTN and ACTA2 respectively from human infarct zone samples (**Fig. 4h**). Additionally, mouse spatial transcriptomics data collected at day 7 post-MI, indicated that *Acta2* and *Postn* expressed in different spatial distributions. *Postn* is enriched within the border zone, whereas *Acta2* is localized to the core of the infarct (**Fig. 4i**). To lineage trace $FAP^+$ fibroblasts, we generated $Fap^{creERT2}Rosa26^{tdTomato}$ mice (**Supplementary Figure. 20**, detailed in methods) and performed Ang II/PE mini-pump implantation (**Fig. 4j**). Using FAPi non-invasive PET imaging, we confirmed early enrichment of FAP at d7 following AngII/PE infusion (**Fig. 4k**). Tamoxifen was administered to label $FAP^+$ fibroblasts on days 1-7 of Ang II/PE infusion and mice were sacrificed at day 14 (**Fig. 4j**). We then performed RNAscope in situ hybridization for *Postn* and immunofluorescence for ACTA2 and overlaid tdTomato signal (**Fig. 4l**). Quantification of $tdTomato^+Postn^+$ and $tdTomato^+ACTA2^+$ cells showed that $FAP^+$ cells contributed towards the Postn lineage and not the Acta2 myofibroblast lineage (**Fig. 4l**).”

Figure 4

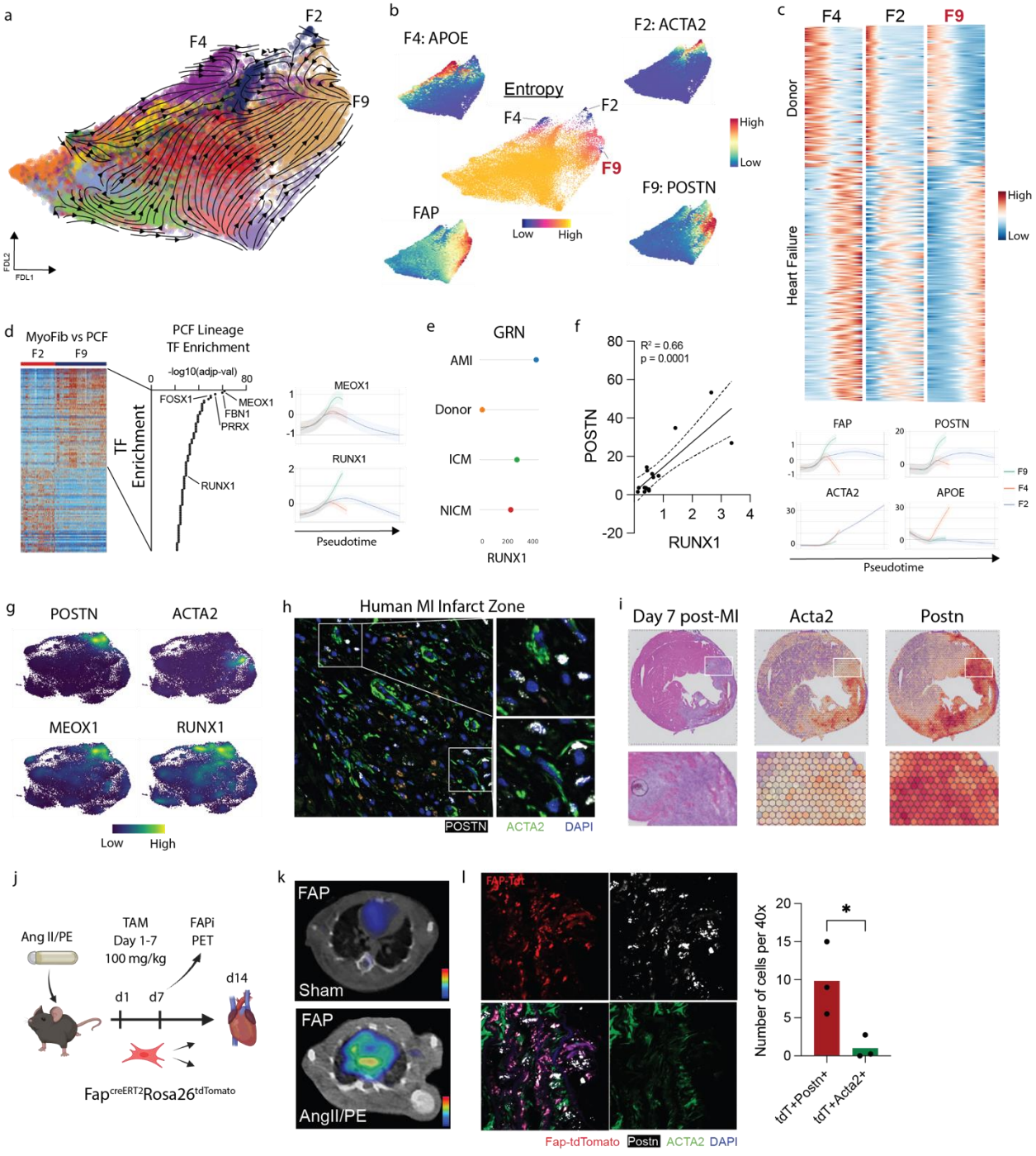
a
F2
F4
F9
FDL2
FDL1
b
F4: APOE
F2: ACTA2
Entropy
F4
F2
F9
High
Low
FAP
F9: POSTN
Low
High
c
F4
F2
F9
Donor
Heart Failure
High
Low
FAP
POSTN
ACTA2
APOE
F9
F4
F2
Pseudotime
d
MyoFib vs PCF
F2
F9
PCF Lineage
TF Enrichment
-log10(adjp-val)
0
80
FOSX1
MEOX1
FBN1
PRRX
RUNX1
TF Enrichment
MEOX1
RUNX1
Pseudotime
e
GRN
AMI
Donor
ICM
NICM
0
200
400
RUNX1
f
R² = 0.66
p = 0.0001
POSTN
RUNX1
g
POSTN
ACTA2
MEOX1
RUNX1
Low
High
h
Human MI Infarct Zone
POSTN
ACTA2
DAPI
i
Day 7 post-MI
Acta2
Postn
j
Ang II/PE
TAM
Day 1-7
100 mg/kg
FAPi
PET
d1
d7
d14
Fap^creERT2 Rosa26^tdTomato
k
FAP
Sham
FAP
AngII/PE
l
FAP-Tdt
Fap-tdTomato
Postn
ACTA2
DAPI
Number of cells per 40x
*
tdT+Postn+
tdT+Acta2+

Additionally, we have created a supplementary figure describing the construction of this new CRE, with the following addition to the methods section:

"**Gene Editing Design**
Analysis of genomic DNA sequence surrounding the target region, using the Benchling (www.benchling.com) guide RNA design tool, identified a gRNA sequence with a suitable target endonuclease site in *Fap* gene start site. Predicted off-target sites for the gRNA (crRNA2-AAGGTTAGTGCGTGCCGTCT) were identified using the specificity model developed and documented by Hsu and colleagues and embedded in the Benchling gRNA design tool. Design considerations for off-target editing were as follows. Higher off-target editing risk was considered when the "Score" is >2.0 with a canonical SpCas9 PAM (NGG), >50.0 with a chromosomally unlinked non-canonical PAM (NAG) or >20.0 with a linked non-canonical PAM yet in an annotated protein coding region. These "Score" thresholds were based on empirical targeted sequencing analysis of 20 different predicted off-target loci in 15 different mouse zygote gene editing experiments.

**Microinjection of gRNAs and plasmid donor DNA repair templates**
*Streptococcus pyogenes* Cas9 (SpCas9) V3 protein and gRNAs were purchased as part of the Alt-R CRISPR-Cas9 system using the crRNA:tracrRNA duplex format as the gRNA species (IDT, USA). Alt-R CRISPR-Cas9 crRNAs (Product# 1072532, IDT, USA) were synthesized using the gRNA sequences specified in the DESIGN section and hybridized with the Alt-R tracrRNA (Product# 1072534, IDT, USA) as per manufacturer's instructions. This gRNA duplex was used in all subsequent gene editing processes. The sequence of the double stranded DNA donor plasmid, that functions as the DNA repair template, was synthesized by Genscript. Features included asymmetric homology arm lengths of 1.6 kb and 2.0 kb, flanking the 2.2 kb insertion sequence. The final concentration of the gRNA, SpCas9 and donor components in the microinjection mixture was 50ng/ul, 100 ng/ul and 10 ng/ul, respectively. All animal work was approved by the Jackson Laboratory Animal Care and Use Committee and adhered to the standards of Guide for the Care and Use of Laboratory Animals set forth by the NIH. Microinjection was performed as described (PMID: 27210041) using C57BL/6J (Stock# 000664, The Jackson Laboratory, USA) donor female mice (3–4 weeks of age).

**Sequence characterization of Founder and N1 mice**
PCR primers flanking the gRNA target site, but outside the repair template homology arms, were used to amplify the region of interest from founder progeny. PCR amplicons were subjected to Sanger sequencing to identify founders with precise desired changes. Founders carrying desired mutations were bred with C57BL/6J mice (Stock #000664, The Jackson Laboratory, USA) to produce N1 progeny. N1 animals were confirmed by the same PCR-Sanger sequence analysis the founder population was subjected to. In contrast to founders, N1 animals are obligate heterozygotes, with one allele derived from an un-manipulated chromosome, enabling deconvolution of the two alleles in the mixed PCR amplicon. PCR primer sequences were as follows: Short Range PCR, Fap SR forward and Cre SR reverse; 5'-AGAACGCCCCCAAAATCTGT-3' and 5'- ATTCAACTTGCACCATGCCG-3', left homology arm PCR, Fap LHA forward and Cre SR reverse; 5'-GCTGATGGCTTTCTCTCGGA-3' and 5'-ATTCAACTTGCACCATGCCG-3', and right homology arm PCR, ERT RHA forward and Fap RHA reverse; 5'-CGGGCTCTACTTCATCGCAT-3' and 5'-CAGGTGACATGCTGAGGTGT-3'.
"

Supplementary Figure 20

a

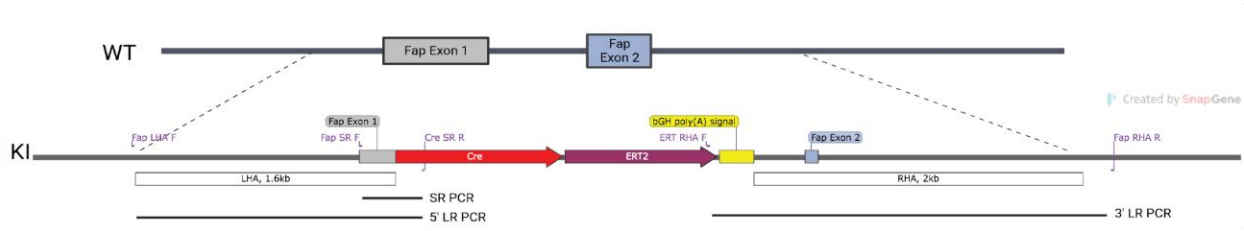


b


c

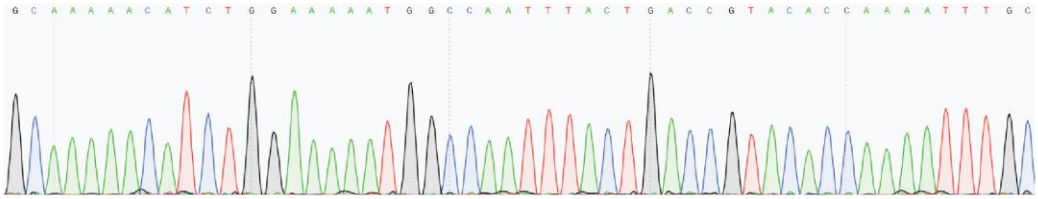

WT GCAAAAACATCTGGAAAAATGAAGGTTAGTGCGTGCCGTCTCGGGGACGACC
KI GCAAAAACATCTGGAAAAATGGCCAATTTACTGACCGTACACCAAAATTTGC
CRE M A N L L T V H Q N L

d

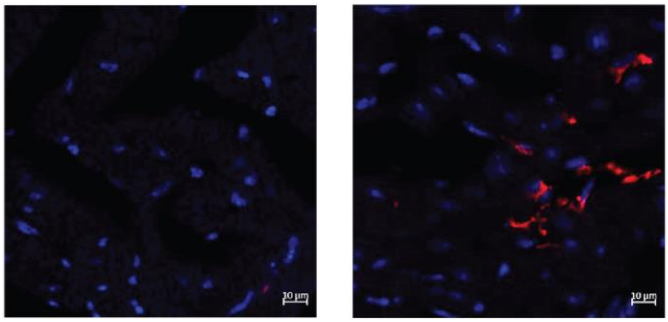

Regarding this statement: “Furthermore, RUNX1 and MEOX1 increased along the F9 lineage but not the other lineages (Fig. 2L)”, did the authors investigate the other fibroblast clusters or just F2 v F9 as shown in Fig 2L? All clusters should be analyzed.

We thank the reviewer for this comment. We used Palantir to identify 3 distinct branches (**Fig. 4b**) and plotted RUNX1 and MEOX1 expression along these 3 lineages (**Fig. 4d**). The F2 vs F9 differential expression was performed specifically to compare transcription factors which specify fate in these 2 populations previously thought to be a single cell type. We have shown MEOX1/RUNX1 in all 3 lineages (**Fig. 4d**) and shown expression of donor and heart failure associated genes also across all 3 lineages (**Fig. 4c**).

Figure 2N is labeled as betweenness centrality in the legend and differential ATAC accessibility in the results. Both would be interesting to see.

We thank the reviewer for this important comment. Initially, we had a limited number of samples in the Multiome dataset which precluded a robust un-biased analysis. However, we have added many new Multiome donor and HF samples for a total of 23. Using this expanded dataset, we performed an un-biased analysis between donor and HF chromatin accessibility, leveraged the multi-omic RNA/ATAC element via peak-2-gene linkage to identify key genes whose RNA and chromatin changes in HF. We have performed this additional analysis and amended figure 2 to reflect these changes and have added the following to the main text:

“We first computed the differential accessibility in fibroblasts between non-failing donors and failing hearts (**Fig. 2l**). We found 15,373 features up and 12,701 features down in heart failure. Using the peak to gene links, we identified nearby genes linked to these differentially accessible peaks based on a high correlation between gene accessibility and expression within the same nuclei – we found 3,167 unique genes linked to differentially accessible peaks (**Fig. 2m**). We overlapped this gene list with the pseudobulk RNA differential expression gene list between donor and heart failure and found 234 overlapping genes (**Fig. 2m**). We then used intersecting genes (those which are increased in heart failure at the RNA and chromatin level) and looked for enrichment in different fibroblast cell states – we found that the F9 fibroblast had the greatest enrichment of this gene set and a gene set score of the intersecting genes as a dot plot shows greatest expression within F9 (**Fig. 2n**).”

For the differential ATAC accessibility, how many of the other marker genes in this cluster also have differential ATAC accessibility and in how many of the cases does it move in the predicted manner (e.g. more accessible, more transcribed)? Is accessibility of the gene body or a nearby regulatory element considered?

We thank the reviewer for this important comment. Initially, we had a limited number of samples in the Multiome dataset which precluded a robust un-biased analysis. However, we have added many new Multiome donor and HF samples for a total of 23. Using this expanded dataset, we performed an un-biased analysis between donor and HF chromatin accessibility, leveraged the multi-omic RNA/ATAC element via peak-2-gene linkage to identify key genes whose RNA and chromatin changes in HF. We have performed this additional analysis and amended figure 2 to reflect these changes and have added the following to the main text:

“We first computed the differential accessibility in fibroblasts between non-failing donors and failing hearts (**Fig. 2l**). We found 15,373 features up and 12,701 features down in heart failure. Using the peak to gene links, we identified nearby genes linked to these differentially accessible

peaks based on a high correlation between gene accessibility and expression within the same nuclei – we found 3,167 unique genes linked to differentially accessible peaks (**Fig. 2m**). We overlapped this gene list with the pseudobulk RNA differential expression gene list between donor and heart failure and found 234 overlapping genes (**Fig. 2m**). We then used to intersecting genes (those which are increased in heart failure at the RNA and chromatin level) and looked for enrichment in different fibroblast cell states – we found that the F9 fibroblast had the greatest enrichment of this gene set and a gene set score of the intersecting genes as a dot plot shows greatest expression within F9 (**Fig. 2n**)."

Figure 2

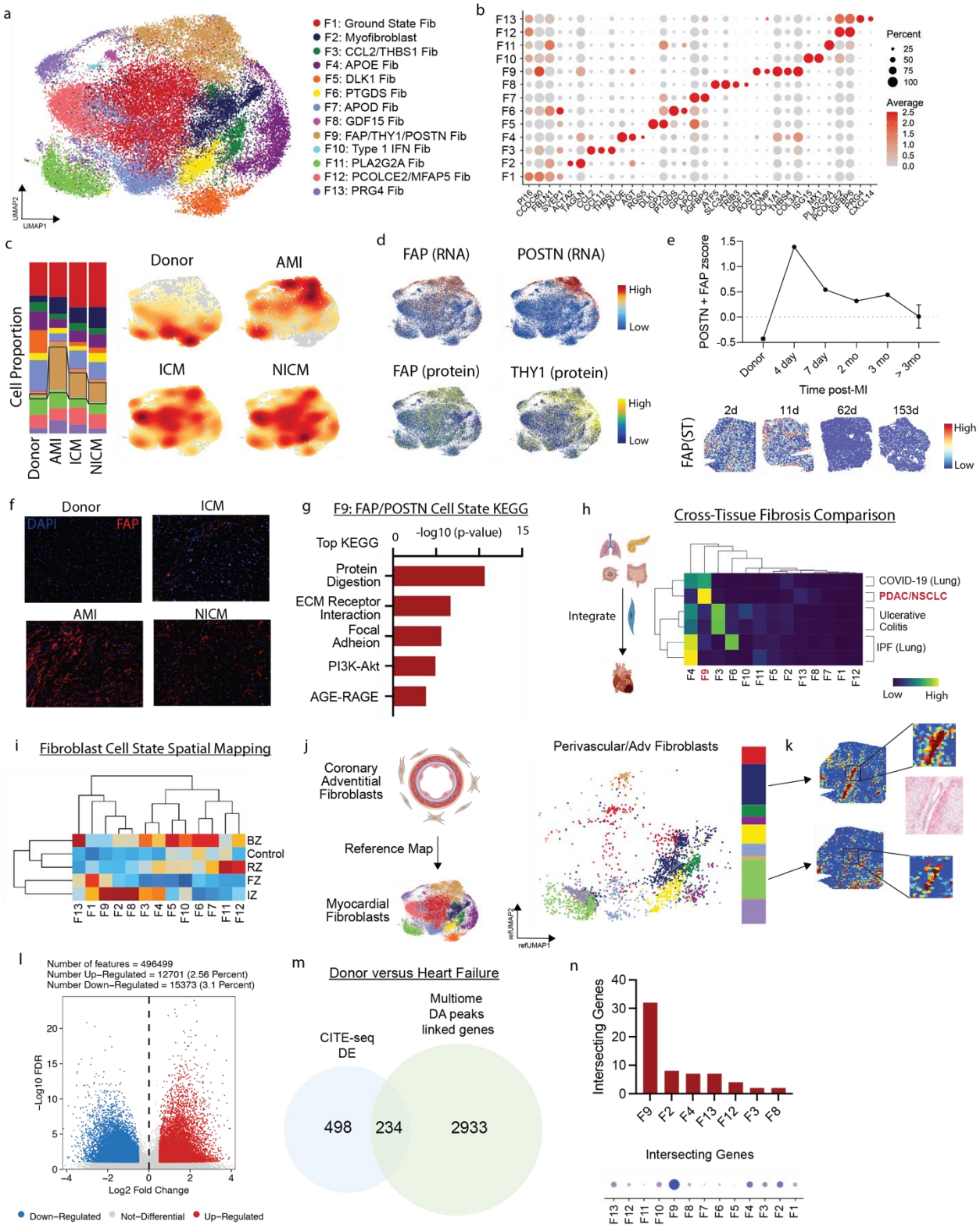
a
F1: Ground State Fib
F2: Myofibroblast
F3: CCL2/THBS1 Fib
F4: APOE Fib
F5: DLK1 Fib
F6: PTGDS Fib
F7: APOD Fib
F8: GDF15 Fib
F9: FAP/THY1/POSTN Fib
F10: Type 1 IFN Fib
F11: PLA2G2A Fib
F12: PCOLCE2/MFAP5 Fib
F13: PRG4 Fib
UMAP1
UMAP2
b
Percent
Average
c
Donor
AMI
ICM
NICM
Cell Proportion
d
FAP (RNA)
POSTN (RNA)
FAP (protein)
THY1 (protein)
High
Low
e
POSTN + FAP zscore
Donor
4 day
7 day
2 mo
3 mo
>3mo
Time post-MI
2d
11d
62d
153d
FAP(ST)
f
DAPI
FAP
g
F9: FAP/POSTN Cell State KEGG
Top KEGG
-log10 (p-value)
Protein Digestion
ECM Receptor Interaction
Focal Adheion
PI3K-Akt
AGE-RAGE
h
Cross-Tissue Fibrosis Comparison
Integrate
COVID-19 (Lung)
PDAC/NSCLC
Ulcerative Colitis
IPF (Lung)
Low
High
i
Fibroblast Cell State Spatial Mapping
BZ
Control
RZ
FZ
IZ
j
Coronary Adventitial Fibroblasts
Reference Map
Myocardial Fibroblasts
Perivascular/Adv Fibroblasts
k
l
Number of features = 496499
Number Up-Regulated = 12701 (2.56 Percent)
Number Down-Regulated = 15373 (3.1 Percent)
-Log10 FDR
Log2 Fold Change
Down-Regulated
Not-Differential
Up-Regulated
m
Donor versus Heart Failure
CITE-seq DE
Multiome DA peaks linked genes
498
234
2933
n
Intersecting Genes

The comparison with previously published mouse scRNA-seq data is a strength of this work. Regarding these analyses: what is meant by ‘strong mapping across all populations’? I understand the coloring in SFigure 6B, but as a control, what comparison would produce weak mapping? What would this look like?

We thank the reviewer for this comment. Strong mapping across all populations implies that as per Seurat (https://satijalab.org/seurat/articles/multimodal_reference_mapping) there is a high prediction score for mapping a given cell from the query onto the reference dataset. Specifically, if there are n clusters in the reference dataset then the reference mapping procedure for a given cell in the query dataset will compute a prediction score for that cell to be mapped into each of the reference clusters 1, …, n and the final annotation is assigned based on which cluster has the highest mapping score from 0 to 1. A strong mapping is obtained when there is a high mapping score to a given cluster and a weak mapping score would have a low mapping score to the “most likely” cluster. A comparison of strong and weak mapping can be seen when comparing the in vitro and in vivo data Figure 3. Specifically, the in vivo data shows strong mapping as highlighted by the high mapping scores whereas the in vitro data shows lower mapping scores as highlighted by the histogram in Figure 3h. Please find attached below.

Figure 3

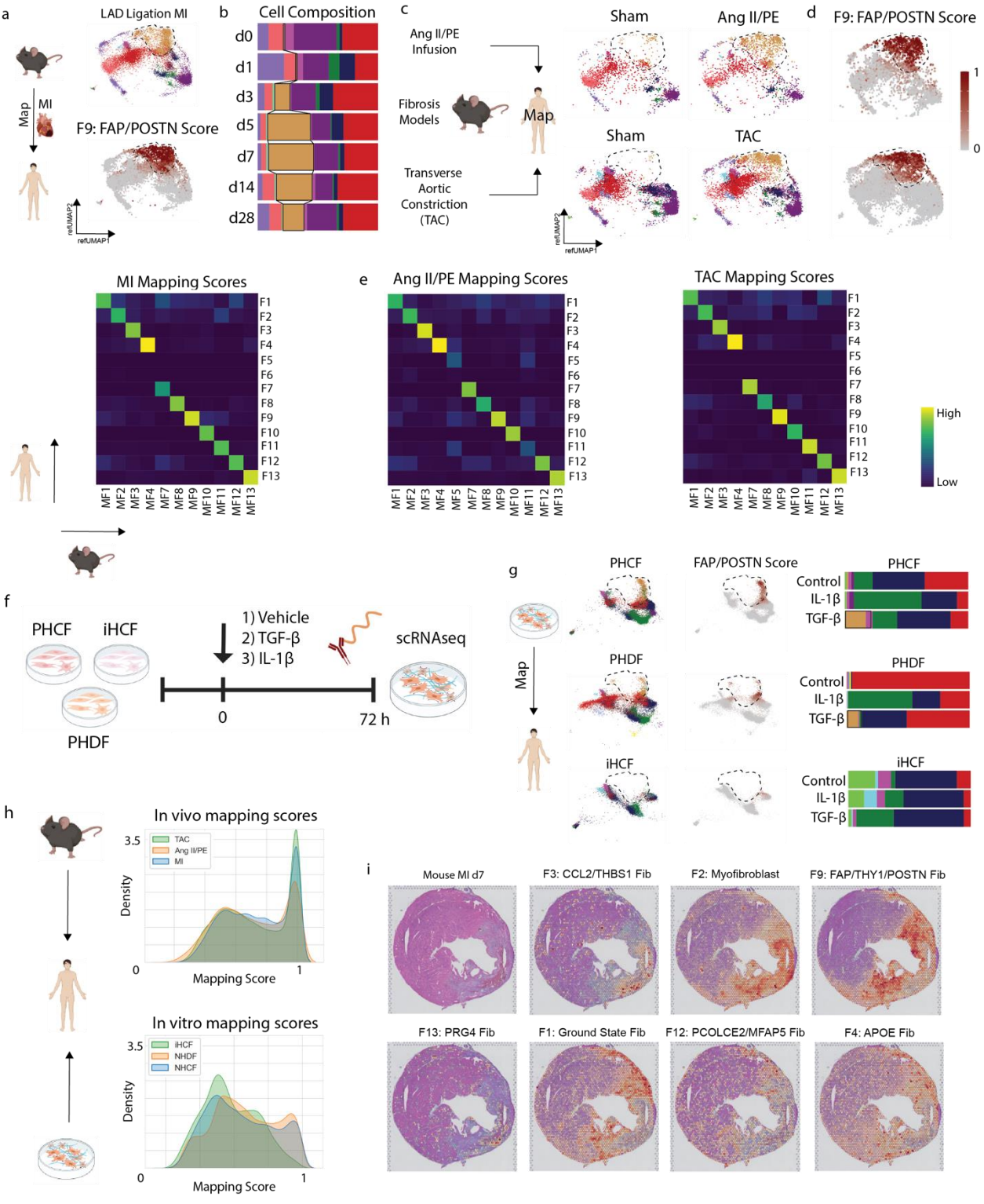
a
LAD Ligation MI
Map
MI
F9: FAP/POSTN Score
refUMAP2
refUMAP1
b
Cell Composition
d0
d1
d3
d5
d7
d14
d28
c
Ang II/PE Infusion
Fibrosis Models
Transverse Aortic Constriction (TAC)
Map
Sham
Ang II/PE
Sham
TAC
d
F9: FAP/POSTN Score
1
0
MI Mapping Scores
e
Ang II/PE Mapping Scores
TAC Mapping Scores
F1
F2
F3
F4
F5
F6
F7
F8
F9
F10
F11
F12
F13
MF1
MF2
MF3
MF4
MF5
MF7
MF8
MF9
MF10
MF11
MF12
MF13
High
Low
f
PHCF
iHCF
PHDF
1) Vehicle
2) TGF-β
3) IL-1β
0
72 h
scRNAseq
g
PHCF
FAP/POSTN Score
PHDF
iHCF
Map
Control
IL-1β
TGF-β
h
In vivo mapping scores
TAC
Ang II/PE
MI
Density
Mapping Score
In vitro mapping scores
iHCF
NHDF
NHCF
i
Mouse MI d7
F3: CCL2/THBS1 Fib
F2: Myofibroblast
F9: FAP/THY1/POSTN Fib
F13: PRG4 Fib
F1: Ground State Fib
F12: PCOLCE2/MFAP5 Fib
F4: APOE Fib

To address the second point made by the reviewer “what comparison would produce weak mapping? What would this look like?” we used a two-prong approach: (1) we sampled cardiac fibroblasts from the global object (these would be expected to display a strong mapping profile) and mapped them onto the fibroblast cell states (Fig. 2a) and (2) we sampled cardiac endothelial cells from the global object (these would be expected to display a weak mapping profile) and mapped them onto the fibroblast cell states (Fig. 2a). We have created a new Supplementary Figure 25 (attached below) to show this additional analysis. As evident, the fibroblast-to-fibroblast mapping histogram of mapping scores has a peak towards 1 (high mapping scores) while the endothelial cell mapping onto fibroblasts has a lower mapping score with a peak around 0.5.

We have added the following to the manuscript to reflect this additional analysis. “To validate our mapping strategy, we used a two-prong approach: (1) we sampled cardiac fibroblasts from the global object (these would be expected to display a strong mapping profile) and mapped them onto the fibroblast cell states (**Fig. 2a**) and (2) we sampled cardiac endothelial cells from the global object (these would be expected to display a weak mapping profile) and mapped them onto the fibroblast cell states (**Fig. 2a**). Fibroblast-to-fibroblast mapping histogram of mapping scores has a peak towards 1 (high mapping scores) while the endothelial cell mapping onto fibroblasts has a lower mapping score with a peak around 0.5 (**Supplementary Figure. 15**).”

Supplementary Figure 15

a Mapping cardiac fibroblasts onto fibroblast cell states

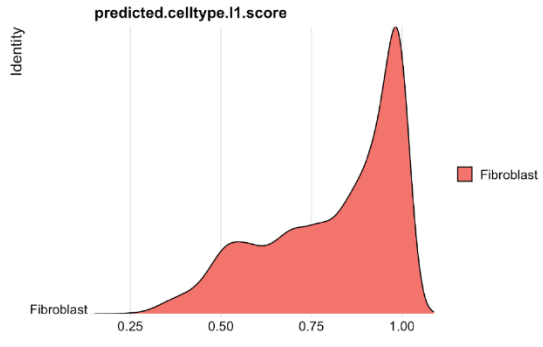


b Mapping cardiac endothelium onto fibroblast cell states

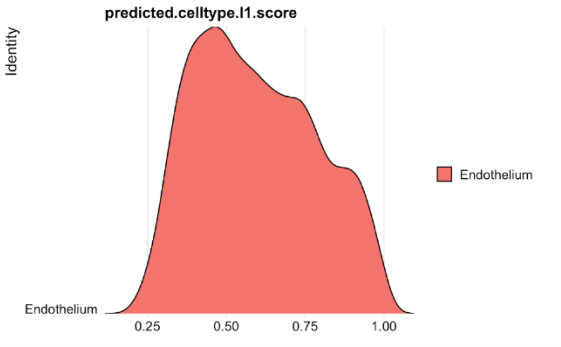

If you map previously published data onto your CITED-seq clusters, how do you avoid overfitting? This analysis gives the impression that one would generate the same clusters from these different datasets with the same data analysis methods, but without using the cell type assignments from one to label the other. But I do not think this is what has been done here. Do you regenerate the clusters in Figure 6A without reference to the CITED data in your study? It sounds like you are using the already generated clusters and mapping onto them the expression data from other mouse studies. If this is the case, how similar are the data if you just cluster them completely independently of each other (i.e. cluster the mouse data without reference to the human data)? Either way, please make this clearer in results and figures. These same questions apply to Figure 3.

We thank the reviewer for addressing this important point. The purpose of mapping the previously published and newly generated mouse data from cardiac injury models was to view the populations in the same nomenclature of the human heart cell states and to test whether the mouse failing cardiac fibroblasts recapitulate the diversity seen in human hearts. The reviewer makes a very good point regarding overfitting and to expand on this point, it is important to note that reference mapping will mapping any given query cell onto the reference. However, if the query has poor mapping it will be reflected by the mapping scores. As an example, to show what strong vs weak mapping would look like we used a two-prong approach: (1) we sampled cardiac fibroblasts from the global object (these would be expected to display a strong mapping profile) and mapped them onto the fibroblast cell states (Fig. 2a) and (2) we sampled cardiac endothelial cells from the global object (these would be expected to display a weak mapping profile) and mapped them onto the fibroblast cell states (Fig. 2a). We have created a new Supplementary Figure 25 (attached above) to show this additional analysis. As evident, the fibroblast-to-fibroblast mapping histogram of mapping scores has a peak towards 1 (high mapping scores) while the endothelial cell mapping onto fibroblasts has a lower mapping score with a peak around 0.5.

The purpose of mapping mouse fibroblasts to human fibroblasts was to dissect which human states are present in mouse models of cardiac injury and the transcriptional similarity between human and mouse as evident by the mapping scores.

To address the reviewer's point, we have independently clustered the mouse MI, Ang II/PE, and TAC fibroblast single cell RNA-seq data. We next created gene signatures for the human CITE-seq fibroblast cell states using the key marker genes (Supplementary Figure 3) and plotted these in the independent mouse clusters and constructed dot plots to show which mouse clusters are enriched with the different human fibroblast cell state gene signatures. To reflect this additional analysis, we have created a new Supplementary Figure 26 attached below. Notably, we see that all the clusters which showed evidence of mapping also mapped to mouse clusters. F11 was not present in either of the 3 mouse datasets and from the human coronary artery fibroblast mapping, F11 is associated with adventitial fibroblasts. F6 was also largely absent from the mouse datasets as the F6 signature did not map to any of the mouse clusters. Using 2 orthogonal methods, we show good concordance between human and mouse clusters.

We added the following to the manuscript to reflect this additional analysis: "We independently clustered the mouse MI, Ang II/PE, and TAC fibroblast single cell RNA-seq data and created gene signatures for the human CITE-seq fibroblast cell states using the key marker genes. To assess concordance of clustering, we plotted these signatures in the independent mouse clusters and constructed dot plots to show which mouse clusters are enriched with the different human fibroblast cell state gene signatures. Notably, we see that all the clusters which showed evidence of mapping also mapped to mouse clusters. F11 was not present in either of the 3

mouse datasets and from the human coronary artery fibroblast mapping, F11 is associated with adventitial fibroblasts. F6 was also largely absent from the mouse datasets as the F6 signature did not map to any of the mouse clusters (**Supplementary Fig. 16**)."

Supplementary Figure 16

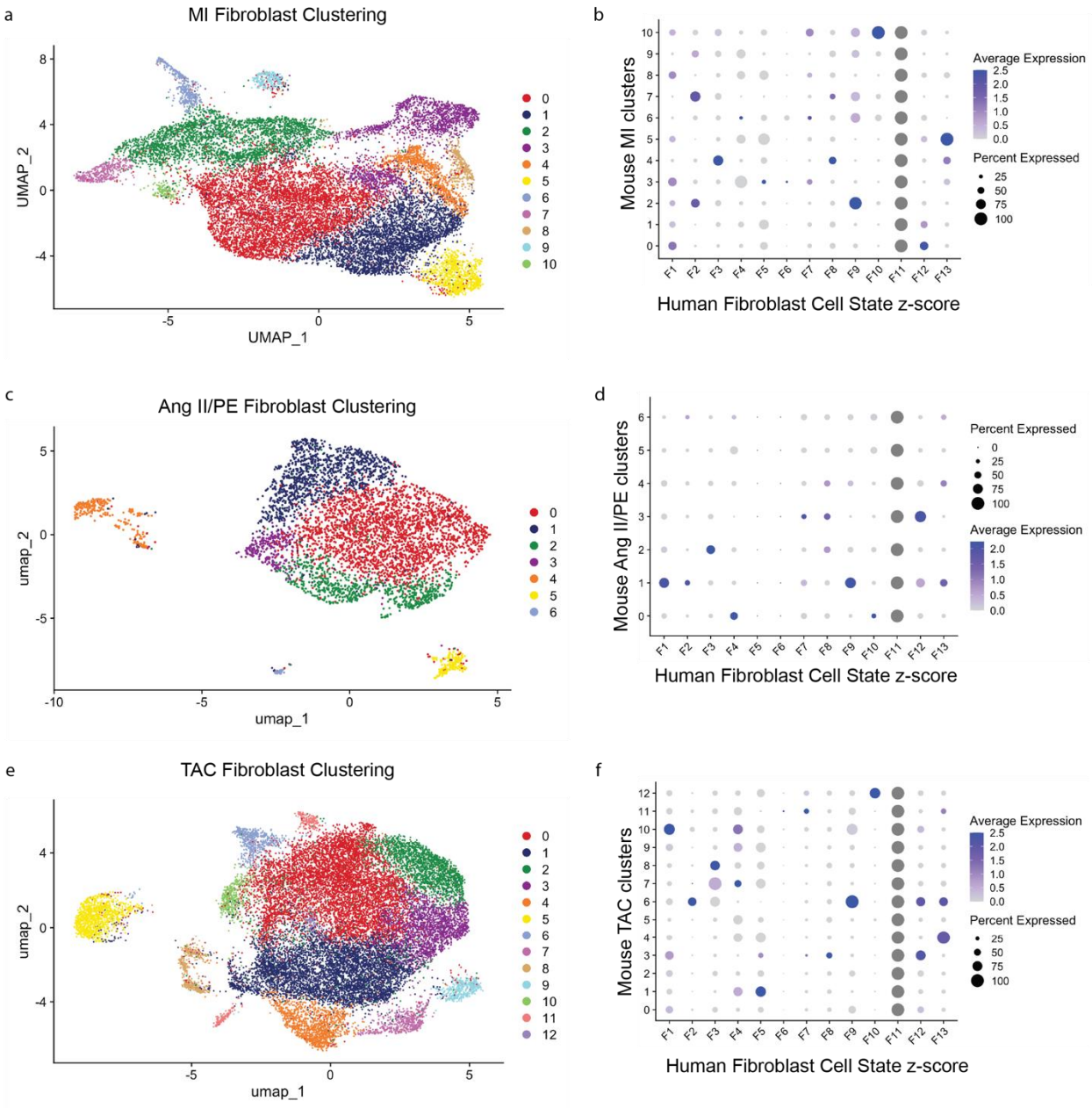

Regarding this statement: “Multiple biological and technical replicates were included, individually hash tagged, and pooled to minimize any potential batch effects (Fig. 3F).” If the replicates were separately bar coded, the authors should be able to retrieve the individual sample information and analyze this variability. Such analyses would be very useful to the field towards the goal of understanding variability in single cell measurements.

We thank the reviewer for this comment. As described in the manuscript, “Multiple biological and technical replicates were included, individually hash tagged, and pooled to minimize any potential batch effects (Fig. 3f).” Furthermore, we performed clustering and data integration within each in vitro sample with control, TGF-β, and IL-1β treatment. We have shown the clustering with marker genes for each in vitro cell culture system in Supplementary Figure 11. Additionally, we have done sample level QC and overlaid technical and biological replicate meta data on the integrated UMAP in Supplementary Figure 10. To assess the variability among technical and biological replicates under treatment, we clustered all replicates together, and then constructed a stack plot of relative compositions by biological/technical replicate and have created a new Supplementary Figure (Supplementary Figure 27). We do not find much variability between technical replicates, but interestingly, we do find some variability across biological replicates. This variability exists in the baseline condition suggesting a very important point the reviewers bring up, that there can be batch effects in baseline plated fibroblasts given their source and transcriptional plasticity. These are important considerations for planning future experiments as it emphasizes the need for multiple hash tagged biological replicates to improve the robustness of biological findings.

We have added the following to the main text of the manuscript to highlight this important point: “Hashed biological and technical replicates were de-multiplexed to identify potential batch effects and inherent variability across different replicates – we found that while there was minimal variability amongst technical replicates, there was some biological variability across batches, highlighting the baseline plasticity inherent in cultured fibroblasts models (**Supplementary Fig. 19**).”

Supplementary Figure 19

a

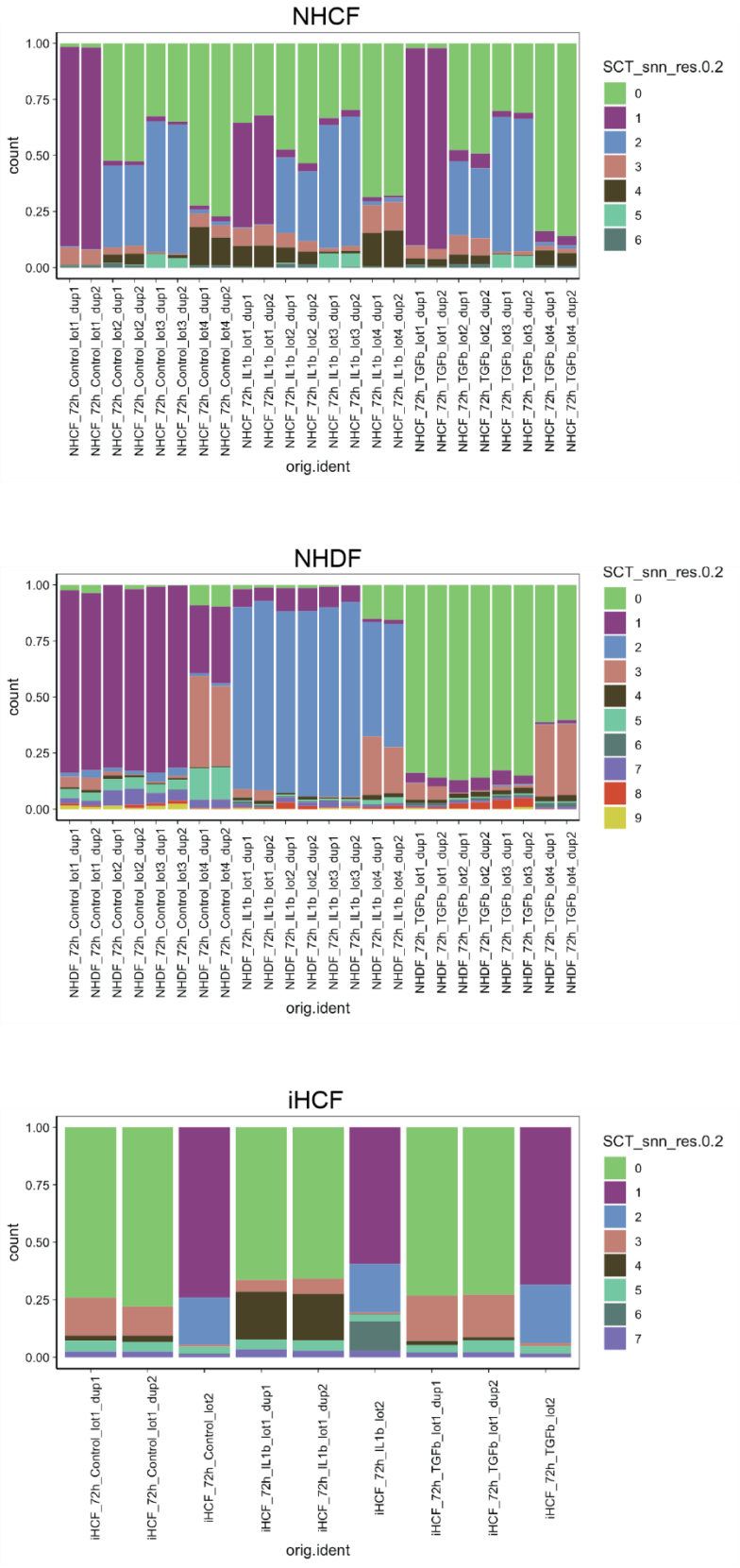

How Figure 4J was generated and what it shows is unclear. Also, for Figure 4M. The relationship between ‘spatial niches’ and ‘spatial clusters’ is unclear.

We thank the reviewer for this important comment. We apologize for the confusing terminology, but “spatial niches” and “spatial clusters” are intended to refer to the same thing. The original Figure 4j (now Figure 5g) was generated by performing clustering and UMAP embedding construction on the spatial spots to identify transcriptionally distinct spatial niches. Figure 4m (now Figure 5j) is a heatmap of the top differentially expressed genes across the different spatial niches computed using standard differential expression in Seurat – the goal of this analysis was to find marker genes for the different spatial niches. Throughout the manuscript, we have only used the term “spatial niches” to avoid any confusion.

Please show level of Il1beta and Il1 receptor protein expression in control, Il1rflox/flox dermo1-cre, and both strains with AngII/PE in macrophages and cardiac fibroblasts. Also, the level of circulating Il1beta should be tested in all these conditions.

We thank the reviewer for this comment. Given the chronic and relatively mild nature of the Ang II/PE injury model, there is a small rise in serum cytokine levels and other groups have already performed extensive cytokine analysis under Ang II/PE infusion (PMID 31511695). As such, we did not measure the circulating levels of IL-1β.

To validate the knockdown of Il1r in our Dermo1-Cre fibroblasts, we sorted macrophages and fibroblasts as the reviewer suggests and performed qPCR for Il1r1 in these cell in IL-1R$^{flox/flox}$ and IL-1R$^{flox/flox}$Dermo1$^{Cre}$ mice 7 days after Ang II/PE infusion. We have added the following to the results section of the manuscript and created a new supplementary figure displaying these results: “To validate knockdown of the *IL-1R*, we sorted macrophages fibroblasts from IL-1R$^{flox/flox}$ and IL-1R$^{flox/flox}$Dermo1$^{Cre}$ mice 7 days after Ang II/PE infusion (**Supplementary Fig. 26a**) – using qPCR on sorted cells, we verify decreased *IL-1R* expression in fibroblasts but not macrophages (**Supplementary Fig. 26b**).”

Supplementary Figure 26

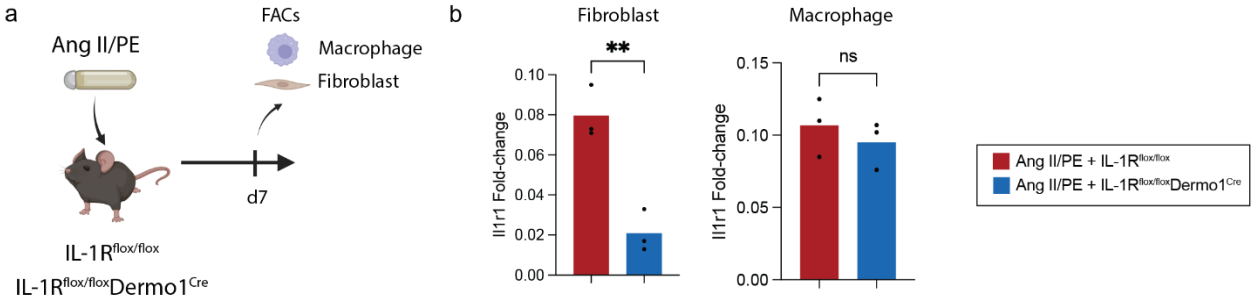

The ability of Il1beta to influence ventricular remodeling by inhibiting fibrosis has been known for some time (PMID: 11691538). The experiments in Figure 5 add detail to the molecular features of the different cells contributing to this phenomenon. The investigators need to show whether Il1b mAb treatment influences fibrosis in this model and the effects on systolic and diastolic cardiac function.

To address the relevant source of IL-1β and the effect of IL1-β on fibrosis and cardiac function, we genetically deletion of IL-1β in monocytes and monocyte-derived macrophages. We chose this approach as neutralizing antibody treatment may not completely ablate the effects of IL-1β. To this end, we generated IL-1β $^{flox/flox}$ Ccr2$^{creERT2}$ mice to specifically knockout IL-1β in monocytes and monocyte-derived macrophages. We focused specifically on CCR2 monocytes and macrophages because both the human and mouse data support that these are the dominant cell types which produce IL-1β in heart failure. We then performed Ang II/PE pump implantation with continuous tamoxifen dosing throughout the duration of the experiment and characterized early Fap activation at day 7 by flow cytometry, fibrosis, and systolic and diastolic function with echocardiography at 28 days post Ang II/PE pump implantation. Briefly, we found that the IL-1β $^{flox/flox}$ Ccr2$^{creERT2}$ mice had fewer FAP+ fibroblasts at day 7, decreased fibrosis, and improved systolic and diastolic function compared to IL-1β $^{flox/flox}$ mice. We have amended figure 6 and the main manuscript text to reflect these new experiments and additional analysis.

"***IL-1β derived from CCR2+ monocytes and macrophages is causally linked to fibrosis and diminished cardiac function.***
To determine whether IL-1β derived from CCR2$^{+}$ monocytes and macrophages is necessary for cardiac fibrosis, we generated mice that lack IL-1β in CCR$^{2+}$ monocytes and macrophages (IL-1β$^{flox/flox}$ Ccr2$^{creERT2}$). Control and IL-1β$^{flox/flox}$ Ccr2$^{creERT2}$ mice underwent sham surgery or received Ang II/PE eluting osmotic minipumps (**Fig. 6i**). To characterize early fibroblast activation, mice were sacrificed after 7 days of Ang II/PE infusion and hearts enzymatically digested for flow cytometry. Quantification of flow cytometry data revealed an increase in the proportion of FAP$^{+}$ fibroblasts in Ang II/PE treated animals compared to sham surgeries and importantly fewer FAP$^{+}$ fibroblasts in IL-1β$^{flox/flox}$ Ccr2$^{creERT2}$ mice compared to IL-1β$^{flox/flox}$ mice (**Fig. 6j**). Transthoracic echocardiography (TTE) was performed after 28 days of Ang II/PE infusion to characterize the impact of IL-1β deletion in CCR2+ cells on cardiac function. TTE showed a significant decrease in E/e' and end systolic volume (ESV) with a significant improvement in fractional shortening (FS) an ejection fraction (EF) in IL-1β$^{flox/flox}$ Ccr2$^{creERT2}$ mice compared to IL-1β$^{flox/flox}$ mice (**Fig. 6k, l**). Fibrosis was quantified after 28 days of Ang II/PE infusion by trichrome staining. Ang II/PE infusion resulted in deminished interstitial fibrosis in IL-1β$^{flox/flox}$ Ccr2$^{creERT2}$ mice compared to IL-1β$^{flox/flox}$ mice (**Fig. 6m**)."

Figure 6

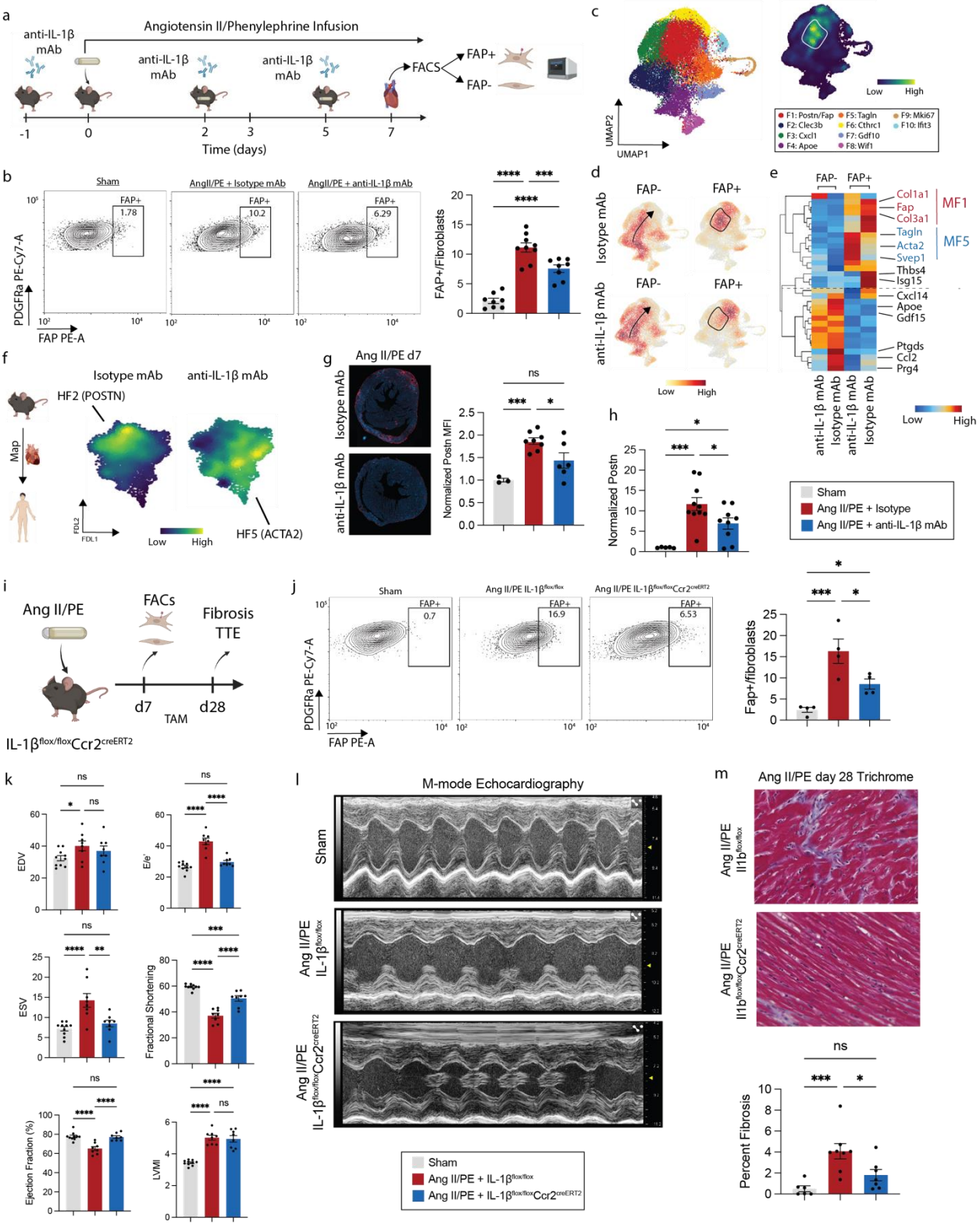
a
anti-IL-1β mAb
Angiotensin II/Phenylephrine Infusion
anti-IL-1β mAb
anti-IL-1β mAb
FACS
FAP+
FAP-
-1
0
2
3
5
7
Time (days)
b
Sham
AngII/PE + Isotype mAb
AngII/PE + anti-IL-1β mAb
FAP+
1.78
10.2
6.29
PDGFRa PE-Cy7-A
FAP PE-A
FAP+/Fibroblasts
c
UMAP2
UMAP1
Low
High
F1: Postn/Fap
F2: Clec3b
F3: Cxcl1
F4: Apoe
F5: Tagln
F6: Cthrc1
F7: Gdf10
F8: Wif1
F9: Mki67
F10: Ifit3
d
FAP-
FAP+
Isotype mAb
anti-IL-1β mAb
Low
High
e
FAP-
FAP+
Col1a1
Fap
Col3a1
MF1
Tagln
Acta2
Svep1
MF5
Thbs4
Isg15
Cxcl14
Apoe
Gdf15
Ptgds
Ccl2
Prg4
anti-IL-1β mAb
Isotype mAb
anti-IL-1β mAb
Isotype mAb
Low
High
Sham
Ang II/PE + Isotype
Ang II/PE + anti-IL-1β mAb
f
Isotype mAb
anti-IL-1β mAb
HF2 (POSTN)
Map
FDL2
FDL1
Low
High
HF5 (ACTA2)
g
Ang II/PE d7
Isotype mAb
anti-IL-1β mAb
Normalized Postn MFI
h
Normalized Postn
i
Ang II/PE
FACs
Fibrosis
TTE
d7
TAM
d28
IL-1β^flox/flox Ccr2^creERT2
j
Sham
Ang II/PE IL-1β^flox/flox
Ang II/PE IL-1β^flox/flox Ccr2^creERT2
FAP+
0.7
16.9
6.53
PDGFRa PE-Cy7-A
FAP PE-A
Fap+/fibroblasts
k
EDV
E/e'
ESV
Fractional Shortening
Ejection Fraction (%)
LVMI
l
M-mode Echocardiography
Sham
Ang II/PE IL-1β^flox/flox
Ang II/PE IL-1β^flox/flox Ccr2^creERT2
Sham
Ang II/PE + IL-1β^flox/flox
Ang II/PE + IL-1β^flox/flox Ccr2^creERT2
m
Ang II/PE day 28 Trichrome
Ang II/PE Il1b^flox/flox
Ang II/PE Il1b^flox/flox Ccr2^creERT2
Percent Fibrosis

Given the known role of Il1b in fibrosis, it is uncertain how the reader will use the information in this paper for future studies. Efforts by the authors to make clearer how to repeat identification and characterization of the fibroblast subpopulations described in this study, and whether these subpopulations are differentially involved in the effects of Il1b, would increase the impact of the study.

We thank the reviewer for this very important comment. Considering the very relevant suggestions made by the reviewer, we have expanded the work in the manuscript with additional human data, computational analysis, and novel mouse models to better characterize immune-fibroblast crosstalk in the failing human heart. Below, we outline the novel elements of the work herein and how it relates to and advances prior work in the field. Points 3-4 highlight our revisions that provide additional in vivo evidence that support our conclusions.

1. We added extensive new human data for a total of 22 CITE-seq from fresh hearts and 23 Multiome (RNA/ATAC) from frozen hearts. Both these data elements are novel and there are currently no studies which have profiled RNA, protein, and ATAC from failing human hearts. Importantly, the CITE-seq was performed in fresh explanted hearts from non-failing donors, acutely infarcted tissues (within a week of MI), and chronically failing hearts. These data offer an unprecedented opportunity to characterize cells from diseased human hearts and identify cell states at high granularity. We believe that this data can be of use to the broader field to identify new hypothesis, annotate existing datasets at higher resolution, leverage the ever-growing computational models to gain deeper insights from these data, and interpret newly generated human and mouse omics data in the context of these high-resolution state annotations. To facilitate these applications, we will be working with the human cell atlas to share out data in a user-friendly portal as well as the Seurat team to build an Azimuth reference so future studies can seamlessly map their data onto this reference for imputation of cell states and surface protein information.

2. An important consideration for translational studies for new targets is the applicability of experimental findings to human disease. Here in, we have utilized published data and generated additional single cell data from the 3 most widely used in vivo models of cardiac injury (MI, Ang II/PE infusion, and TAC) and compared this to newly generated single cell RNA sequencing data from human cell culture systems of fibroblast activation. Using integrated cell mapping, we show that the in vivo models are better surrogates for the populations identified in human hearts as compared to the cell culture systems. These findings are useful for the field as they can leverage our human data to compare how in vivo and in vitro perturbations may affect the corresponding human heart cell states which can have tremendous translation value.

3. Using the human CITE-seq data, we identify transcriptionally distinct myofibroblast and POSTN cell states which have previously largely considered a single population. Recent studies have leveraged immunomodulator approaches like CAR T cells to target activated fibroblasts marked by fibroblast activator protein (FAP) to target cardiac fibrosis which highlights the therapeutic potential of this cell state. Importantly, to deplete these cells or modify their cell state transitions, it is critical to understand the precise markers of this population in humans as well as the lineages they go down in the injured heart. Given the plastic nature of fibroblasts and the dearth of genetic tools to study FAP+ fibroblasts, there is no data on how these fibroblasts evolve in the injured heart as well as their molecular markers in human tissue. Using an array of orthogonal techniques: single cell RNA-sequencing, immunofluorescence, and in vivo lineage

tracing with a novel Fap-cre mouse, we show that these populations are distinct transcriptional states and come from different lineages in the failing heart. These are very important findings and tools for future studies targeting activated fibroblasts.

4. We further leverage the human multi-omic data in additional to integration with published spatial transcriptomics data to identify IL-1β as a potential therapeutic target to hinder macrophage fibroblast crosstalk. Within the human data, show that CCR2 monocytes and macrophages are producing the IL-1β which is predicted to signal to activated fibroblasts and drive fibrosis in heart failure. We generated mice lacking the IL-1R on fibroblasts and showed that in Ang II/PE infusion there is decreased fibroblast activation and less fibrosis compared to controls. Additionally, we use a monoclonal anti-IL-1β neutralizing antibody to show that IL-1β suppression reshapes the early activation landscape of fibroblasts. To mechanistically implicate CCR2 monocytes and macrophages as the causal cell state in driving fibrosis, we generated mice lacking the IL-1β ligand in CCR2 cells showed that in Ang II/PE infusion there is decreased fibroblast activation, less fibrosis, and improved systolic and diastolic function compared to controls. Our findings highlight the potential for targeting IL-1β in patients with heart failure, a finding that is consistent with secondary analysis of the CANTOS clinical trial (PMID 28845751).

**Reviewer Reports on the First Revision:**

Referee expertise:

Referees' comments:

Referee #1 (Remarks to the Author):

The revised manuscript by Amrute et al. has improved however the claims are still insufficiently supported by functional validation. The points that would need to be addressed in order to be considered appropriate for publication in Nature are listed below.

Major Points:
1. The GRN analysis presented in Figure 4 (and linked supplementary figures should be provided), which is central to the main message of the paper, lacks functional validation. More specifically, the authors have still not experimentally validated the inferred relationship between IL1b and IL1R signaling and the downstream transcriptional activities that drive the F9 phenotype. This analysis should help to strengthen the weak and indirect connection between POSTN and RUNX1 and address the absence of any convincing connection with MEOX1.
2. While the manuscript title suggests a cross-talk between the immune and fibroblast compartments the data do not currently support the authors' thesis. The functional evidence in support of macrophage-to-fibroblast communication is reasonable the evidence in support of the opposite is lacking. The manuscript would be greatly improved by the inclusion of functional data showing that CCR2+ monocytes/macrophages receive essential signal from fibroblasts. For example, is F3 a key source of CCL2 for CCR2+ monocytes/macrophages in the setting of cardiac stress?
3. Are monocyte-derived macrophages or tissue-resident macrophages, both of which express CCR2 in the heart, more important for driving the F9 phenotype? The data presented in Figure 5k and S10 do not convincingly show that CCR2/IL1B+ monocytes occupy the same niches as POSTN/RUNX1+ fibroblasts. Can the authors use a higher resolution method to further evaluate this spatial interaction?
4. Figure 5a suggests that TGFB is a major component of the cell-cell communication circuit. Does TGFB contribute to the F9 phenotype in addition to IL1B (which only partially contributes to the expansion of POSTN+ fibroblasts)?

Minor Point:
5. In lines 421-422 the authors incorrectly referred to FBN1 and FOSX1 as transcription factors. The text and accompanying figure should be corrected.

Referee #2 (Remarks to the Author):

In this revised version of the manuscript the authors have addressed several critical points raised in the first revision, including: some location issues of the pathogenic fibroblasts subsets and their interaction with macrophages, the identity of CCR2+ infiltrating monocyte/macrophage as a relevant source of IL1b in cardiac pathogenic contexts, and the paracrine IL1b responsiveness of fibroblasts through IL1R. While the data generally validates the conclusions of the paper, there are still a substantial number of minor limitations that need to be addressed. In particular, the authors have ignored some of my previous comments and continue to abuse the use of computational tools that generate confusion (including to this reviewer) rather than useful data, and the quality of many of the panels and figures is still low and can be improved substantially. Importantly, the issue of immune-fibroblastic niches remains in my opinion unclear with the tools used here. Finally, I find that a lot of the supplementary data based on reanalysis of the datasets in multiple different ways are not essential and in fact overload and distract from the flow of the paper and dilute the main message (see e.g. the analyses shown for Suppl Fig. 15 and 16).
I hope that these comments help to improve and otherwise interesting paper with profound therapeutic implications, as detailed below:
- the paper continues to abound in statements that direct to main or suppl. figures that are packed with data but fail to rigorously show the claim. For example, the claim that fibroblast populations localize in defined perivascular and interstitial spatial niches in Suppl Figs.7b-d. It is impossible to assess if this is the case and there is a lack of quantification. The text of these panels is also very small and difficult to follow. The authors have ignored my previous comments and instead have packed the figures even more in ways that I find counterproductive for the clarity of the message and for the readers.
- Related to the above, the claim that F9 fibroblasts associates most with myeloid cells and F2 with other vascular cells is central to the model proposed in the paper. This is assessed using spatial correlation analyses in Suppl Fig.10. The relevant panels here are in low resolution, with text difficult to read, and not assessing the different groups with recognizable names, such as F2 or F9, for example. This makes evaluation difficult if not impossible but also suggests rushed analyses that exclusively aim to validate a hypothesis, without actual rigorous demonstration.
- More on this, the relevant point that Postn, Runx1, Ccr2 and 1lb co-localize spatially in MI sections is presented in an image with low resolution and no quantification, so the claim remains largely unsupported by the data. It is unclear why immunofluorescence is not performed in MI samples to directly validate this claim at the protein level.
- The change in FAP+ fibroblasts in the different experimental groups (Il1b-floxed mice, etc.) cannot be shown by this cytometric assay that does not match or explain the fibroblast diversity described through the paper and is in fact the basis of their finding. Imaging, sc transcriptomics or other consistent measured should be used. Also, it remains unclear to me why FAP+ vs FAPneg fibroblasts were sorted for scRNAseq in the control and anti-IL1b-treated mice, rather than just analyzing the total fibroblast compartment to examine for altered population frequencies particularly in the FAP/Postn subset. This data needs to be better organized and explained, ideally presenting only the experiments that justify the conclusion that anti-IL1b prevents the maturation towards the matrifibroblast state.
- The resolution and contrast of Fig.2f showing FAP staining needs to be improved. It is very difficult to

discern in a printout.
- In Pag.13, lines 439-441: “Using 68Ga-FAPi-46 non-invasive PET imaging, we confirmed early enrichment of FAP at d7 following AngII/PE infusion (Fig. 4k)”. These panels are not supported by any quantification or statistics.
- I don't understand the added value of Fig.4c beyond what is already shown as prediction in Figs.4a-b.
- Fig6g, it is difficult at this size and resolution to discriminate Postn staining, the authors should make a general effort to improve the images included in the different figures.
- Misspelling: line 69: “shoewed”
- Misspelling: line 680: therapy instead of therapeutic?
- typo: line 454 should be Fig5C, not 7C, right?
- typo: line 457 should be Fig5C, not 9C, right?
- Supplementary Figures 21a-f are not referred in the main document.
- Supplementary Figure 27 is not referred in the main document.
- The number of samples for each condition indicated in the text (Lines 166-169) does not match the information in Fig.1a
- It is difficult to follow changes in different fibroblasts subsets since those are referred as F1-13 in text and this information is not reflected in referred figures (i.e. Supl.Fig10a-d, Sspl.Fig12b)). Please standarize nomenclature
- Consider re-spelling. Lines 372-374: “F11 (associated with adventitial 373 fibroblasts) was not present in either of the 3 mouse datasets and from the human coronary artery fibroblast mapping, F11 is associated with adventitial fibroblasts”

Referee #3 (Remarks to the Author):

The authors have responded extensively to my concerns raised in first review. I have one comment regarding their response to the question of using IL-1b mAb to target IL-1b in vivo.

In the original paper, the authors state: “To dissect the therapeutic impact of IL-1b inhibition on fibroblast cell state transitions, we implanted mice with Ang II/PE osmotic minipumps treated animals with an IL-1b neutralizing antibody (anti-IL-1b mAb) or isotype control every 3 days (Fig. 5A).”

This experimental design posits that mAb against IL-1b will affect IL-1b and have a ‘therapeutic impact…on fibroblast cell state transitions.” The experiments in new Figure 6 B-H require the context of whether this mAb treatment affects the phenotypes measured elsewhere in this paper…in other words, does the mAb against IL-1b have a therapeutic benefit or not?

Thus I am confused by the authors’ response to my original request of “The investigators need to show whether Il1b mAb treatment influences fibrosis in this model and the effects on systolic and diastolic cardiac function.”, to which they replied “To address the relevant source of IL-1β and the effect of IL1-β on fibrosis and cardiac function, we genetically deletion [sic] of IL-1β in monocytes and monocyte-derived macrophages. We chose this approach as neutralizing antibody treatment may not completely ablate the effects of IL-1β.”

In fact, this is exactly what the reader needs to know: if the mAb intervention is used to identify the cell populations in Fig 6B-H, is this taking place in the context of effective IL-1b inhibition and rescue of the phenotype? If the mAb does not ablate the effects of IL-1b, as the authors anticipate, this is important to know in the context of the rest of the paper.

**Author Rebuttals to First Revision:**

**Referee #1 (Remarks to the Author):**

The revised manuscript by Amrute et al. has improved however the claims are still insufficiently supported by functional validation. The points that would need to be addressed to be considered appropriate for publication in Nature are listed below.

Follow up comment: I believe the authors of the Lavine manuscript have done a superb job with addressing almost all of the outstanding points and questions. While not every one of my comments was addressed I can overlook them because the other points have been rather definitively addressed. The impact of various perturbations/gene deletions/treatments did not completely resolve pathology or reverse cell differentiation states which is not unexpected in biological studies of this complexity. However, it is important that the authors of both papers not overstate their findings.

We are grateful for your invaluable comments and have made every effort to tone down the claims made in the manuscript. Additionally, we have highlighted which analyses are predictions throughout the manuscript. All high-quality pdf files for figures are available at:

(https://www.dropbox.com/scl/fo/bvrwsild7pnct26kcyu6c/AGphrJLw49Szs45A0tvExHM?rlkey=tlissrp3qs49c2b1cqfk6kwsu&dl=0).

Major Points:
1. The GRN analysis presented in Figure 4 (and linked supplementary figures should be provided), which is central to the main message of the paper, lacks functional validation. More specifically, the authors have still not experimentally validated the inferred relationship between IL1b and IL1R signaling and the downstream transcriptional activities that drive the F9 phenotype. This analysis should help to strengthen the weak and indirect connection between POSTN and RUNX1 and address the absence of any convincing connection with MEOX1.

We thank you for this very important comment. The key message of our manuscript is that IL1b constitutes a direct signal from monocyte-drive macrophages to cardiac fibroblasts that drives the emergence of FAP+POSTN+ fibroblasts, myocardial fibrosis, and LV remodeling. To causally validate this inferred interaction, we generated conditional KO mice where we deleted IL1b specifically in monocyte derived macrophages ($Ccr2^{creERT2}$) and deleted the receptor for IL1b (Il1r1) in fibroblasts ($Dermo1^{cre}$).

The GRN analysis is presented to highlight the utility of human heart Multiome (RNA/ATAC) data and how it can be applied to infer regulatory networks for the pathogenic fibroblast cell states we see in heart failure. These analyses are meant to be hypothesis generating and provide a resource for the community to shed light on potential regulatory mechanisms driving fibroblast state diversification in the human heart. This integrated analysis predicted MEOX1 and other transcription factors (including RUNX1) to be the most active regulator of the POSTN cell state. Importantly, our colleagues have co-submitted a manuscript where they dissect the epigenetic mechanism in detail of IL1b signaling within fibroblasts connecting MEOX1 to the FAP/POSTN+ fibroblast cell fate.

We acknowledge, that we do not causally explore the epigenetic mechanism within our manuscript and have amended the text and our conclusions to reflect that these are predictions made from human data and have made a stronger effort to connect our findings with the manuscript co-submitted from the Srivastava lab – the central message being IL1b as a regulator of fibrosis in humans with extensive animal validation. The human data support the

epigenetic mechanisms studied in the co-submitted manuscript by our colleagues and we have cited their paper as appropriate throughout the discussion.

2. While the manuscript title suggests a cross-talk between the immune and fibroblast compartments the data do not currently support the authors' thesis. The functional evidence in support of macrophage-to-fibroblast communication is reasonable the evidence in support of the opposite is lacking. The manuscript would be greatly improved by the inclusion of functional data showing that CCR2+ monocytes/macrophages receive essential signal from fibroblasts. For example, is F3 a key source of CCL2 for CCR2+ monocytes/macrophages in the setting of cardiac stress?

We appreciate the potential importance of fibroblast to macrophage signaling and agree that this is an area worthy of detailed investigation. However, our manuscript focused on signaling events that drive the emergence of FAP+POSTN+ macrophages (specifically macrophage to fibroblast signaling) and feel that dissecting the crosstalk from fibroblasts to macrophages is outside the scope of our manuscript. A prior study (PMID: 15774854) has shown that CCL2 in cardiac injury has an important role in macrophage recruitment, activation, and myofibroblast accumulation. While it is certainly feasible that the CCL2+ fibroblast subset interacts with the macrophages in the pathogenesis of heart failure, we feel that investigating this concept is outside the scope of the current manuscript as it would require extensive experimentation (including genetic models) to rigorously address. We hope that our human multi-omic dataset and analyses presented herein serves as a resource for the community to further study novel mechanisms of heart failure with fascinating targets such as CCL2 as pointed out by the reviewer.

3. Are monocyte-derived macrophages or tissue-resident macrophages, both of which express CCR2 in the heart, more important for driving the F9 phenotype? The data presented in Figure 5k and S10 do not convincingly show that CCR2/IL1B+ monocytes occupy the same niches as POSTN/RUNX1+ fibroblasts. Can the authors use a higher resolution method to further evaluate this spatial interaction?

We thank the reviewer for this very important point. CCR2+ macrophages are monocyte-derived as prior studies have shown (PMID: 30582448, 25349429, 24439267, 29892064, 36034743). Tissue-resident macrophages do not express CCR2. We specifically used a $Ccr2^{creERT2}$ to target monocytes and monocyte-derived macrophages (and not the tissue resident macrophages) as our human data suggest that the CCR2+ monocyte-derived cells are the source of the IL1b. We provide 3 orthogonal approaches that monocyte-derived macrophages are the source of IL1b: 1) From the human CITE-seq data, we overlaid CCR2 with IL1b to show these cells co-express CCR2 and IL1b, 2) Using a CCR2-GFP reporter mouse model with Ang II/PE infusion, we co-stained for GFP and IL1b to show that CCR2+ macrophages are the source of IL1b, and 3) we generated a new mouse ($Il1b^{flox/flox}$ $Ccr2^{creERT2}$) to specifically delete IL1b from monocytes and monocyte-derived macrophages using a tamoxifen dosing strategy that selectively labels monocytes (https://www.biorxiv.org/content/10.1101/2023.12.24.573263v1). Deletion of IL1b from monocytes and their progeny (monocyte-derived macrophages) results in reduced Postn+ fibroblasts, diminished myocardial fibrosis, and improved LV function.

To dissect co-localization between CCR2+ monocytes and macrophages with fibroblast cell states in an un-biased manner we leveraged spot deconvolution using cell-2-location along with predictive modeling with MistyR. We applied this framework on 7 spatial transcriptomic samples from infarcted hearts and have presented the additional analysis in Figure 4f in the amended manuscript. We found that CCR2+ monocytes and macrophages were spatially localized with

F9 (POSTN) and F3 (CCL2+) fibroblasts but not F2 (myofibroblasts) whereas resident macrophages were spatially localized with F4 fibroblasts.

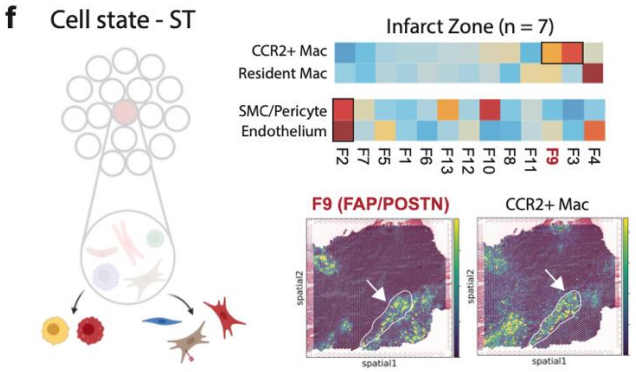


Furthermore, we also performed immunofluorescence for FAP/CD68/CCR2 to show co-localization of FAP+ fibroblasts with CCR2+ macrophages (Fig. 4g) in human HF samples. To quantify co-expression of myeloid IL1B and fibroblast POSTN, we ran a regression analysis at the patient level of IL1B expression in CCR2+ macrophages harvested from these hearts with POSTN expression in fibroblasts harvested from the same hearts and found a strong positive correlation (Fig. 4g).

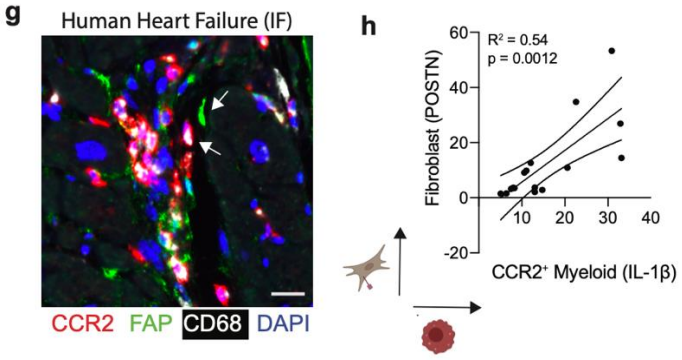


To further validate the co-localization of CCR2+ macrophages with POSTN+ fibroblasts, we performed RNAscope in infarcted human hearts and quantified CCR2+ cells in POSTN-low and POSTN-high fields and saw a significantly greater number of CCR2+ macrophages in POSTN-high fields (Fig. 4i).

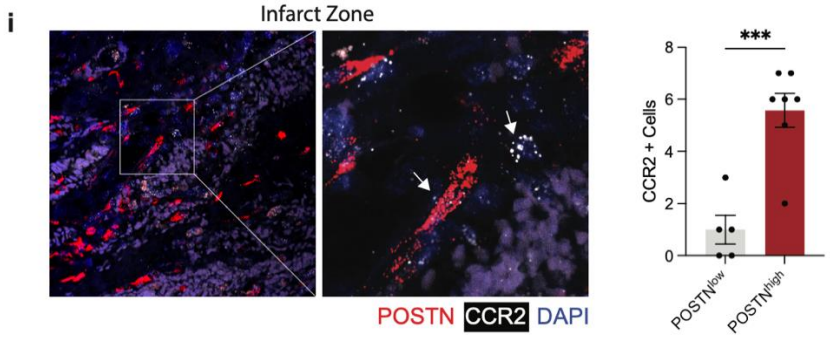

We have added the following to the results section to highlight this additional analysis:

"To dissect which myeloid and fibroblast cell states localize in space, we performed spot deconvolution using cell2location at the cell state level and MISTYr[29,35] for predictive modeling across multiple infarcted samples (n = 7) to co-localize CCR2+ macrophages (predictor cell type) with all fibroblast cell states (target cell type) which showed inflammatory CCR2+ macrophages co-localize with F9 fibroblasts while resident macrophages co-localize with F4 fibroblasts (**Fig. 4f, Supplementary Table 18**). Notably, F2 fibroblasts co-localized with SMC/Pericyte/Endothelium and did not co-localize with CCR2+ macrophages (**Fig. 4f, Supplementary Table 18**). We used immunofluorescence for CCR2/FAP/CD68 in human LV sections to show co-localization of FAP+ fibroblasts with CCR2+ macrophages in the failing LV (**Fig. 4g, Supplementary Table 18**). To further infer macrophage-fibroblast crosstalk at the patient level we performed a linear regression of pseudobulk macrophage IL-1β expression with fibroblast *POSTN* expression and observed a strong correlation (**Fig. 4h**). To validate our findings in a broader cohort of specimens, we performed RNAscope for POSTN and CCR2 and quantification showed more CCR2+ cells in POSTN-high fields compared to POSTN-low fields in post-MI hearts (**Fig. 4i**)."

4. Figure 5a suggests that TGFB is a major component of the cell-cell communication circuit. Does TGFB contribute to the F9 phenotype in addition to IL1B (which only partially contributes to the expansion of POSTN+ fibroblasts)?

We thank the reviewer for the interesting comment. We agree that many signaling molecules play an important roles in human heart failure pathogenesis and fibrosis. Prior studies have characterized the impact of TGFb as a putative regulator of cardiac fibrosis (PMID 32997468, 17967775, 19919989, 28891814). While evaluating the impact of dual IL1b/TGFb blockade would be fascinating, we feel that rigorous genetic experiments are needed to address this scenario and the underlying mechanisms of synergy. Such an extensive analysis is outside the intended scope of the current manuscript. We hope that the Multi-omic human data presented herein in addition to the computational analysis serves as an important resource for the heart failure and cardiac immunology community. We have presented an unbiased analysis to prioritize key targets with human relevance and show in detail using conditional KO mouse models the potential of targeting Il1b in heart failure.

Minor Point:
5. In lines 421-422 the authors incorrectly referred to FBN1 and FOSX1 as transcription factors. The text and accompanying figure should be corrected.

We thank the reviewer for this comment and edited the text accordingly.

**Referee #2 (Remarks to the Author):**

In this revised version of the manuscript the authors have addressed several critical points raised in the first revision, including: some location issues of the pathogenic fibroblasts subsets and their interaction with macrophages, the identity of CCR2+ infiltrating monocyte/macrophage as a relevant source of IL1b in cardiac pathogenic contexts, and the paracrine IL1b responsiveness of fibroblasts through IL1R. While the data generally validates the conclusions of the paper, there are still a substantial number of minor limitations that need to be addressed. In particular, the authors have ignored some of my previous comments and continue to abuse the use of computational tools that generate confusion (including to this reviewer) rather than useful data, and the quality of many of the panels and figures is still low and can be improved substantially. Importantly, the issue of immune-fibroblastic niches remains in my opinion unclear with the tools used here. Finally, I find that a lot of the supplementary data based on reanalysis of the datasets in multiple different ways are not essential and in fact overload and distract from the flow of the paper and dilute the main message (see e.g. the analyses shown for Suppl Fig. 15 and 16).

We thank the reviewer for being meticulous and thorough in the review of our manuscript. We apologize for the image quality – all high-quality pdf files for figures are available at

(https://www.dropbox.com/scl/fo/bvrwsild7pnct26kcyu6c/AGphrJLw49Szs45A0tvExHM?rlkey=tlissrp3qs49c2b1cqfk6kwsu&dl=0).

Furthermore, we recognize and appreciate that abundant data analysis is distracting. We have made every effort to address the important concerns made by all reviewers, which warranted the additional figures and analyses. In the revised manuscript, we have extensively re-organized the figures into main, extended data, and supplementary figures prioritizing key analyses and removing less informative information as pointed out by the reviewer. We have also streamlined the text.

I hope that these comments help to improve and otherwise interesting paper with profound therapeutic implications, as detailed below:
- the paper continues to abound in statements that direct to main or suppl. figures that are packed with data but fail to rigorously show the claim. For example, the claim that fibroblast populations localize in defined perivascular and interstitial spatial niches in Suppl Figs.7b-d. It is impossible to assess if this is the case and there is a lack of quantification. The text of these panels is also very small and difficult to follow. The authors have ignored my previous comments and instead have packed the figures even more in ways that I find counterproductive for the clarity of the message and for the readers.
- Related to the above, the claim that F9 fibroblasts associates most with myeloid cells and F2 with other vascular cells is central to the model proposed in the paper. This is assessed using spatial correlation analyses in Suppl Fig.10. The relevant panels here are in low resolution, with text difficult to read, and not assessing the different groups with recognizable names, such as F2 or F9, for example. This makes evaluation difficult if not impossible but also suggests rushed analyses that exclusively aim to validate a hypothesis, without actual rigorous demonstration.
- More on this, the relevant point that Postn, Runx1, Ccr2 and 1lb co-localize spatially in MI sections is presented in an image with low resolution and no quantification, so the claim remains largely unsupported by the data. It is unclear why immunofluorescence is not performed in MI samples to directly validate this claim at the protein level.

We are very grateful to the reviewer for being thorough and pointing out these important points. For clarity and visualization purposes we have kept fibroblast cell state naming convention consistent throughout the manuscript, removed extraneous analyses as suggested, and provided high resolution images. Below we outline in detail the un-biased approach we used to characterize fibroblast and myeloid cell state spatial localization.

To dissect fibroblast spatial diversity, we used the following 5 orthogonal approaches:

1) Plotted signatures for each fibroblast cell state from 26 patients and have shown the data in Extended Data Fig. 4f. We found that different fibroblast states are differentially enriched across myocardial regions.
2) For cell state level mapping, we used cell-2-location to deconvolute spatial spots into fibroblast cell states and then used predictive modeling with MistyR and a previously utilized method in human hearts to identify predictor cell types which can predict target cell types to be co-localized within the same spot. An integrated analysis across 7 ischemic samples (Extended Data Fig. 4g) suggested that most fibroblast cell states displayed independent localizations. Only F6-11 and F12-13 displayed strong co-localization signals.
3) Given the stronger localization of F2 fibroblasts with perivascular niches and F9 fibroblasts with interstitial fibrosis, we calculated a distance matrix based on spatial image coordinates and constructed a minimum spanning tree representing the spatial cellular proximity using the SColoc function within CellTrek toolkit. This analysis showed through an orthogonal approach (spatial distance) that F2 fibroblasts are associated with perivascular niches while F9 fibroblasts are more associated with immune cells and F4 fibroblasts (Extended Data Fig. 4h).
4) To further dissect the precise cell states contributing to perivascular (vascular, adventitial) fibroblasts versus interstitial fibroblasts, we utilized human coronary artery single cell data. These vessels travel through the myocardium and are surrounded by adventitial and perivascular fibroblasts. We reference mapped the fibroblast populations to our human cardiac fibroblasts to identify perivascular fibroblasts within our heart dataset. We found that the F2 and F11 fibroblasts were most enriched in the adventitia, whereas F9 fibroblasts were much less abundant (Fig. 2h).

We have amended the manuscript to include the following:

“To characterize the spatial localization of transcriptionally distinct fibroblast cell states, we built an integrated spatial transcriptomics dataset from 26 patients and we carried out 3 orthogonal analyses. First, fibroblast cell state co-localization analysis in different myocardial regions was performed by creating fibroblast cell state gene set scores and constructing heatmaps to characterize how different fibroblast cell states localize across myocardial regions. This analysis showed that different fibroblast cell states were enriched across myocardial sampling locations including the infarct zone (F2, F8, F9), border zone (F5, F6, F7, F10, F13), and remote zone (F11, F12). Some fibroblast cell states (F1, F3, F4) were present across tissue compartments (**Extended Data Fig. 4f**). Second, to dissect the spatial localization of fibroblasts in the infarcted heart, we performed spot deconvolution at 2 levels: cell level using snRNA-seq followed by cell state level using CITE-seq annotations. We then used MISTYr for predictive modeling to identify cell types predicted to be co-localized within the same spot. An integrated analysis across 7 samples (**Extended Data Fig. 4g**) suggested that most fibroblast cell states displayed independent localizations. Only F6-11 and F12-13 displayed strong co-localization signals. Third, we calculated a distance matrix based on spatial image coordinates and constructed a minimum spanning tree representing the spatial cellular proximity using the SColoc function within CellTrek

toolkit. This analysis showed that F2 fibroblasts are associated with perivascular cells (pericytes) while F9 fibroblasts are more associated with myeloid cells and F4 fibroblasts (**Extended Data Fig. 4h**). To further dissect the precise cell states contributing to perivascular (vascular, adventitial) fibroblasts versus interstitial fibroblasts, we utilized human coronary artery single cell data[31]. These vessels travel through the myocardium and are surrounded by adventitial and perivascular fibroblasts. We reference mapped the fibroblast populations to our human cardiac fibroblasts to identify perivascular fibroblasts within our heart dataset. We found that the F2 and F11 fibroblasts were most enriched in the adventitia, whereas F9 fibroblasts were largely absent from perivascular areas (**Fig. 2h**)."

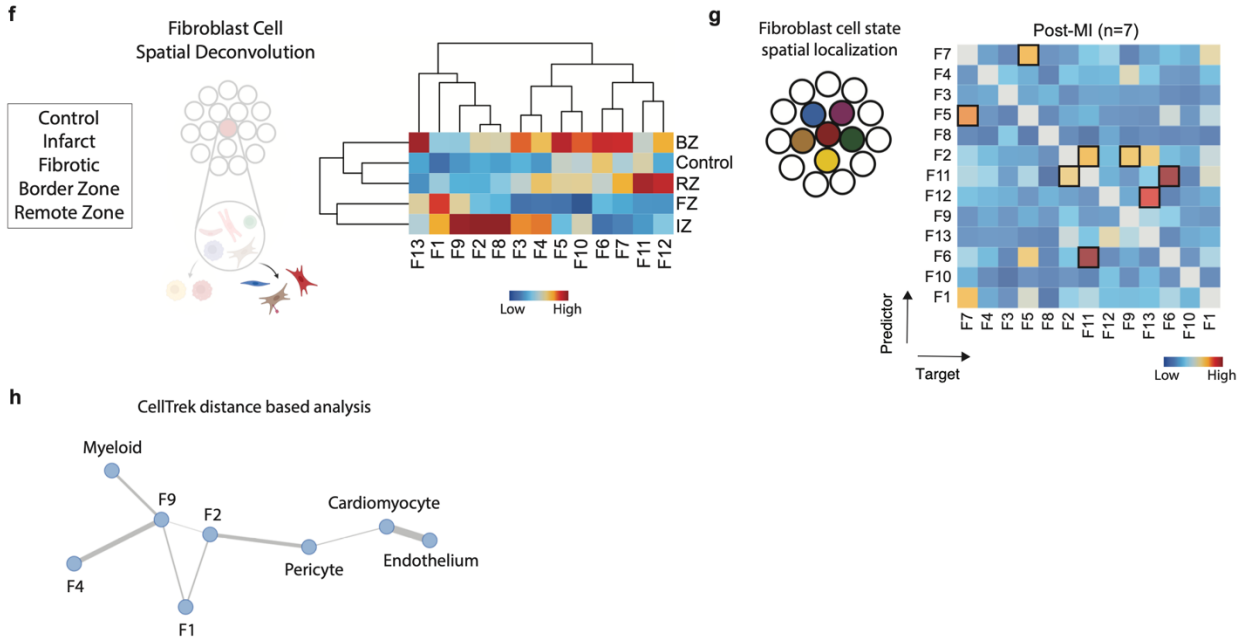


To dissect co-localization of CCR2+ monocytes and macrophages with fibroblast cell states in an un-biased manner we leveraged spot deconvolution using cell-2-location along with predictive modeling with MistyR. We applied this framework on 12 spatial transcriptomic samples from infarcted hearts and have presented the additional analysis in Figure 4f in the amended manuscript. We found that CCR2+ monocytes/macrophages were spatially localized with F9 (POSTN) and F3 (CCL2+) fibroblasts but not F2 (myofibroblasts) whereas resident macrophages were spatially localized with F4 fibroblasts. Furthermore, we also performed immunofluorescence for FAP/CD68/CCR2 to show co-localization of FAP+ fibroblasts with CCR2+ macrophages (Fig. 4g) in human HF samples. To quantify co-expression of myeloid IL1b and fibroblast POSTN, we ran a regression analysis at the patient level of IL1b expression in CCR2+ macrophages harvested from these hearts with POSTN expression in fibroblasts harvested from the same hearts and found a strong positive correlation (Fig. 4g). To further validate the co-localization of CCR2+ macrophages with POSTN+ fibroblasts, we performed RNAscope in infarcted human hearts and quantified CCR2+ cells in POSTN-low and POSTN-high fields and saw a significantly greater number of CCR2+ macrophages in POSTN-high fields (Fig. 4i).

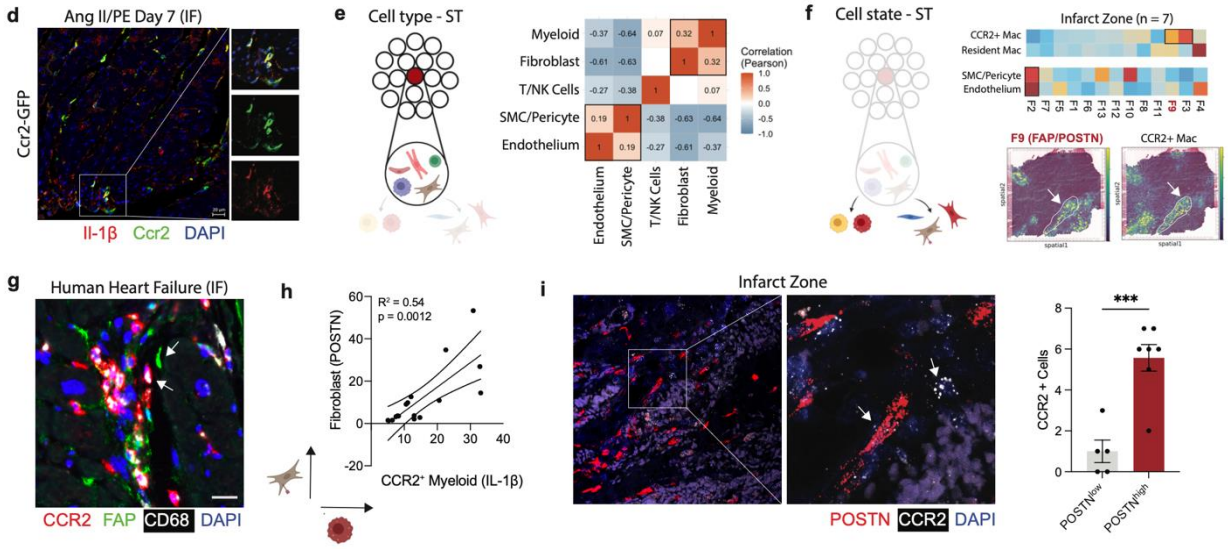


We have amended the manuscript to include:

"To dissect which myeloid and fibroblast cell states localize in space, we performed spot deconvolution using cell2location at the cell state level and MISTYr[29,35] for predictive modeling across multiple infarcted samples (n = 7) to co-localize CCR2+ macrophages (predictor cell type) with all fibroblast cell states (target cell type) which showed inflammatory CCR2+ macrophages co-localize with F9 fibroblasts while resident macrophages co-localize with F4 fibroblasts (**Fig. 4f, Supplementary Table 18**). Notably, F2 fibroblasts co-localized with SMC/Pericyte/Endothelium and did not co-localize with CCR2+ macrophages (**Fig. 4f, Supplementary Table 18**). We used immunofluorescence for CCR2/FAP/CD68 in human LV sections to show co-localization of FAP+ fibroblasts with CCR2+ macrophages in the failing LV (**Fig. 4g, Supplementary Table 18**). To further infer macrophage-fibroblast crosstalk at the patient level we performed a linear regression of pseudobulk macrophage IL-1β expression with fibroblast *POSTN* expression and observed a strong correlation (**Fig. 4h**). To validate our findings in a broader cohort of specimens, we performed RNAscope for POSTN and CCR2 and quantification showed more CCR2+ cells in POSTN-high fields compared to POSTN-low fields in post-MI hearts (**Fig. 4i**)."

- The change in FAP+ fibroblasts in the different experimental groups (Il1b-floxed mice, etc.) cannot be shown by this cytometric assay that does not match or explain the fibroblast diversity described through the paper and is in fact the basis of their finding. Imaging, sc transcriptomics or other consistent measured should be used. Also, it remains unclear to me why FAP+ vs FAPneg fibroblasts were sorted for scRNAseq in the control and anti-IL1b-treated mice, rather than just analyzing the total fibroblast compartment to examine for altered population frequencies particularly in the FAP/Postn subset. This data needs to be better organized and explained, ideally presenting only the experiments that justify the conclusion that anti-IL1b prevents the maturation towards the matrifibroblast state.

We thank the reviewer for this comment. Given FAP is expressed on the cell surface, we used the FAP flow cytometric assay to quantify FAP+ fibroblasts in the different conditions. An antibody flow reagent allows for robust characterization of FAP within the entire tissue which obviates challenges with immunofluorescence quantification in serial sections. In the original analysis we sorted FAP+ and FAP- cells and performed scRNA-seq analysis and importantly the

FAP+ group displays signatures of F9, and pro-fibrotic cells compared to the FAP- group (Extended Data Fig. 12i, j). As the reviewer suggested, we have repeated this experiment sorting out all fibroblasts without creating separate libraries and amended Figure 5 to show this new data and analysis. Notably, we find that anti-IL-1β mAb decreases the proportion of Postn fibroblasts (Extended Data Fig. 12d,e) and decreases pro-fibrotic gene expression in particular *Fap* and *Postn* (Fig. 5j). A pathway analysis using differentially expressed genes between Isotype and anti-IL-1β mAb showed decreased TGF- β signaling in anti-IL-1β mAb fibroblasts (Fig. 5k). Additionally, we would like to highlight that the co-summitted manuscript by the Srivastava lab has performed the same experiment in a TAC model with anti-IL-1β mAb treatment and scRNA-seq of all fibroblasts – in Fig. 5G-N of their manuscript the find anti-IL-1β mAb treatment leads to fewer Postn+ pro-fibrotic fibroblasts highlighting the efficacy of anti-IL-1β mAb treatment to abrogate fibroblast activation. Furthermore, we also performed a 28-day experiment with sham, Ang II/PE + Isotype, or Ang II/PE + anti-IL-1β mAb to show decreased fibrosis in the treatment group.

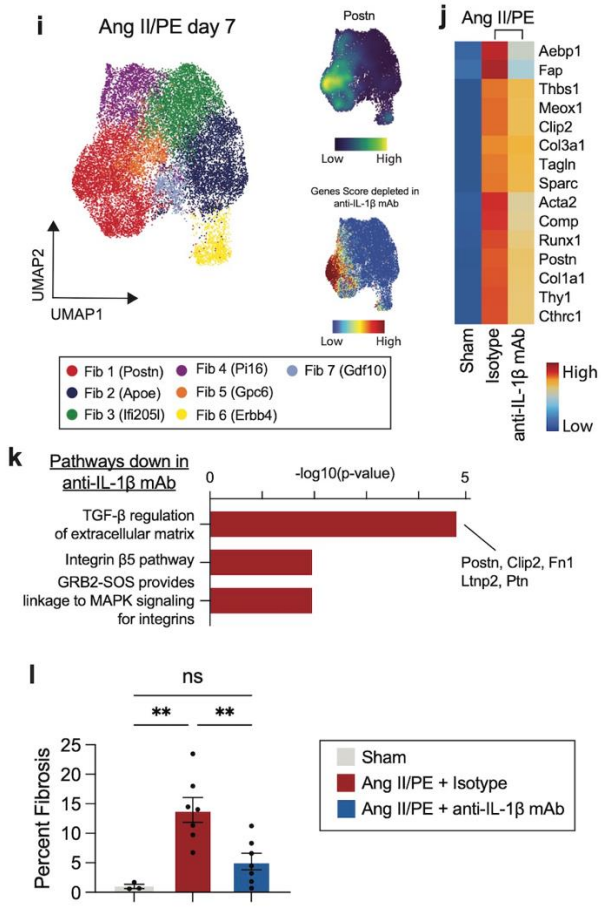


We have reorganized the figure panels and revised the text to better highlight the main message as the reviewer points out.

“To dissect whether anti-IL-1β mAb blunts activated fibroblast maturation, we performed scRNA-seq on sorted fibroblasts at day 7 in sham and Ang II/PE infused mice treated with either isotype or anti-IL-1β mAb. We found 7 transcriptionally distinct fibroblast cell states (**Fig. 5i, Extended Data Fig. 12a-c, Supplementary Table 19**) and expansion of *Postn*+ fibroblasts in Ang II/PE relative to sham (**Extended Data Fig. 12d,e**). We then performed differential expression in the

Ang II/PE group between the isotype and anti-IL-1β mAb treated mice to create a signature of genes downregulated in the anti-IL-1β mAb treatment group which was most enriched in the *Postn*+ fibroblast state (**Fig. 5i**). Notably, the anti-IL-1β mAb group had fewer Postn+ cells (Fib 1; **Extended Data Fig. 12e, bottom panel**) and decreased expression of key pro-fibrotic genes such as *Aebp1, Fap, Thbs1, Meox1, Clip2, Col3a1, Tagln, Sparc, Acta2, Comp, Runx1, Postn, Col1a1, Thy1, Cthrc1* compared to isotype treated mice (**Fig. 5j**). A pathway analysis showed that the TGF-β regulation of extracellular matrix was decreased in the anti-IL-1β mAb group relative to isotype controls (**Fig. 5k, Supplementary Table 20**). We additionally mapped the mouse data onto the human fibroblasts (**Extended Data Fig. 12d-f**) and found fewer F9 imputed fibroblasts in the anti-IL-1β mAb group relative to isotype controls (**Extended Data Fig. 12e, top panel**). These findings are consistent with anti-IL-1β mAb reducing pro-fibrotic fibroblasts in a TAC injury model from the Srivastava Lab[34].”

- The resolution and contrast of Fig.2f showing FAP staining needs to be improved. It is very difficult to discern in a printout.

We apologize for the image quality and have improve the resolution of the FAP staining. All high-quality pdf files have been uploaded to the link above.

- In Pag.13, lines 439-441: “Using 68Ga-FAPi-46 non-invasive PET imaging, we confirmed early enrichment of FAP at d7 following AngII/PE infusion (Fig. 4k)”. These panels are not supported by any quantification or statistics.

We thank the reviewer for this comment. Considering the prior comment pertaining to Fap+ fibroblast quantification we repeated the $^{68}$Ga-FAPi-46 non-invasive positron emission tomography (PET) imaging experiment in sham, Ang II/PE with isotype or anti-IL-1β mAb treatment at day 7 to define a treatment response. Using a large cohort of animals, we quantified FAPi signal in the heart and found that Ang II/PE infusion for 7-days substantially increased FAPi signal in the heart. Notably, anti-IL-1β mAb treatment reduced $^{68}$Ga-FAPi-46 uptake consistent with our flow cytometric and scRNA-sq data. We have included this additional analysis below and in Fig. 5h and amended the manuscript.

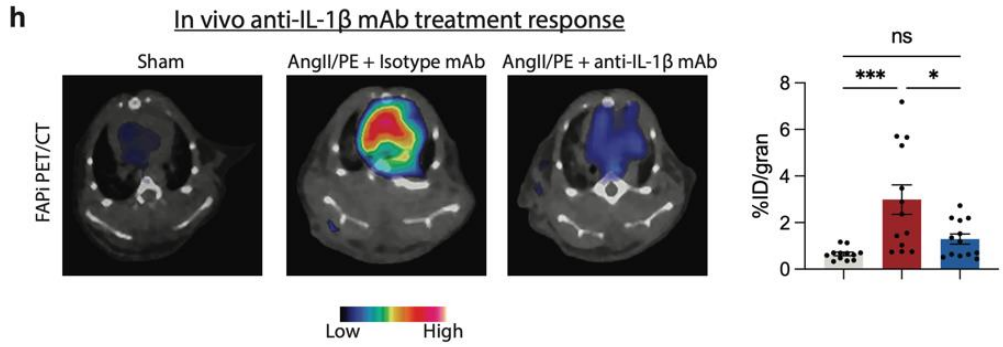


“To further characterize the treatment response of anti-IL-1b mAb treatment we performed $^{68}$Ga-FAPi-46 non-invasive positron emission tomography (PET) imaging to detect early fibroblast activation[39]. Ang II/PE treated mice had greater FAPi signal compared to sham. Mice treated with anti-IL-1β mAb demonstrated less $^{68}$Ga-FAPi-46 enrichment compared to mice treated with isotype control (**Fig. 5h**).”

- I don't understand the added value of Fig.4c beyond what is already shown as prediction in

Figs.4a-b.
- Fig6g, it is difficult at this size and resolution to discriminate Postn staining, the authors should make a general effort to improve the images included in the different figures.
- Misspelling: line 69: “shoewed”
- Misspelling: line 680: therapy instead of therapeutic?
- typo: line 454 should be Fig5C, not 7C, right?
- typo: line 457 should be Fig5C, not 9C, right?
- Supplementary Figures 21a-f are not referred in the main document.
- Supplementary Figure 27 is not referred in the main document.
- The number of samples for each condition indicated in the text (Lines 166-169) does not match the information in Fig.1a
- It is difficult to follow changes in different fibroblasts subsets since those are referred as F1-13 in text and this information is not reflected in referred figures (i.e. Supl.Fig10a-d, Sspl.Fig12b)). Please standarize nomenclature
- Consider re-spelling. Lines 372-374: “F11 (associated with adventitial 373 fibroblasts) was not present in either of the 3 mouse datasets and from the human coronary artery fibroblast mapping, F11 is associated with adventitial fibroblasts”

We thank the reviewer for the meticulous comments and will correct all redundancies, textual errors, and appropriate references to figures throughout the text including uploading all high-quality pdf documents to a server link.

Andres Hidalgo

**Referee #3 (Remarks to the Author):**

Follow-up comment: I have read over the comments in detail. In my view, the authors have done a great job addressing concerns raised in review. I would be in favor of accepting both papers. My only feedback will be that these analyses and discussion should make it into the paper to the extent this is possible.

We greatly appreciate your thorough review of out manuscript. The co-submitted manuscript by our colleagues demonstrated in vivo that treatment with an anti-IL1b mAb leads to improved LV function (Fig. 5G,H, Supplementary Fig. 10). We have also repeated this experiment in our Ang II/PE model as you suggested, and we found a decrease in cardiac fibrosis at day 28 with anti-IL-1β mAb treatment relative to isotype control. As you suggested we have also elaborated on the discussion of the synergy between both manuscripts.

The authors have responded extensively to my concerns raised in first review. I have one comment regarding their response to the question of using IL-1b mAb to target IL-1b in vivo.

In the original paper, the authors state: “To dissect the therapeutic impact of IL-1b inhibition on fibroblast cell state transitions, we implanted mice with Ang II/PE osmotic minipumps treated animals with an IL-1b neutralizing antibody (anti-IL-1b mAb) or isotype control every 3 days (Fig. 5A).”

This experimental design posits that mAb against IL-1b will affect IL-1b and have a ‘therapeutic impact…on fibroblast cell state transitions.” The experiments in new Figure 6 B-H require the context of whether this mAb treatment affects the phenotypes measured elsewhere in this paper…in other words, does the mAb against IL-1b have a therapeutic benefit or not?

Thus I am confused by the authors’ response to my original request of “The investigators need to show whether Il1b mAb treatment influences fibrosis in this model and the effects on systolic and diastolic cardiac function.”, to which they replied “To address the relevant source of IL-1β and the effect of IL1-β on fibrosis and cardiac function, we genetically deletion [sic] of IL-1β in monocytes and monocyte-derived macrophages. We chose this approach as neutralizing antibody treatment may not completely ablate the effects of IL-1β.”

In fact, this is exactly what the reader needs to know: if the mAb intervention is used to identify the cell populations in Fig 6B-H, is this taking place in the context of effective IL-1b inhibition and rescue of the phenotype? If the mAb does not ablate the effects of IL-1b, as the authors anticipate, this is important to know in the context of the rest of the paper.

We thank the reviewer for this important comment. The co-submitted manuscript by our colleagues demonstrated in vivo that treatment with an anti-IL1b mAb leads to improved LV function (Fig. 5G,H, Supplementary Fig. 10). We have also repeated this experiment in our model as suggested with sham, isotype, and anti-IL-1β mAb treatment and found a decrease in cardiac fibrosis at day 28 in Ang II/PE infusion with anti-IL-1β mAb treatment relative to isotype control. We have amended the figures and provided the following to the results section:

“Furthermore, we found that after 28 days of Ang II/PE infusion via osmotic minipumps anti-IL-1β mAb treatment decreased cardiac fibrosis (**Fig. 5I, Extended Data Fig. 12r**). Consistent with these findings, concurrent work from the Srivastava lab further showed that anti-IL-1β mAb treatment improved cardiac function and reduced fibrosis in a TAC heart failure model[34].”

As suggested, we have amended parts of the discussion and results sections to better highlight the synergy of the co-submitted manuscript from the Srivastava lab.

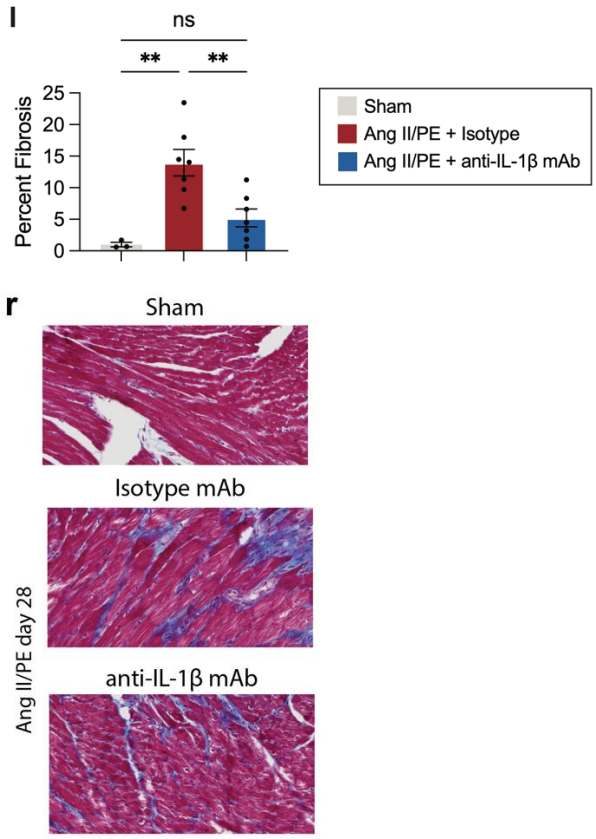

**Reviewer Reports on the Second Revision:**

Referees' comments:

Referee #1 (Remarks to the Author):

The authors have addressed most of my concerns. However, a few key points require more attention.

1) As previously highlighted, the data are not sufficient to justify using “crosstalk” in the title and throughout the manuscript, and the language should be toned down accordingly.
2) Relatedly, the authors should not overstate the role of IL1B signaling alone given that inhibition does not rescue all functional parameters even when genetically depleted.
3) The variability in fibrosis induction and reduction across studies is concerning and should be addressed or at least discussed, as it affects the robustness of the work.
4) The authors have removed FBN1 and FOSX1 from the text but they remain in Figure 2o. They should be removed for consistency and clarity.
5) The manuscript remains extremely dense and challenging to read. Streamlining the main figures could help with accessibility to the general readership of Nature.

Referee #2 (Remarks to the Author):

While the paper by Amrute et al. has improved and addresses many of my original comments, it remains a bit chaotic and dependent to a certain extent on the accompanying paper by the Srivastava group. For example, the statistics are indicated for some panels and not others, and there is wrong analysis e.g. in the FACS data in Fig.5g showing fraction of fibroblasts while the density plots shows that there is only one population whose intensity changes. The conclusions/analysis of this experiment are therefore not precise. I would suggest the authors to carefully address all these small but relevant technical concerns before the paper published.

Referee #3 (Remarks to the Author):

No further comments on this very interesting and important study.

**Author Rebuttals to Second Revision:**

Referee #1 (Remarks to the Author):

The authors have addressed most of my concerns. However, a few key points require more attention.

1) As previously highlighted, the data are not sufficient to justify using “crosstalk” in the title and throughout the manuscript, and the language should be toned down accordingly.

We have removed the word cross-talk from the title and toned down claims and highlighted important limitations in the discussions section.

2) Relatedly, the authors should not overstate the role of IL1B signaling alone given that inhibition does not rescue all functional parameters even when genetically depleted.

We have included a discussion of limitations including other relevant signaling axis in the discussion: “Our current study has potential limitations. First, we are not powered to assess the effects of demographics (age, sex, ethnicity) on the cell state diversity post-MI, thus, we included patients of diverse ethnicities, sex, and broad age ranges to remain inclusive in the generation of the human dataset. Given the challenge acquiring fresh acutely infarcted cardiac tissue, we validated our CITE-seq findings in a broad array of patients using multiple experimental approaches. Secondly, we studied the in vivo mechanism in a single pressure overload model with Ang II/PE which has inherent variability in degree of fibrosis induction across strains and batches[3,4,7,39] – further studies in a myocardial infarction model are necessary to generalize the findings presented herein. Finally, blocking IL-1b does not completely blunt cardiac remodeling suggesting there may be concurrent pro-fibrotic stimuli such as TGF-b contributing to cardiac fibrosis. Future studies are needed to clarify the interaction between IL-1b and TGF-b in fibroblast fate specification[39,45] and elucidate mechanisms by which fibroblasts communicate with immune cells such as macrophages, a possibility that is supported by recent findings[46].”

3) The variability in fibrosis induction and reduction across studies is concerning and should be addressed or at least discussed, as it affects the robustness of the work.

We have added the following discussion with citations in our discussion to highlight the comment made by the reviewers: “Secondly, we studied the in vivo mechanism in a single pressure overload model with Ang II/PE which has inherent variability in degree of fibrosis induction across strains and batches[3,4,7,39] – further studies in a myocardial infarction model are necessary to generalize the findings presented herein.”

4) The authors have removed FBN1 and FOSX1 from the text but they remain in Figure 2o. They should be removed for consistency and clarity.

Removed from the figure.

5) The manuscript remains extremely dense and challenging to read. Streamlining the main figures could help with accessibility to the general readership of Nature.

We have streamlined figures, moved detailed analyses to SI, and condensed the text to improve the clarity and readability of the manuscript.

Referee #2 (Remarks to the Author):

While the paper by Amrute et al. has improved and addresses many of my original comments, it remains a bit chaotic and dependent to a certain extent on the accompanying paper by the Srivastava group. For example, the statistics are indicated for some panels and not others, and there is wrong analysis e.g. in the FACS data in Fig.5g showing fraction of fibroblasts while the density plots shows that there is only one population whose intensity changes. The conclusions/analysis of this experiment are therefore not precise. I would suggest the authors to carefully address all these small but relevant technical concerns before the paper published.

We have streamlined figures, moved detailed analyses to SI, and condensed the text to improve the clarity and readability of the manuscript. We have also corrected axis headings to clarify details in flow panels. We have also indicated statistics for all relevant panels with p-values shown in the figure and statistical test used shown in the figure legends.

Referee #3 (Remarks to the Author):

No further comments on this very interesting and important study.

Thank you for your thoughtful comments in improving our manuscript.